OPTOFLUIDIC ADD-ON DEVICES FOR LIGHT SHEET FLUORESCENCE MICROSCOPY OF *CAENORHABDITIS ELEGANS* WITH CONVENTIONAL WIDE-FIELD MICROSCOPES

By

Mehran Behrouzi

A THESIS SUBMITTED TO THE FACULTY OF GRADUATE STUDIES

IN PARTIAL FULFILLMENT OF THE REQUIREMENTS FOR THE DEGREE OF

MASTER OF APPLIED SCIENCE

GRADUATE PROGRAM IN MECHANICAL ENGINEERING

YORK UNIVERSITY

TORONTO, ONTARIO

February 2022

Abstract

Caenorhabditis elegans (C. elegans) is a widely used model organism for studying molecular, cellular, and behavioural mechanisms underlying human diseases. Light-sheet fluorescence microscopy (LSFM) is an emerging fluorescent imaging technique suitable for non-invasive volumetric imaging of *C. elegans*. These promising microscopy systems, however, are scarce in academic and research institutions due to their high cost and technical complexities. Simple and low-cost solutions that enable the conversion of commonplace wide-field microscopes to LSFM platforms promote widespread adoption of this technology by a biologist for studying the cells, neurons and organs of *C. elegans*. In this respect, the primary goal of this thesis was to develop optofluidic add-on microdevices that can convert the commonplace wide-field microscope to an LSFM platform in a low-cost manner.

The first objective of the thesis was to perform immobilization-free and fast LSFM imaging of *C. elegans* with a standard fluorescent microscope at high contrast and resolution using a simple and low-cost optofluidic microdevice. The second objective of the thesis was to increase the throughput of the platform and perform continuous fluorescent imaging of groups of *C. elegans*. The developed optofluidic chips contained an integrated PDMS cylindrical lens for on-chip generation of the light-sheet across a microchannel. Cross-sectional LSFM images of *C. elegans* were acquired by the native objective of the host microscope as worms were flown in an L-shape microchannel and through the light sheet. Optical characterization of the developed device for fulfilling the first objective suggested a full width half maximum (FWHM) width of the point spread function as 1.1 μm and 2.4 μm in the lateral and axial directions, respectively. On-chip

LSFM imaging of *C. elegans* strains using the developed optofluidic LSFM platform demonstrated the possibility of visualizing the entire neuronal system in few seconds (2s) at single-neuron resolution, with high contrast, and without worm immobilization. Volumetric visualization of the neuronal system from the acquired cross-sectional 2D images was also demonstrated, enabling the standard microscope to acquire 3D fluorescent images of *C. elegans*.

For the second objective of the thesis, the optofluidic device was modified to enable easy passing of worms through the L-shaped channel to perform continuous imaging of groups of *C. elegans*. The flow characterization of the device suggested 20 µl/min as the operating flow rate for the continuous assay. The obtained results of the continuous imaging of the BZ555 *C. elegans* strain suggested an imaging throughput of 12 worms per minute. To investigate the performance of the platform for quantitative fluorescent imaging, *C. elegans* BZ555 worms were exposed to established dosages of 6-OHDA neurotoxin and imaged with the LSFM optofluidic device. The obtained results demonstrated the ability of the LSFM platform in detecting the toxin-induced neurodegeneration phenotypes in the worms as they were continuously passed through the device. We envision this simple and low-cost optofluidic LSFM platform can be used for high-content and potentially high-throughput imaging of *C. elegans* with the conventional wide-field microscopes.

Acknowledgments

I would like to express my sincere gratitude and appreciation to Professor Tabatabaei and Professor Rezai for their support and guidance throughout my research. I would also like to express my heartfelt thanks to Dr. Youssef for all his helps and kindness throughout this research.

Table of Contents

List of Figures

List of Tables

Chapter 1
Introduction

1.1. Introduction and Research Motivation

Caenorhabditis elegans (C. elegans), shown in Figure 2-1, is a widely used model organism for studying molecular, cellular, and behavioural mechanisms underlying human diseases [5], [6]. The success of such investigations frequently relies on the availability of imaging platforms with high spatial and temporal resolutions with minimal photodamage. Wide-field (WF) fluorescent microscopy is commonplace in biology but suffers from poor image contrast due to out-of-focus/background fluorescence. Confocal fluorescent microscopy (CM), on the other hand, offers high-contrast images but is inherently slow and, similar to WF, and prone to photodamage and photobleaching [7], [8].

To overcome the above limitations, light-sheet fluorescence microscopy (LSFM) techniques, also known as selective plane illumination microscopy (SPIM), have been proposed [9]–[12]. LSFM systems illuminate the sample only in the detection objective's focal plane to enable the acquisition of high contrast images with minimal photodamage. Enhancement in imaging speed, compared to CM, is a key advantage of LSFM as the image is acquired in a widefield manner [13]. To date, several variants of LSFM have been developed and tailored for imaging biological samples, particularly for imaging *C. elegans* [14]–[17]. These stand-alone systems, however, are normally complex and costly because they require two dedicated illumination and detection objectives, and controlled or motorized translation of immobilized *C. elegans* through the light-sheet for image

acquisition. These limitations have effectively hindered the widespread adoption of LSFM by biologists.

In an attempt to make LSFM more accessible, a collection of recent works has focused on making LSFM compatible with the commonplace WF microscopes [3], [18]–[22]. For example, replacing the epi-illumination of the host conventional microscope with light-sheet illumination has been shown to enable the acquisition of light-sheet fluorescent images with a high signal-to-background ratio (SBR) [19], [21]. Another example is the work of Hsieh et al. [20], in which a volume holographic optical element was developed to create a light-sheet for high contrast imaging of *C. elegans* with the conventional WF microscope. However, these promising works were quite complex and slow as *C. elegans* had to be immobilized and translated through the light sheet via precision motorized components. These constraints preclude the use of such systems in large-scale studies involving continuous imaging of large numbers of *C. elegans* to test various experimental conditions with high statistical confidence. In another approach, on-chip platforms (e.g., microfluidics devices) were integrated into conventional LSFM systems to enable fast fluorescent imaging of groups of *C. elegans* [23]. While these approaches have enhanced the LSFM speed by acquiring images of *C. elegans* as they flew through the light-sheet, the proposed solutions were still costly because of the utilization of the stand-alone light-sheet microscopy systems. Developing a low-cost, simple, and continuous-flow LSFM platform compatible with commonplace wide-field microscopes can promote wide-spread use of this imaging technology for studying the cellular and neuronal fluorescent expressions of *C. elegans*, which was the overall goal of this thesis.

1.2. Research Opportunity and Thesis Objectives

Although LSFM has proven to be a powerful non-invasive imaging platform, there are no reports on the development of a simple and low-cost LSFM platform for fast and continuous imaging of groups of *C. elegans*. This thesis attempts to narrow the gap between the required resources for implementing a sophisticated microscopy method and those available to less-specialized research labs. To do so, the goal of this project is to develop optofluidic add-on devices that can convert the commonplace wide-field microscope to an LSFM platform in a low-cost manner. Optofluidic chips enable the miniaturization of the LSFM by integrating its illumination path within the same chip used for flow-based translation of *C. elegans*. Also, the fluidic-based scanning approach of the platform can be suitable for large-scale studies as the groups of *C. elegans* can potentially be continuously imaged while passing through the light sheet. In particular, we will focus on fabricating inexpensive microfluidic sample holders with integrated optical components that will allow on-chip light-sheet microscopy. To achieve our goal, the following thesis objectives will be pursued.

1. Fast and immobilization-free light-sheet imaging of adult *C. elegans* with the conventional wide-field microscope using a simple and low-cost optofluidic microdevice.

2. Continuous fluorescent imaging of groups of *C. elegans* and performing validation study for quantitative fluorescent imaging using an established neurotoxin exposure assay.

1.3. Thesis Organization

The first chapter of this thesis provides a general introduction and motivation of this research, followed by the research gaps and defined thesis objectives.

The second chapter of the thesis starts with providing an overview of the *C. elegans* model organism and its importance in biological sciences, followed by the manipulation methods of this organism. Next, an overview of the widely used fluorescent techniques is provided, followed by a comprehensive review of the LSFM background, principle, and application in *C. elegans* research.

The third chapter describes the conceptual design of the optofluidic LSFM platform, including the mechanical and optical design. Also, this chapter provides the fabrication procedure of the devices and *C. elegans* preparation protocol, along with data processing.

The fourth chapter provides the obtained results and the corresponding discussions. The first section of the chapter presents the results of LSFM imaging of *C elegans* neurons with the add-on optofluidic device, confirming the feasibility of high-resolution immobilization-free fluorescent imaging of *C. elegans* with the conventional wife-field microscope (thesis objective 1). The second section provides the quantitative results obtained for continuous imaging of *C. elegans* with the modified optofluidic device and assessing the effect of 6-OHDA neurotoxin exposure on worms that express fluorescence in their dopaminergic neurons (thesis objective 2).

The fifth chapter summarizes the findings of the presented study and suggests recommendations for further research.

Chapter 2
Literature Review

2.1. *C. elegans* Model Organism

This section is divided into four subsections, starting with a brief introduction on model organisms, followed by a review on *C. elegans* model organism and its manipulation methods, and ending with a survey on different imaging methods, focused on fluorescent methods, in *C. elegans* research.

2.1.1. Introduction to Model Organisms

Model organisms are non-human species that have long been associated with biological and medical research. Even though human clinical trials are unquestionably the most accurate approach for studying human diseases and drug screening, practical and ethical constraints exist in using human samples in these cases. Failure of drug discovery investigations due to inadequate drug distribution and absorption and chemical toxicity is an example of the limitations associated with clinical studies [5], [24]. The use of models to explore system biology and disease is frequently a trade-off between the model's ability to imitate the actual situation and its ease of manipulation. While mammalian species such as mice have shown to be valuable models for human diseases and preclinical drug screening, studies with these animals can not be conducted in a cost-effective and rapid manner. In this respect, researchers have become interested in using small non-mammalian model organisms such as the fruit fly (*Drosophila (D.) melanogaster)* [23], the zebrafish (*Danio*

(D.) rerio) [27], and the worm (*Caenorhabditis (C.) elegans)* [28], that can reduce the use mammals and the failure rate of preclinical animal assays. These are promising models for molecular, genetic, cellular, and organ-based research in human biology and disease, owing to their similar genetic patterns and simplified cellular/tissue structures. Such studies improve our lives by lowering the cost and time required to investigate disorders [24], [29].

2.1.2. *C. elegans* as a Human Biology and Disease Model

C. elegans have proven to be a promising model for studying human biology and disease, owing to its appealing experimental and biological characteristics. *C. elegans* is typically cultivated on agar plates seeded with a food source of *E. coli* OP50 strain bacteria containing a variety of nutrients, as illustrated in Figure 2-1 (A) [53]. This invertebrate organism reproduces in a three-day life cycle that begins with the embryonic stage and continues through four larval stages (L1-L4) and adulthood (Figure. 2-1 (B)). Experimental advantages of this versatile roundworm include fast growth, body transparency, the small size of 1 mm at the adult stage, and mapped neuronal connectivity. Also, maintaining and culturing the worm in a laboratory environment is easy and cost-effective, making it a widely used whole model organism for biology research [5], [30].

Numerous biological processes and disorders have been mimicked in *C. elegans* using genetically encoded and mutant strains due to the amenability of the worm to molecular genetic techniques. Cell-specific expression of fluorescent labels, such as green fluorescent protein (GFP) on dopaminergic neurons (DNs), can be achieved by these genetic manipulations. High-resolution imaging and quantification of these fluorescent expressions is an essential step in biological investigations that utilize these worm strains. By employing these strains as disease models, we

can better understand the pathologies, processes, and pathways underlying various diseases, including muscular dystrophy, ageing, diabetes, and neurodegeneration (e.g., Huntington's disease, HD; Parkinson's disease, PD) [5], [30]. As an example, a fluorescent image of a *C. elegans* BZ555 strain, which expresses GFP in the DNs as a model for PD is demonstrated in Figure. 2-1 (C).

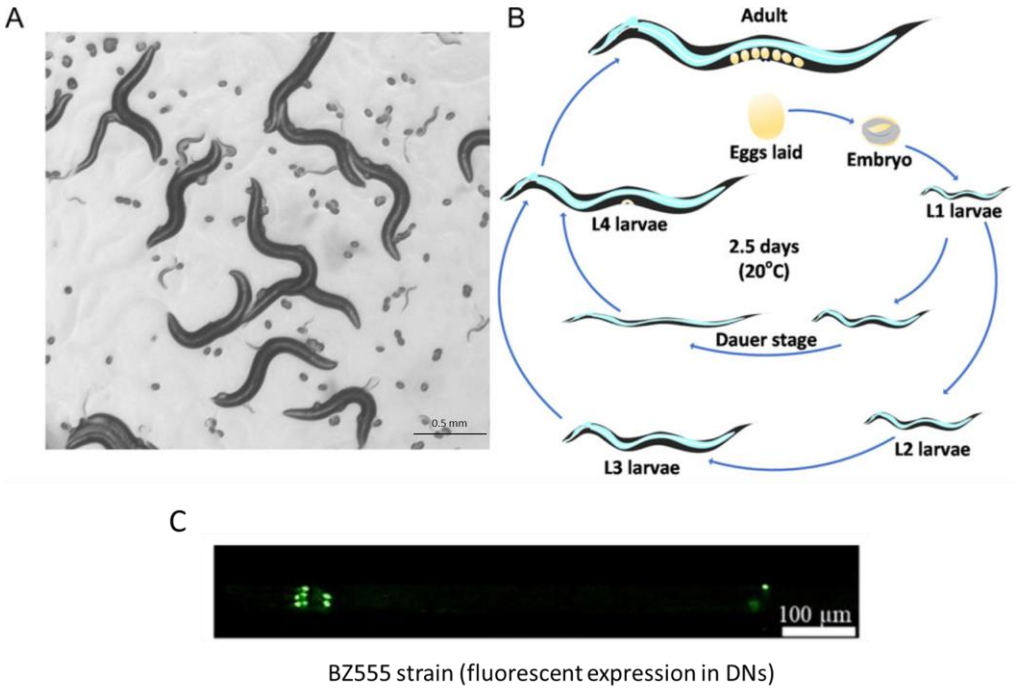

Figure 2-1. Caenorhabditis elegans and its life cycle. A) A culture of C. elegans on the OP50 seeded agar plate showing adult worms, L1 stage worms and spherical embryos. B) life cycle of C. elegans at 20°C is roughly three weeks, including embryogenesis, four larval stages and adulthood. [31] *C) BZ555 C. elegans PD model, expressing green fluorescent protein (GFP) in its DNs.*

In order to mimic diseases, two main strategies are used in worm research to induce neurological dysfunction, degeneration, or death, i.e., genetic mutation (like gene knockout or knockdown) or pharmacological interventions (like neurotoxin exposure). For example, PD is a neurological condition characterized by the degeneration of DNs in the substantia nigra and the widespread aggregation of the protein α-synuclein (α-syn), which results in motor deficits and, eventually,

cognitive dysfunction. *C. elegans* genome research revealed six orthologs of recognized genes related to familial PD in humans (i.e. Parkin, DJ-1, PINK1, UCHL-1, LRRK2, PARK 9, and NURR1) [32]. Thus, multiple transgenic worm strains expressing a variety of PD-related traits have been produced for neural and behavioural tests. Also, investigations on these strains have helped identify chemical compounds/drugs that can suppress the abnormalities [31]. The work of Fu *et al*. [33] is an example that investigated the effect of acetylcorynoline, as a potential drug, on PD using the *C. elegans* model organism. In this study, BZ555 (fluorescent expression in DNs, Figure 2-1 (C)) and OW13 (expression of human α-syn in muscle cells) strains were exposed to 6-hydroxydopamine (6-OHDA) toxicant, which leads to DN degeneration. Acetylcorynoline-treated worms demonstrated a significant reduction in DN degeneration in BZ555 and accumulation of α -syn in OW13, implying that the chemical compound acetylcorynoline could be used as a possible anti-PD medication.

Due to the conserved signaling pathways between *C. elegans* and mammals, including humans, this invertebrate is also a valuable model for understanding other diseases such as diabetes. As *C. elegans* possesses an insulin growth factor-1 signaling pathway, its mechanism of metabolic regulation is studied through observation of fluorescently-tagged body muscle cells. For instance, it has been shown that increasing the amount of glucose in the diet causes the mitochondria in germ and muscle cells of *C. elegans* to swell and accordingly disfunction. Also, the efficacy of metformin, a commonly used medicine to treat type 2 diabetes, was measured by examining changes in the intensity of mitochondrial fluorescence following treatment [31].

All the achievements and discoveries listed above are tightly connected to our ability to image the worm body, organs, and cells while quantifying the fluorescent expressions in them. To obtain

reliable biological outcomes, it is essential to image *C. elegans* at substantially high spatial and temporal resolutions without damaging the specimen [34]. However, manipulation and secure immobilization of *C. elegans* are often required to do high-resolution imaging without affecting the worms' physiological condition [31]. The following section provides an overview of the techniques used to manipulate *C. elegans*, conventionally and using microfluidic platforms.

2.1.3. Methods for *C. elegans* Assays

C. elegans are known for their voluntary locomotory behaviour that hinders their ease of manipulation and handling, especially when considering their small size of 80-µm diameter and 1-mm length at adulthood. In this respect, different techniques have been introduced to control and manipulate the worms without severely harming the organism.

2.1.3.1. Conventional Methods for C. elegans Research

The conventional laboratory approaches for studying *C. elegans* rely on manual manipulation of the worm in a Petri dish or a multiwell plate [35]. Traditionally, worms were imaged with a microscope by mounting them on agarose pads on a glass slide using immobilizing drugs such as sodium azide or levamisole. Manual transferring of a worm to the glass slide for imaging is time-consuming; also, immobilizing with the drugs can alter gene expression or other phenotypes of the *C. elegans*. For instance, sodium azide obstructs the mitochondrial electron transport chain and disturbs the activity of cells [34], [35]. Additionally, when worms are fixed on glass slides, their orientation is variable, making it challenging to image the worm's specific orientation. Lastly, the entire procedure is sometimes lethal and hence not reversible, making later stage experiments like

aging studies on the same worm impossible. While these mentioned conventional manipulation approaches are well established, they are time-consuming, cumbersome, and difficult to scale up.

C. elegans are an established model for chemical screening applications, owing to the availability of its mutants and disease models. The purpose of a chemical screen is to evaluate a collection of compounds in order to find those that exhibit the desired effect. For instance, as indicated in section 2.1.2, chemical screening using *C. elegans* disease models discovered multiple inhibitory candidates against neuronal toxicity [35]. Chemical screens are frequently carried out using multi-well plates. For instance, Petrascheck et al. [36] screened 88,000 compounds in 384-well plates to identify candidates for life-span reducing chemicals. Although high throughput screening is made possible with these platforms, complex robotic sorters and imaging systems are often needed, which are expensive and mostly inaccessible to academic labs.

To address some of the limitations of conventional worm manipulation and screening methods, microfluidics technology has emerged, which offers an environment to manipulate and study *C. elegans* in a precise, automated, low-cost, and high-throughput manner [37]–[39]. The following section provides a brief overview of the developed microfluidic devices for *C. elegans* manipulation and chemical or gene screening.

2.1.3.2. Microfluidic Methods for C. elegans Manipulation

Microfluidics is the field of understanding and handling fluid flow at the scale of micrometers. Since its introduction as a tool for *C. elegans* research, microfluidics has provided numerous inherent benefits for addressing major limitations in the handling, manipulation, and screening of *C. elegans*. This technology enables precise visualization and quantification of biological processes owing to its miniaturized nature [23], [40]. Channels in microfluidic devices typically

range from a few to hundreds of micrometers, matching the worm's size throughout its life stages. Numerous microfluidic devices have been created to accomplish complex operations on a chip, such as manipulating worms for accurate spatial placement and controlling the physical, chemical, and biological milieu to which the organism is subjected. These devices have contributed to the advancement of *C. elegans* research in various areas such as neuro-behavioural studies, screening applications, axotomy and cell ablation [41]. Secure and reversible immobilization of worms is critical to conducting the studies mentioned above. For instance, genetic screens for fine phenotypes based on micron-sized features typically are performed using high-resolution imaging, which necessitates immobilization of the worm during the process. To address this challenge, several microfluidic-based immobilization methods have been created to accommodate the requirements of these assays [41], [42]. Unlike conventional immobilization methods that work based on gluing and anesthetic drugs, the microfluidic-based methods employ different physical principles to immobilize the worm in a rapid, reversible, and efficient way. These techniques can be classified as mechanical force-based [43]–[47], gel-based [48]–[50], temperature-based [51]–[53], Gas-based [43], [54], electric-based [55]–[58], and acoustic-based methods [59].

Mechanical manipulation. Mechanical clamping is a robust and reversible method of worm immobilization. Different mechanical approaches are employed to securely confine a worm inside a microchannel based on suction flow, PDMS membrane pressure, and channel geometry [42]. Hulme *et al*. [47], for the first time, introduced a single PDMS layer microfluidic device with tapered channels to confine an individual worm. Pressure difference was applied between the inlet and outlet of the device and directed the worms to the array of 128 microchannels with a wedge shape (Figure 2-2 (A)). In other works, a flexible PDMS membrane was employed to apply pressure and restrict the worm. These devices mostly work based on the applied pressure of the

controlled layer that is above the main chamber. The worm is restricted in the channel of the main layer by the deflection of the thin membrane in the second layer [42].

Gel manipulation. Immobilizing the worm by utilizing the biocompatible Pluronic F127 polymer was proposed by Krajniak *et al*. [49], [50]. They developed microfluidic devices to handle the reversible thermo-sensitive sol-gel transition of the polymer on a chip (Figure 2-2 (B)). *C. elegans* were immobilized by the Gel phase of the material. This platform offers minimal physical deformation to the sample, avoiding alterations in physiological processes and the specimen's anatomy. However, this method is unsuitable for high-throughput studies due to the long sol-gel transition time (45-60s) [42].

Temperature manipulation. A worm can be immobilized by decreasing or increasing its temperature to specific levels. For instance, worms were immobilized once their temperature was decreased to 4 °C [51], [52]. This operation was performed by supplying a cooling liquid through a control layer of the microfluidic device (Figure 2-2 (C)). This technique showed good throughput characteristics (up to 400 samples per hour) and did not impact the morphological phenotypes. However, it is not feasible to implement the device for long-term assays involving physiologically active specimens [42].

Gas manipulation. It has been shown that subjecting the worm to the N_2 and CO_2 gasses result in long-time immobilization [43], [54]. Chokshi *et al.* [43] developed a microfluidic device to pass the pure CO_2 through the control layer of the device to expose and immobilize the *C. elegans* in the microchannel for an extended time (Figure. 2.2 (D)). No physiological effect was reported in the short-time period (1 min) of CO_2-based immobilization.

Electric manipulation. Electric fields have been utilized to confine *C. elegans* passively within a microchannel for long-time periods. For instance, Rezai *et al.* [57] demonstrated the behaviour of

C. elegans once exposed to electricity and showed that worms stop in the presence of low frequency alternating current electric field (Figure 2.2 (E)).

Acoustic manipulation. Ding *et al.* [59] presented a manipulation method using a single-layer PDMS device that works based on the standing surface acoustic wave (SAW). The developed acoustic tweezer employed the wide resonance band of interdigital transducers to control a SAW field, enabling contact-free and precise manipulation of samples such as *C. elegans*. However, in the required input power to enable *C. elegans* manipulation, temperature increases to 31°C, which can harm the nematode [42].

For performing large-scale studies for screening applications, the mechanical and electrical manipulation methods have been widely used because of their higher assay speeds [39]. For example, gel manipulation method is not suitable for high-throughput studies as the long sol-gel transition time lowers the assay speed (45-60s) [42]. On the other hand, using the mechanical manipulation method, and specifically the narrow channel technique shown in Figure 2.2 (A), one can restrict the worms in one direction while flowing it across the imaging spot on the chip for continuous image acquisition as needed in the second objective of this thesis.

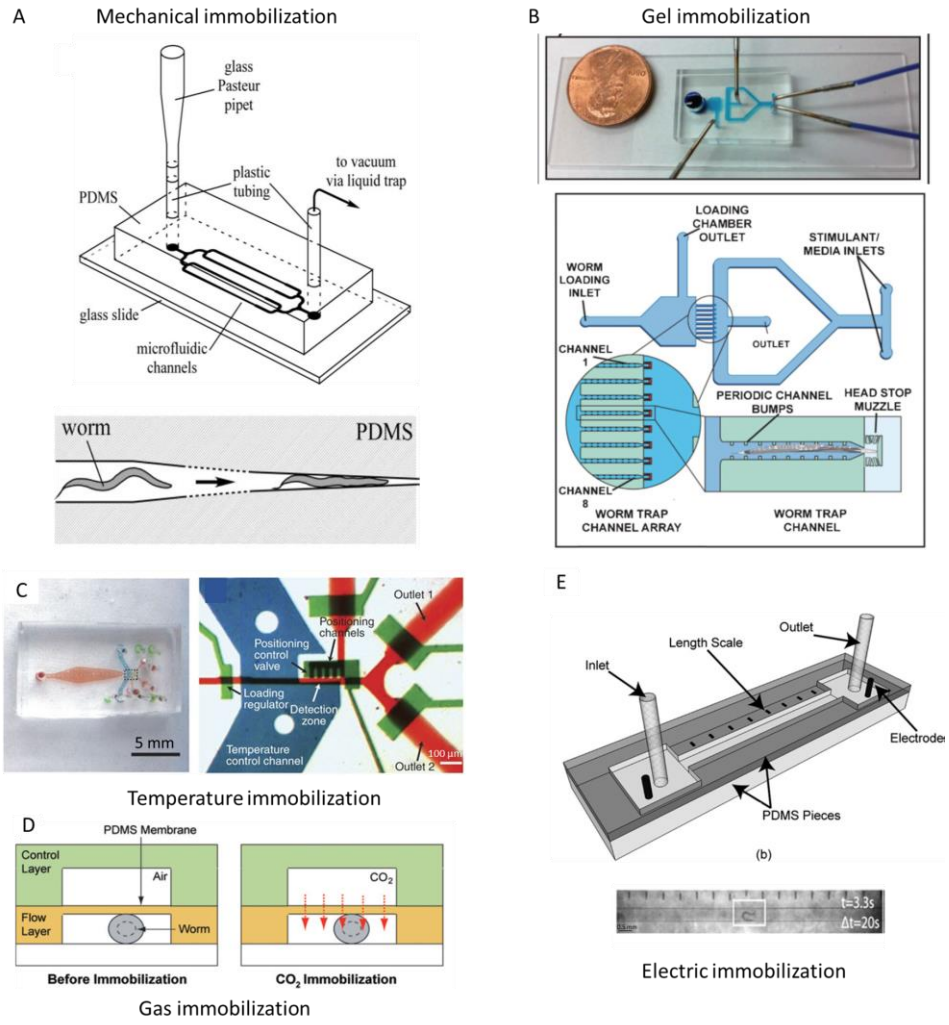

Figure 2-2. C. elegans manipulation using microfluidics devices. A) Mechanical manipulation using a PDMS device (top). Schematic of the tapered microfluidic channel of the device to restrict the worm's motion (bottom) [47]. *B) Gel immobilization using the PDMS device (top) consisting of trapping channels (bottom)* [49]. *C) Temperature-dependent manipulation with the double-layer PDMS device (left). Optical image of the device showing temperature control channel (blue), valves (green), sample-loading channel (red)* [52]. *D) Manipulation of the worm by passing a CO2 stream from a control layer to the main layer.*[54] *E) Electric manipulation of the worm using a single layer PDMS device with an alternating current electric field* [57], [58]. *(Panels A, B, D, E reproduced from ref* [44, 46, 51, 54] *respectively, with permission from the Royal Society of Chemistry. Panel C adopted from ref* [52]*, with permission from Springer Nature, Nature Method).*

2.1.4. Imaging Methods in *C. elegans* Research

In all *C. elegans* studies, whether conducted using traditional approaches or in the microfluidics environment, obtaining high resolution images is a critical step after worm manipulation. This section aims to provide an overview of the imaging technologies used in *C. elegans* research as a major observation and quantification tool, focusing on fluorescent microscopy to quantify gene expressions and cell toxicity levels after genetic manipulations and pharmacological treatments [8].

Macroscopy, automated microscopy, and microplate reader technology are the methods used in traditional well plate-based *C. elegans* phenotypic studies. Macroscopy is a low-throughput and low-content tool historically used to assess the morphology and locomotion of live *C. elegans*. Microplate reader is also a low-content instrument used in drug screening applications to measure the overall fluorescence of the wells without taking images. Optical microscopy is a high-content and high-throughput tool used in many applications, including fluorescent and non-fluorescent assays [60]. Optical microscopy with traditional manipulation methods of worms is time-consuming and labor-intensive as the worms should be manually picked, put on the optical imaging platform and immobilized using anesthetics before imaging. Therefore, several microfluidic-based manipulation techniques that were reviewed above have been integrated with optical microscopy systems to enhance the imaging speed and quality.

The imaging technologies used to study *C. elegans* in microfluidics can be categorized into two broad types: 1) conventional optical (fluorescent and non-fluorescent) and 2) lens-free optical microscopy [42]. Lens-free imaging systems are compact and miniaturized tools that include optofluidic contact microscopy [61], [62], shadow imaging [63], holographic imaging [64]–[66],

and microelectrode grid imaging [67]. However, conventional optical microscopy is the dominant imaging platform in biology laboratories. They are well-developed commercially available systems that normally offer a higher resolution than lens-free systems. Table 2-1 compares some important imaging methods [42], [68]. The following section provides an overview of conventional fluorescent microscopy as the most widely used imaging technique in *C. elegans* research from the optical perspective.

Table 2-1 Imaging Methods for *C. elegans* in Microfluidics

Imaging method	Size	Technology	Field of View	Resolution	Application
Fluorescent Microscopy	Large	Assembling	Small	High	Neuro-behavioral phenotyping, Chemical/Genetic screening, Drug screening Neurobiology
Non-fluorescent Microscopy	Large	Assembling	Small	High	Behavioural phenotyping, Monitoring
Optofluidic microscopy	Compact	PDMS layer on imaging sensor	Large	Moderate	Monitoring
Shadow imaging	Compact	Polycarbonate with polyester film	Large	Low	Monitoring
Digital holography	Compact	Sample plane on printed circuit board	Large	Moderate	Monitoring, Neuronal study

2.1.4.1. Fluorescent Imaging Techniques

Due to the worm's ease of genetic modification and optical transparency, it is possible to observe the worm's interior organs and cells directly using fluorescence microscopy without jeopardizing the animal's normal physiology. By expressing fluorescent markers, biologists can investigate

many biological matters *in vivo*; it is also feasible to track the neurons' dynamic activity by expressing genetically encoded fluorescent calcium indicators within the worms [5], [69].

The majority of fluorescence microscopes in use today are epifluorescence widefield (WF) microscopes. These microscopes are frequently used in biology labs and serve as the foundation for more sophisticated designs such as confocal and light-sheet microscopes. In WF microscopy, the emission fluorescent signal is focused on the detector using the same objective used to excite the specimen. The dichroic mirror functions as a wavelength-specific filter, transmitting the fluorescence toward the eyepiece or detector (Figure 2.3 (A)) [69]. For example, in work by Krajniak et al. [49], an epifluorescence microscope was utilized for long-term live imaging of immobilized *C. elegans*. In this experiment, the *C. elegans* body was immobilized in a microfluidic device using the gel behaviour of PF127 polymer. Fluorescently-tagged lipid droplets in intestinal cells of *C. elegans* were recorded over 3h period (Figure 2-3 (B)). The performance of the microdevice in maintaining the normal physiological condition over time was assessed by measuring the lipid diameter for 3h. However, droplets smaller than 2 μm could not be detected using the epifluorescence microscope at the 40x magnification, highlighting the need for higher resolution optical systems.

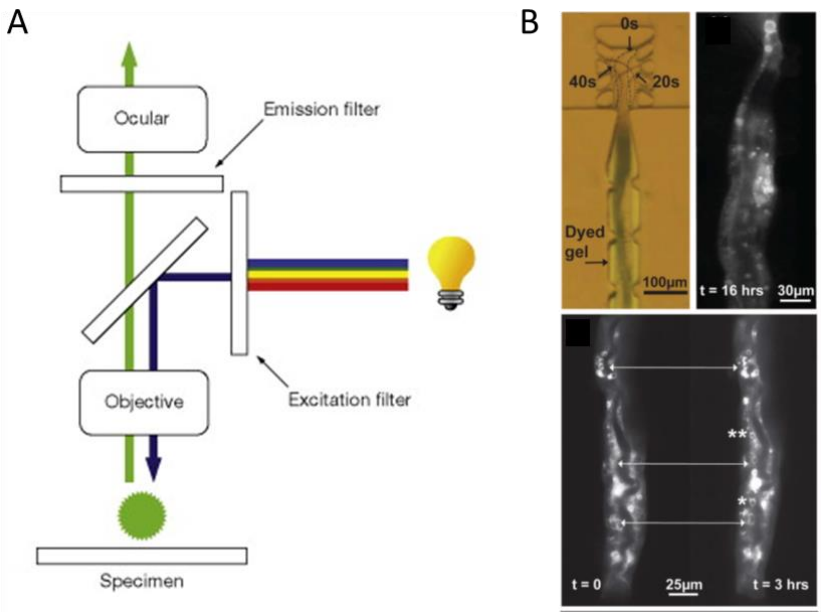

Figure 2-3. WF microscopy in C. elegans studies. A) Working principle of the conventional wide-field microscope [69]. *B) Bright-field and fluorescent images of transgenic C. elegans labeled with GFP in lipid droplets. The top left image shows the worm's head in different time points and its immobilized body. Bottom images show the change of droplets over 3h* [49], *reprinted with permission from the Royal Society of Chemistry.*

The conventional WF microscope suffers from poor spatial contrast as the images are formed from the sample's focal plane plus superimposed out-of-focus signal. Therefore, when higher resolution and high contrast 3D images are required to observe finer features and phenotypes, confocal microscopy (CM) is favoured over WF. In contrast to typical epi-fluorescence microscopy, which illuminates the entire field simultaneously and excites fluorescence across the specimen's depth, CM illuminates a single point in the focal plane that is scanned in the lateral direction to provide a full image. The optical system is equipped with a confocal imaging aperture, which prevents almost all light emanating from regions above and below the focal plane from contributing to the final image. Increased contrast and SBR in the final image result from reduced stray light not only from out-of-focus object planes, but also from the optical device itself [69]. The working principle

schematic of CM is shown in Figure 2-4 (A) [70]. For example, Ham *et al*. [71] studied the formation of α-synuclein inclusions using a confocal microscope to identify the involved cellular factors in their formation and finally get insight into the molecular origin of PD. Eighty genes were found to suppress the α-synuclein inclusion formation by observing the transgenic *C. elegans* strains that did not contain the targeted gene (Figure 2-4 (B)).

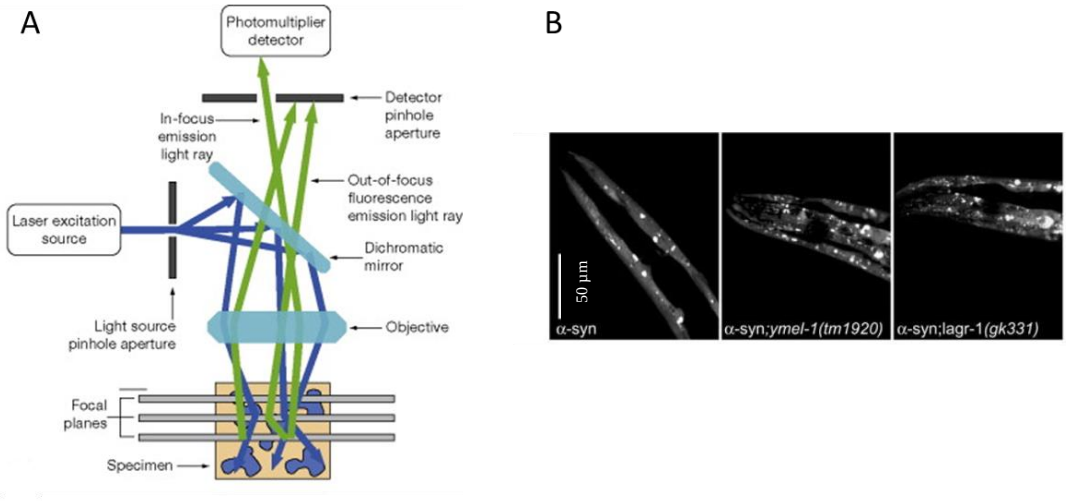

Figure 2-4. CM in C. elegans studies. A) Working principle of the point-scanning confocal microscope. 67], *reprinted with permission from Springer Nature, Nature Biotechnology. B) Confocal images showing a worm strain with α-synuclein-YFP tagged muscle cells (left), and the other strains (middle and right) with deleted target gene showing increased α-synuclein inclusions* [71]. *Adopted from Ref.* [71] *under the terms of the Creative Commons Attribution License.*

While confocal microscopy is a high-resolution 3D imaging technique, the high cost of purchasing (~ $200k-$500k) and operating CM systems, which can be several orders of magnitude more than comparable WF microscopes, often limits their use in smaller research facilities like academic labs [8].

In recent years, researchers have been interested in creating new technologies that can image with high spatial and temporal resolutions while also being low in phototoxicity, such as light-sheet fluorescence microscopy [72]. Before looking into the optical principle and technological background of light-sheet microscopy, it is essential noting why biological and biomedical researchers are interested in this imaging technology. Observing and quantifying biological processes in samples such as living organisms, tissues, and cells demands microscopy techniques that are harmless for the specimen while providing fast, volumetric information with high spatial and temporal resolutions [7]. Conventional WF fluorescent microscopy is low-cost, rapid, and commonplace in biology labs. However, it does not offer clear visualization of features deep in the samples due to the contributions of out-of-focus fluorescence light, which, in return, leads to deterioration of the image contrast. CM, on the other hand, offers high contrast volumetric images by optical sectioning. However, these systems are inherently slow as they work based on the point-scanning measurement scheme. Another significant disadvantage of WF and CM is that the excitation light travels through the sample, resulting in fluorescent excitation all along the optical path. This causes fluorescence emission from locations above and below the focal plane which can deteriorate the image quality [13]. Besides, numerous endogenous fluorescent and nonfluorescent organic components in the sample are stimulated. This is especially important when imaging living specimens over extended periods, as continuous exposure produces undesirable photodamage and phototoxicity. As a result, efforts have been undertaken in recent decades to create imaging alternatives capable of visualizing samples at greater spatiotemporal resolutions while maintaining the sample under low irradiation doses.

2.2. Light Sheet Fluorescence Microscopy (LSFM)

In recent years, researchers have shown an interest in a method known as light sheet fluorescence microscopy (LSFM). The concept of light-sheet microscopy was initially employed in 1903, when a German chemist, Richard Zsigmondy, and a physicist, Henry Siedentopf, collaborated to discover better means of understanding colloidal gold. However, it was a practice that lacked the technology to become a feasible and common imaging system for *in vivo* biological studies at the time. As a practical imaging platform, the resurfacing of light-sheet microscopy was introduced to the life sciences in 2004 and was referred to as selective plane illumination microscopy (SPIM) [11]. This method was initially utilized to study the embryonic development of *Drosophila melanogaster*. However, its application swiftly grew and was used for different studies on various samples, ranging from whole organisms to tissues, cell clusters, and single cells [73]. In this area, a variety of setups have been established in recent years, each tailored to the type of sample used and the demands of the research questions [13]. The section below is aimed at providing the working principle of the LSFM, followed by the main configurations and practical implementations of the technology. Finally, review of the LSFM systems used in the *C. elegans* research is presented and discussed.

2.2.1. Working Principle of LSFM

The working principle of a basic light-sheet microscope is illustrated in Figure 2-5. In this technology, illumination and detection paths are decoupled, contrary to conventional WF and CM, which use a single optical path. SPIM consists of two orthogonally-placed optical arms in its conventional configuration: an illumination arm to generate an excitation light-sheet and a

detection arm that collects the fluorescence emission. In this arrangement, the light-sheet coincides with the detection objective's focal plane and only illuminates a portion of the sample within the focal plane. Thus, contrast enhancement compared to WF is achieved as the out-of-focus fluorescence is removed. Also, unnecessary exposure of the fluorophores outside of the light sheet's thin volume is avoided, and thus, the risk of phototoxicity and photobleaching is minimized. A light-sheet microscope is an intrinsically fast 3D imaging technique as the entire field of view is recorded at once. As a result, higher imaging speed is achievable compared to CM [73].

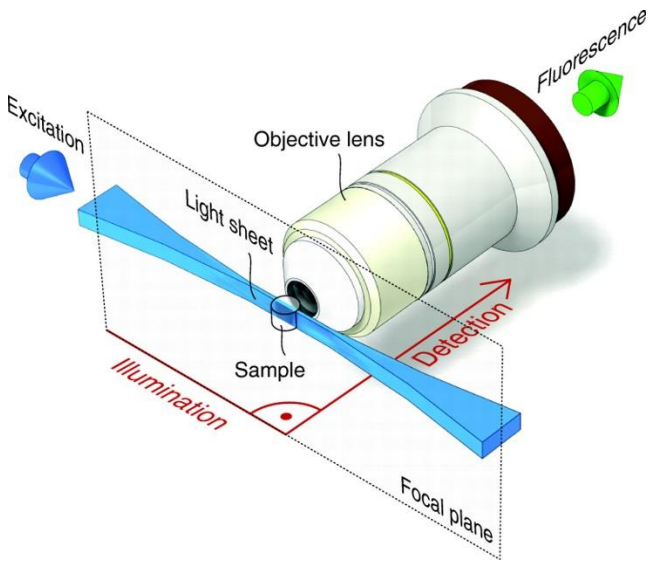

Figure 2-5. Basic schematic of a LSFM. Illumination or excitation path is decoupled from the detection or emission path. A light-sheet excites the section of the sample within a detection objective's focal plane [1]. *Reprinted with permission from The Company of Biologists Ltd.*

As mentioned above, light-sheet microscopy systems typically consist of two independent optical arms, elaborated below.

Illumination arm. In an essence, the purpose of the illumination arm is to create the excitation light-sheet, either in a static or dynamic manner. The static light-sheet is created by a cylindrical lens or combination of cylindrical lens and the objective lens in the illumination arm. In the most basic setup, a cylindrical lens is placed at its focal distance from the imaging plane where the collimated laser beam is shaped into a light sheet (Figure 2-6 (A)). To obtain a diffraction-limited light-sheet, multiple setups such as SPIM have employed a combination of the objective lens and cylindrical lens to minimize aberrations caused by using a single cylindrical lens. In this arrangement, a cylindrical lens is placed in the objective's rear focal plane, and the objective is positioned such that its focal plane matches the detection axis (Figure 2-6 (B)) [13], [74]. Dynamic light sheets also have been proposed (DSLM), in which the entire illumination power is focused on a line and virtual light-sheet is generated by rapid scanning of focused beam across the focal plane. In this approach, incoherent and more homogeneous light sheets are created, leading to less scattering and imaging artifacts, particularly in dense samples [10].

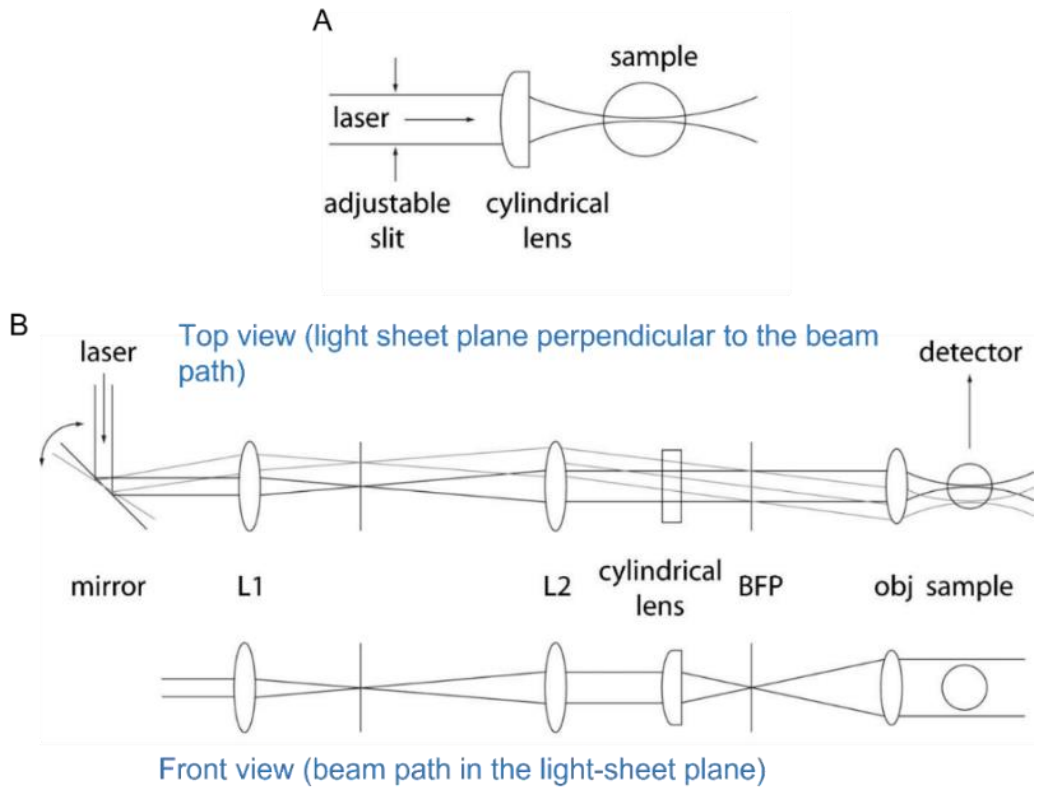

Figure 2-6. Illumination arm of LSFM. A) The simplest arrangement for creating the light sheet that utilizes a single cylindrical lens to focus a collimated beam into the thin section of the specimen. An adjustable slit allows for alteration of the illumination lens's numerical aperture and hence the thickness of the light sheet. B) An enhanced setup to generate a diffraction-limited light sheet in the SPIM. The illumination parts and ray traces are presented in planes perpendicular to the light sheet at the top and parallel to it at the bottom. The mirror is used to align the light sheet with the focal plane of the detection lens (not shown). Lenses (L1 and L2) form a telescope to tune the numerical aperture of the cylindrical lens and accordingly illumination objective (obj). BFP stands for back focal plane [74]. *Panels reprinted with permission from AIP publishing.*

In the standard light-sheet microscopes, typically, a Gaussian beam is used to form the light sheet (see Figure 2-7 (A)). The thickness and length of the Gaussian light-sheet are the crucial properties for the microscope's performance and are selected considering the sample under study. The

thickness of the light sheet is defined as twice the beam waist (w_0) at the focus, and is given by Equation 2-1:

$$2w_0 = \frac{2\lambda}{\pi\, NA_{illumination}} \tag{2-1}$$

Where λ is the wavelength of the illumination light, and $NA_{illumination}$ is the numerical aperture of the illumination lens. The length of the light sheet (twice the Rayleigh length (z_r)) is defined as the distance beyond which the light sheet does not extend more than twice its thickness. The light-sheet remains reasonably uniform over this distance, which is also considered as the usable field of view (FOV) given by Equation 2-2:

$$FOV = 2z_r = 2\frac{\pi {w_0}^2}{\lambda} \tag{2-2}$$

Light-sheet thickness is linked with the system's sectioning capability, and consequently, axial resolution. Thus, thinner light sheets offer superior axial resolution. However, thinner light sheets diverge more rapidly from the focus and, consequently, offer a smaller usable field of view. This results in an intrinsic compromise between the axial resolving power and the usable field of view in LSFM (Figure 2-7 (B)) [13], [75].

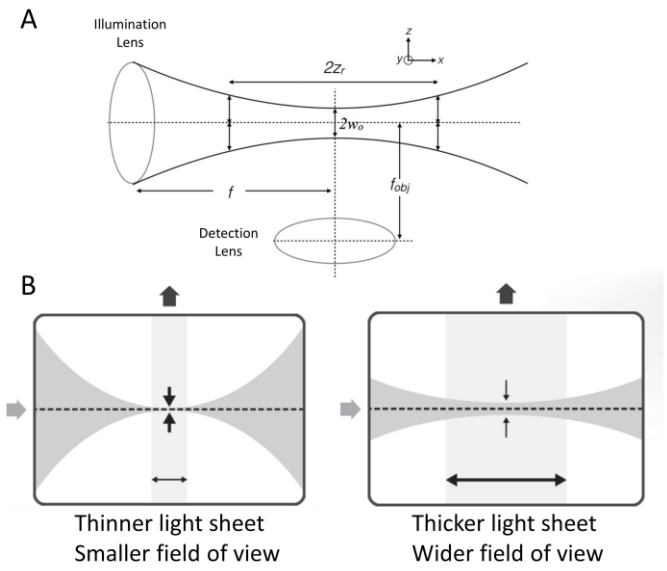

Figure 2-7. Gaussian beam focusing and light sheet characteristics. A) A focused gaussian light beam referred to as light-sheet. Focused beam (light-sheet) coincides with the detection lens' focal plane (f_{obj}). Thickness of light sheet ($2w_0$) and length of light sheet ($2z_r$) are shown. The z_r refers to the Rayleigh length which is proportionate with the waist. B) A thin light sheet propagates uniformly only within a short field of view. In comparison, a wide field of view can only be obtained with a thicker light sheet [73]. *Reprinted with permission from Elsevier.*

Detection arm. The detection unit of the SPIM is similar to the epi-fluorescent of the conventional WF microscopes, which generally consists of a detection objective lens, an emission filter, a tube lens and a widefield 2D detector (e.g., camera). Therefore, the lateral resolution of a light-sheet microscope is equal to a WF system and given by Equation 2-3:

$$R_{lateral} = \frac{\lambda_{em}}{2\,NA_{detection}} \tag{2-3}$$

Where $NA_{detection}$ is the numerical aperture of the detection lens, and λ_{em} is the wavelength of emitted fluorescent light. However, when dealing with the 2D detector such as CCD or CMOS, the camera's characteristics (e.g., pixel density and frame rate) also are essential in determining the final imaging resolution. Electron-multiplying CCD (EMCCD) cameras are typically used for

their high sensitivity, which allows for faster acquisition times. However, they usually offer less spatial sampling and limited imaging field of view due to the large pixels. Instead, scientific CMOS cameras offer enhanced signal-to-noise ratio (SNR) and higher spatiotemporal resolution. Thus, one must carefully consider the camera based on the nature of the study [13], [72].

2.2.2. Configurations and Practical Implementations of LSFM

2.2.2.1. Main configurations

The term “light-sheet microscopy” is used to refer to a variety of microscopy approaches that all rely on projecting a sheet of light to the imaging objective’s focal plane. While the core technological principle is in harmony, implementations vary. For several years, the absence of commercial LSFM platforms prompted biologists and researchers to develop customized systems, each suitable for a specific biological question or application. Indeed, LSFM is particularly appropriate for customization as the system can be built around the sample due to its decoupled nature. This customization has been made in multiple fronts such as components orientation, illumination patterns, sample holders, and image processing approaches. One of the main variations between the LSFM implementations is the relative orientation of the plane created by the two objectives and the plane of the optical table. In the initial SPIM, the plane of objectives is parallel to the bench, as shown in Figure 2-8 (A) [11]. In this configuration, sample positioning is done through the top of the chamber. iSPIM (shown in Figure 2-8 (B)), on the other hand, is an example of vertical orientation, which is usable for specimens that require traditional mounting procedures such as coverslips. Also, these configurations can be integrated into the standard microscope frame, allowing to benefit from all the microscope’s functions [11].

The abovementioned implementations illuminate the sample with a light-sheet through one side. When imaging large, living specimens, the light-sheet propagates through a highly absorbing and scattering environment. Attenuation of the excitation light in such samples causes shadowing, resulting in the deterioration of the image quality. Another disadvantage of one-sided illumination is scattering/widening of the excitation light-sheet deep into thick samples which lowers the imaging resolution. To avoid these complications, dual excitation setups have been developed to enable acquisition of high-resolution images with higher signal to noise ratio in highly dense and opaque samples. As shown in Figure 2-8 (C), multi-directional (m) SPIM illuminates the sample from two sides with two opposing illumination objectives. In mSPIM, the pivoting light-sheet, created by scanning the excitation beam using a resonant mirror, sequentially illuminates the specimen from two opposing directions. This results in a homogeneously illuminated image plane [9]. One can add a fourth lens for detection to acquire images in a faster manner (Figure 2-8 (D)). In this four-lens configuration, called MuVi-SPIM, two dynamic light sheets illuminate the focal plane of the two detection lenses. Here, illumination arms operate in an alternated manner to avoid image fuzziness that occurs in simultaneous illumination due to the increased scattering of two light sheets. However, dedicated software and controllers for data acquisition and image fusion are required in such systems [76]. To achieve a highly isotropic spatial resolution, an extension of inverted SPIM (iSPIM) called Dual illumination Inverted SPIM (diSPIM) has been developed. diSPIM is a symmetrical system with two identical and orthogonal objectives in which each optical arm sequentially excites and collects fluorescent. Images are acquired from two perpendicular views, merged and deconvolved to produce images with 330 nm isotropic resolution. However, post-processing of large data sets can take up to several hours, whereas conventional LSFM systems obtain the final image directly [77].

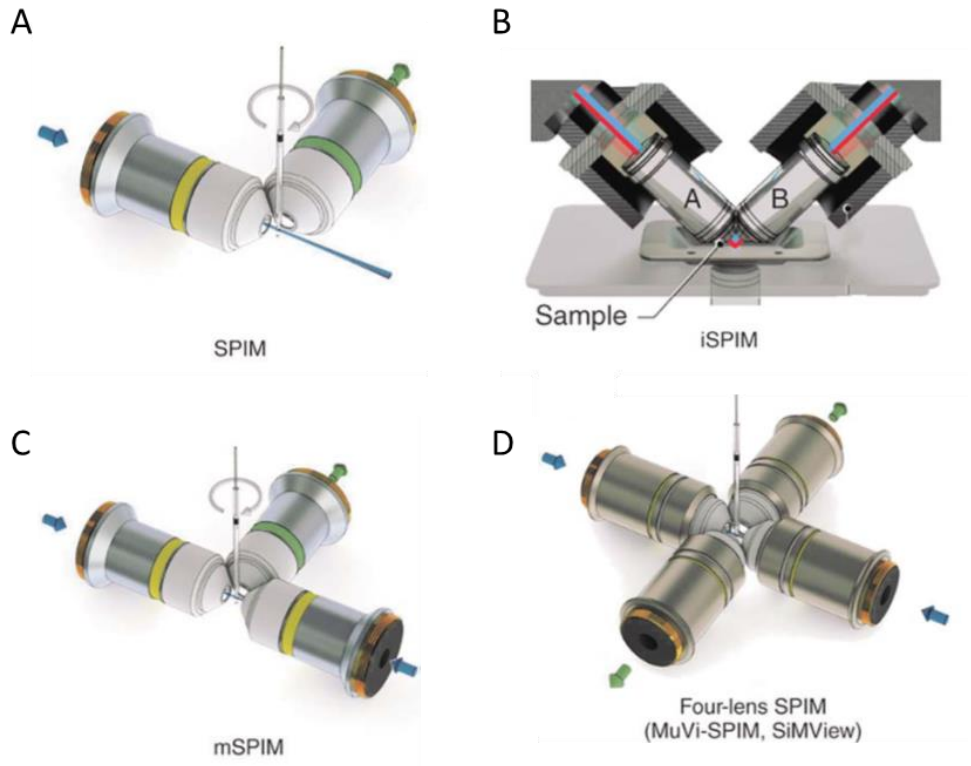

Figure 2-8. Different configurations of SPIM. A) A basic SPIM setup consisting of single illumination and detection objective lenses. B) Inverted SPIM (iSPIM) setup oriented vertically on the frame of a standard microscope. iSPIM will turn to diSPIM if operated in excitation and detection modes sequentially as shown with blue and red lines in B. C) Multidirectional SPIM (mSPIM) excites the sample from both sides and detects the emitted fluorescent from one side. D) Multiview SPIM consists of four lenses, two for illumination and two for detection. Panels A, C, D reprinted from [78] *by permission from Macmillan Publishers Ltd: Nature Methods. Panel B reprinted from* [77] *with permission from Springer Nature, Nature Biotechnology.*

While LSFM is undeniably a beneficial addition to the biologist's microscopy toolset, the complex setups outlined above are far from simple to build and need substantial optics and engineering expertise. LSFM should gradually convert from the dedicated optics laboratory to user-friendly instrumentations available to the larger biological community to be truly effective. Attempts in this regard are enduring by introducing approaches for implementing LSFM on conventional

microscope bodies. Moreover, first generation of commercial LSFM systems have been developed in recent years.

2.2.2.2. Commercially available LSFM

The Lightsheet Z.1 from Zeiss was the first commercially available solution based on Huisken's SPIM [11]. Z.1 is primarily meant for multi-view imaging of large, live samples, but it is also capable of imaging cleaned specimens. This method is well-suited for developmental biology research since it allows for tracking cell dynamics in small model organisms or tissues. Two sides of the sample are illuminated by a light sheet inserted vertically into the chamber from above. The sample is rotated in order to acquire images from several perspectives, which enhances resolution. The MuVi-SPIM microscope from Bruker is a viable alternative that provides faster image collection speeds and increased sample stability. This microscope is based on MuVi-SPIM of Krzic *et al*. [76], which provides four orthogonal views of the sample without requiring rotation. While the MuVi-SPIM is optimized for acquisition speed, the InV-SPIM from the same group is optimized for applications that require prolonged imaging. It is frequently used to monitor cellular and subcellular sites in small model organisms and cell cultures. The Ultramicroscope II of LaVisionBioTech is a feasible alternative, cleared, fluorescently tagged samples. This system is based on the working concept of Dodt and colleagues' ultramicroscope [79], with dedicated software for correcting the refractive indices differences induced by cleared tissues. The Ultramicroscope II has been utilized successfully for neurobiology applications, such as exploring lymph nodes and developmental modes in animal models; however, only at cellular resolution as the light sheet thickness below 4 μm is not achievable. The Lattice LightSheet microscope from 3i (Intelligent Imaging Innovations) is the commercially available microscope that provides a

homogeneous light sheet with a sub-micrometre thickness based on Chen and coworkers' innovation [12]. A 0.4 µm light sheet can be created with a Bessel beam and extended for 50 µm, making the technique ideal for imaging at the sub-cellular level [13], [75]. Although commercial LSFM systems are a beneficial tool for biological studies, the high cost of these systems (normally > $400k) hinders their wide-spread adoption in regular labs.

2.2.2.3. LSFM on conventional fluorescent microscopes

The typical configuration of LSFM with two (or more) perpendicular objective lenses limits its broad application in the biological sciences since it can not be easily integrated with standard microscope bodies. As a result, several laboratories have aimed to create solutions for LSFM implementation on conventional fluorescent microscopes.

Deschout *et al*. [2] proposed the use of microfabricated sample holders to enable high-resolution light-sheet microscopy on a standard fluorescent microscope. As seen in Figure 2-9 (A), the sample holder is a microfluidic chip with a planar waveguide. Generation of a 9-µm-thick light sheet was made possible by coupling an optical fibre to a planar waveguide. The design application in monitoring single particles in biological fluids was demonstrated.

In another work, Guan and colleagues [21] created a compact device suitable for imaging multicellular organisms such as zebrafish. Their planar illumination plugin (PIP) module could be installed on the stage of an epifluorescence microscope. It comprised a short sliding rail on which the optical components and a compact laser diode were attached and a tiny chamber in which the sample was held and aligned to the light sheet using an FEP tube. The light sheet thickness and field of view could be adjusted, with the beam waist thickness ranging between 5.5 and 10 µm and the field of view ranging from hundreds of micrometers to millimetres. The primary benefits of

this compact add-on are its ease of integration with the conventional inverted microscope and its low price. It is not, however, suitable for research needing a high level of axial resolution.

In another approach, Paie *et al*. [3] developed an integrated optofluidic chip using laser micromachining (Figure 2-9 (B)). On-chip generation of a 5.5 µm light-sheet was accomplished by employing an integrated lens that focussed the laser beam emanating from an optical fibre. The device was used with a standard fluorescence microscope to continuously image a group of 300 µm spheroids travelling through a glass microchannel. This platform offered increased throughput compared to conventional LSFM systems as the spheroids were imaged while moving inside the channel. However, the device was fabricated using femtosecond laser micromachining, which is sophisticate, expensive and hence not a commonly used technique for microfluidics applications.

To enable super-resolution light-sheet microscopy on a conventional fluorescent microscope, Gebhardt *et al.* [4] proposed a relatively simple and powerful platform called reflected light-sheet microscopy (RLSM). A high-NA illumination objective lens was replaced with the condenser of the host inverted microspore to produce the illumination beam (Figure 2-9 (C)). In such an arrangement, a focused Gaussian beam is sent in the opposite direction of the detection lens, and a sub-micrometer light-sheet is formed by horizontally reflecting the elliptical beam using an AFM cantilever. The technology's ability to image single fluorescent proteins of mammalian cells with a temporal resolution of up to 100 Hz was demonstrated. However, requiring an additional objective lens and an AFM cantilever adds high instrumentational complexity to the setup.

In a more practical approach, Single-objective SPIM (SoSPIM) has been proposed, producing the light-sheet through the same objective lens used for fluorescence detection. In the SoSPIM developed by Zagato *et al*. [80], microfabricated devices with integrated micromirrors made by silicon and polymer were developed for on-chip generation of 2µm-thick light sheets. Breast

cancer cell spheroids were imaged using microfabricated devices to demonstrate their applicability for soSPIM imaging.

Overall, development of LSFM systems compatible with the commonly used wide-field microscopes has enhanced the platform's accessibility and adoption by a broader range of researchers.

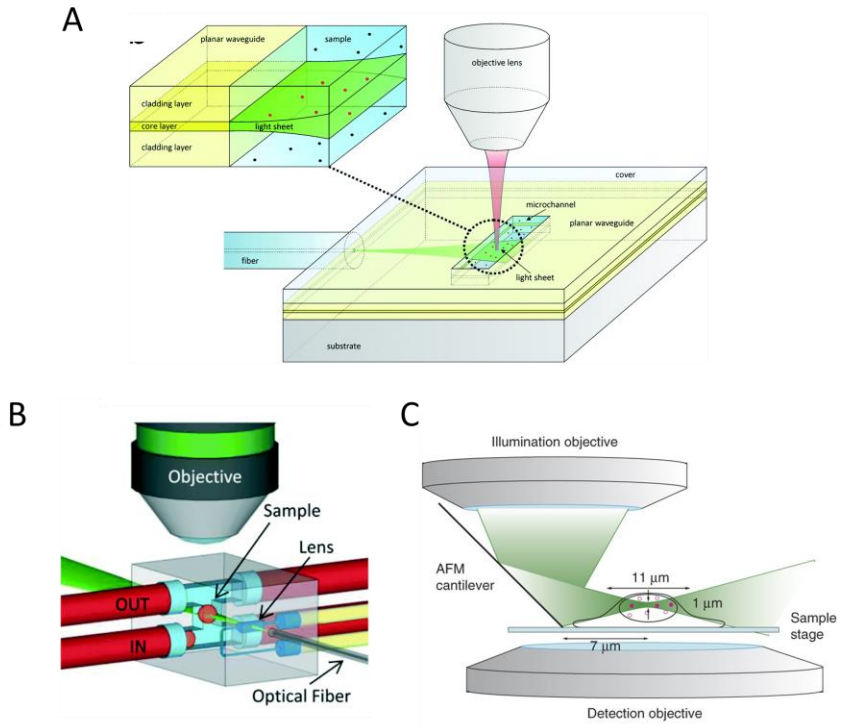

Figure 2-9. Techniques that integrate the light-sheet microscopy on conventional fluorescent microscopes. A) A microfluidic device developed by Deschout et al. [2]. *The laser beam paths through a planar waveguide and forms a light sheet in the channel. Fluorescent is acquired by an objective lens placed above or below the device. Reprinted with permission from the Royal Society of Chemistry. B) Optofluidic device fabricated by laser micromachining for spheroid imaging. An embedded cylindrical lens focuses the laser beam emanating from a fiber into a glass microfluidic channel* [3]. *Reprinted with permission from the Royal Society of Chemistry. C) A Reflected Light Sheet Microscope (RLSM). The laser beam that comes from an altered condenser is reflected horizontally on the sample by a mirror. The emitted fluorescent is collected by the detection objective of the host microscope* [4]. *Reprinted with permission from Springer Nature, Nature Methods.*

LSFM is intrinsically a 3D imaging technique in which volumetric data sets are acquired through different approaches. The following section covers the different approaches for acquiring optical sections of a sample with the goal of obtaining a three-dimensional representation of the sample.

2.2.2.4. Different Optical Sectioning Approaches in LSFM

Mechanical scanning of the sample. In conventional light-sheet microscopes such as SPIM, the light sheet and detection objective are fixed. Thus, the sample is mechanically moved through the static light sheet in order to obtain optical sections of the entire volume (Figure 2-10 (A)). Typically, this mechanical movement is performed using a stepper or a piezoelectric motor. Additionally, sample rotation is used to improve image quality in some implementations [75]. While mechanical scanning is a relatively straightforward and inexpensive approach, it generates sample vibrations that may disturb delicate biological specimens and cause image artifacts. Besides, such translations may not be fast enough to monitor quick dynamic processes over the entire volume. Most importantly, mechanical scanning requires individual mounting of samples which makes imaging of population of samples time consuming. In this regard, new approaches for acquiring 3D images have been established [11], [13].

Mechanical scanning of the system. In some cases, it is desirable to avoid moving the sample and maintain it utterly static during the study. This is conceivable in LSFM if the illumination and detection arms can be scanned synchronously while maintaining a constant relative distance. As executed in the objective-coupled planar illumination (OCPI) system, illumination optics is coupled to the detection arm, leading to fast scanning of the imaging system through the static sample (Figure 2-10 (B)). While OCPI is powerful at rapidly acquiring volumetric images, it needs movement of the bulky imaging system, making it a complex instrumentation system [81], [82].

Optical scanning. The techniques described above do not provide fast enough volumetric imaging speeds for applications such as imaging zebrafish heartbeats. It is possible to obtain extremely fast volumetric images without mechanical translation of either the sample or the imaging apparatus by incorporating an electrically tunable lens (ETL) into the LSFM's detection path. As illustrated in Figure 2-10 (C), ETL aligns the detection objective's focal plane with the scanned light sheet. The technique enables volumetric imaging at a rate of 30 volumes per second from a beating zebrafish heart [83]. Volumetric imaging speeds of 73 volume per second have also been achieved using decoupled illumination detection LSFM system (DID-LSFM). A cubic phase mask was inserted in the detection path in this system, extending the objective's depth of focus [37].

Fluidic-based scanning. Given that the abovementioned LSFM implementations often require samples to be mounted in gel-based media, they are not suitable for large-scale studies. Integration of microfluidics technology with light-sheet microscopy has been established in recent years, enabling high-throughput imaging of specimens. As shown in Figure 2-10 (D), in such approaches, samples are flowed in a microfluidic channel while optically sectioned images are acquired continuously as the sample passes through the static light sheet. In this circumstance, volumetric imaging speed is restricted solely by the camera speed, given that high sample velocities are often achievable by tuning the flow rate [84].

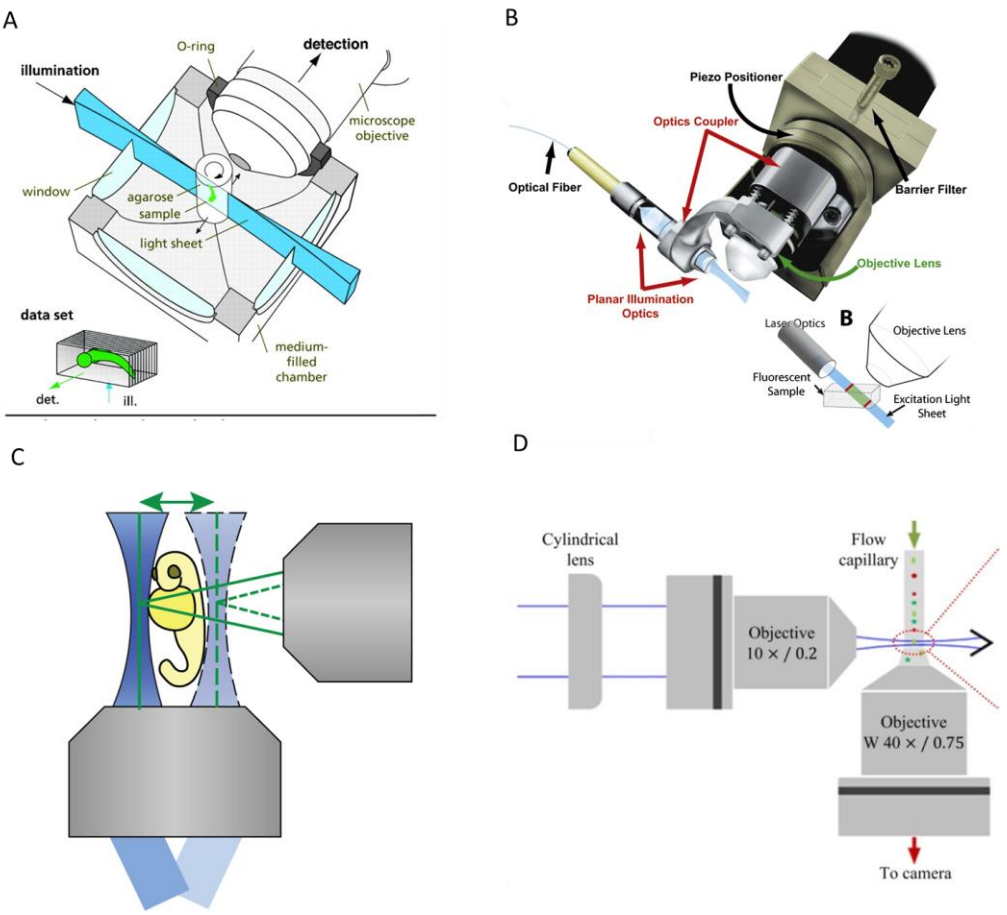

Figure 2-10. Different approaches of scanning for volumetric image acquisition. A) standard sample mounting approach in SPIM [11]. *Sample is fixed in agar-based media and translated via motorized mechanical components. Reprinted with permission from American Association for the Advancement of Science, Science. B) Mechanical scanning of the imaging system. Illumination arm is coupled to the detection objective lens. Z-axis scanning is performed by translating the detection lens with a piezoelectric positioner, which accordingly results in scanning of the light-sheet* [82]. *Reprinted with permission from Elsevier, Neuron. C) Optical scanning approach. Light-sheet is scanned with a galvo-mirror and detection lens is remotely focused accordingly using an electrical tunable lens* [83]. *Reprinted with permission from the Optical Society. D) Scanning the sample using flow. samples are flown through a capillary or channel across the fixed light-sheet* [84]. *Reprinted with permission from John Wiley & Sons.*

As described above, each optical sectioning method has its pros and cons. However, for the applications requiring large number of samples such as chemical screening assays, the fluidic-based scanning approach is preferable since worm samples can be continuously scanned while passing through the light sheet.

2.2.3. LSFM in *C. elegans* Research

This section presents and discusses the light-sheet microscopy implementations employed to investigate the model organism *C. elegans*.

Molecular actors required for *C. elegans* neurodevelopment have previously been identified [85]. However, phototoxicity and slow imaging speed of conventional imaging systems have hindered comprehensive investigation of the mechanisms involved in forming the neural circuit during embryonic neurulation. Wu *et al*. [17] proposed the inverted SPIM (iSPIM), a high-speed and minimally invasive imaging technique, which enabled the investigation of previously unreachable dynamic neurodevelopmental processes. As shown in Figure 2-11 (A), iSPIM comprises two optical arms equipped with excitation and detection objectives mounted on an inverted microscope body. This technological advancement enabled imaging of nematode embryos with the speed of a volume per two seconds for the entire period of embryogenesis, with no observable phototoxicity (Figure 2-11 (B)).

In another step forward by the same group, diSPIM was developed for obtaining isotropic spatial resolution. In iSPIM, the axial resolution was limited as the orthogonal orientation of objectives prohibited using objectives with the highest numerical apertures. diSPIM enabled isotropic resolution by alternatively operating the same two objectives in excitation and illumination modes.

Thus, diSPIM offered more comprehensive and detailed information on the neuron's wiring development in embryogenesis compared to iSPIM (Figure 2-11 (C)). However, this system's instrumentation is more sophisticated, requiring the addition of immense imaging hardware to the inverted microscope [77].

In another technological advancement, Gao *et al*. [86] developed high-resolution light-sheet microscopy by tiling the thin light-sheet in the propagation path, thus increasing the effective field of view without compromising the axial resolution. In this technique, a binary phase spatial light modulator is incorporated in the illumination optics to shift the excitation beam. A 500-nm thick light sheet was achieved in a large field of view, allowing for acquiring images with higher axial resolution than previous works. However, this method's imaging speed was lower than non-tiling methods as multiple images needed to be acquired in a single imaging plane [86].

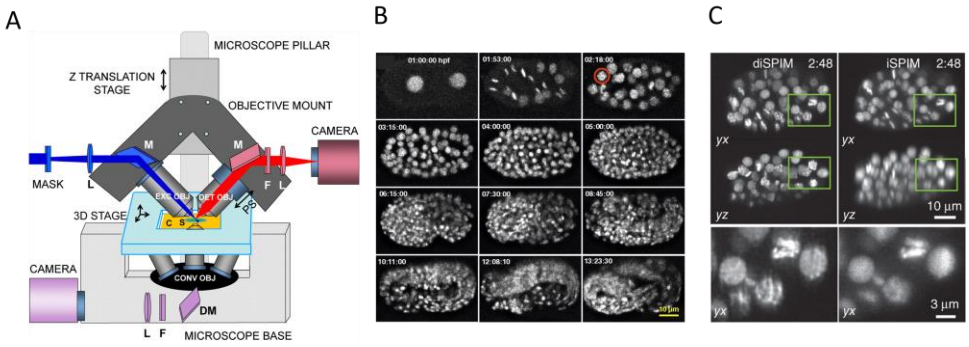

Figure 2-11. LSFM systems for C. elegans embryo imaging. A) Schematic of the Inverted SPIM (iSPIM) system [17]. *Illumination and detection water-immersion objectives are placed onto an inverted microscope's frame. The light sheet is generated using the optical illumination elements, including rectangular slit (MASK), lenses (L) and excitation objective (EXC OBJ). The emitted fluorescence is acquired (DET OBJ) by the mirrors (M), filters (F), lenses (L). B) High-speed imaging of the C. elegans embryo from the two-cell stage till hatching. Embryos containing GFP-histones were volumetrically imaged at a rate of 30 vol/min. Representative maximum-intensity projection images show different developmental stages. C) improved axial resolution in the embryo images using diSPIM compared to iSPIM* [77].

Riecker *et al*. [16] created a custom-built LSFM system for observing the protein dynamics in adult *C. elegans*. The device was tuned to image adult *C. elegans* at high speed for an extended period during ageing with little photobleaching. As illustrated in Figure 2-12 (A), the imaging platform is composed of two intricate illumination and detection arms, as well as an indexed-match stage that allows for movement and rotation of immobilized *C. elegans*. Figure 2-12 (B) depicts volumetric reconstructions of adult *C. elegans* expressing GFP in body wall muscles from different angles.

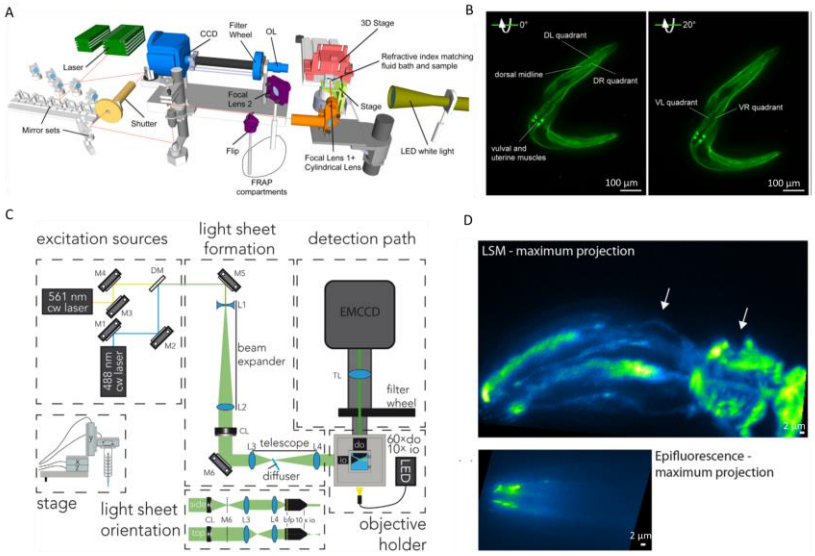

Figure 2-12. Dedicated LSFM systems for C. elegans neuronal study. A) schematic of the customized light-sheet microscope. The laser beam is directed by a flexible mirror set to the cylindrical lens, focusing the beam, and creating the light sheet. A 3D stage is employed to scan the fixed sample mechanically. B) Representative volumetric images of C. elegans expressing GFP in muscles. Body wall muscle quadrants and vulval muscles are characterized. Scale bars are 100µm. [16] *C) Schematic of the light-sheet microscope. D) 3D imaging of C. elegans expressing amphid expressing EGFP in amphid neurons. The top image is the maximum projection of 115 frames of the head region, and the bottom image is the maximum projection of 15 frames of the same area using epifluorescence* [15]. *Panels A and B, reprinted under permission of Creative Commons License. Panels C and D reprinted from* [15] *with permission from John Wiley & Sons.*

In another recent work, Krugten *et al*. [15] developed a variant of SPIM with a high-NA detection objective for live volumetric imaging of young adult *C. elegans*. As shown in Figure 2-12 (C), a cylindrical lens is inserted in the illumination path to generate a 2µm-thick light sheet, and data were gathered using a 0.6 NA water immersion objective. *C. elegans* is immobilized and embedded in an agar-based medium, coupled to a custom-designed sample positioner. As seen in Figure 2-12 (D), the platform improved image quality in volumetric neural imaging of *C. elegans* compared to epifluorescence microscopy due to the elimination of out-of-focus light.

Given the numerous advantages that microfluidics devices provide, particularly in the field of *C. elegans*, several approaches have been proposed to combine the LSFM with on-chip platforms. This integration enables high-speed and volumetric imaging of *C. elegans*, suited for large-scale experimental studies [34], [87].

Following the direction to develop light-sheet microscopy systems for applications demanding high-content and high-throughput imaging, McGorty *et al*. [14] created an open-top SPIM. As illustrated in Figure 2-13 (A) and (B), open-top SPIM is a stand-alone platform with all the optical equipment positioned beneath the sample stage. The unique feature of the open-top SPIM is a water prism that compensates for the aberrations induced by imaging through a 45-degree cover glass. A volumetric image of an adult *C. elegans*, tagged with fluorescent in PVD neurons (Figure. 2-13 (C)), is acquired while the sample stage moves through the steady 6-µm-thick light sheet. However, *C. elegans* imaging was performed by fixing the sample on a cover slip and scanning it using motorized mechanical components [14].

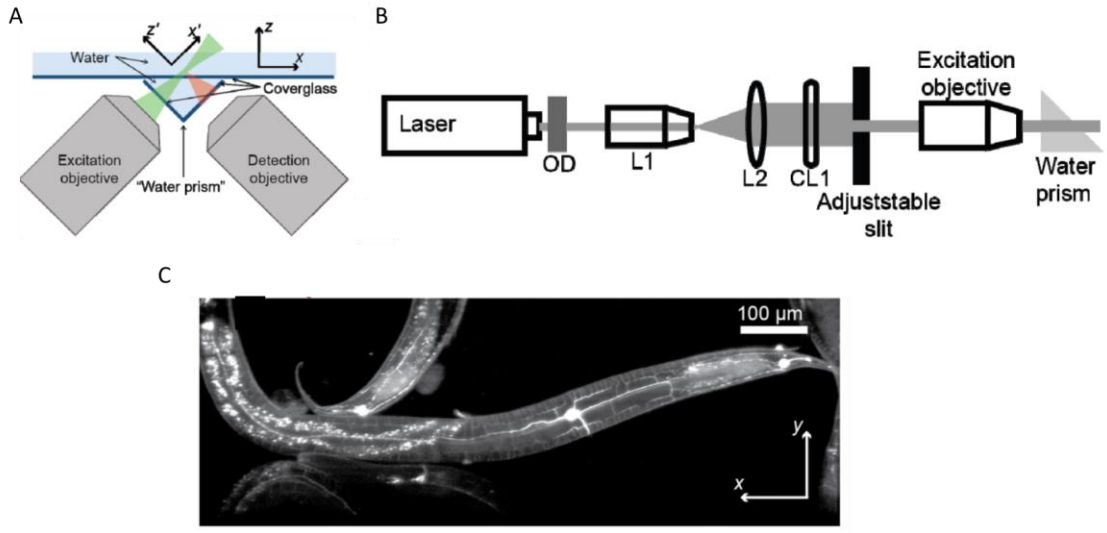

Figure 2-13. C. elegans imaging with open-top SPIM. A) Schematic of the open-top SPIM system with the two objective lenses below the sample stage. B) Excitation path of the system, consisting of the laser, optical density filter (OD), 10 × objective (L1), lens (L2), a cylindrical lens (CL1), slit aperture, and a 20 × 0.42NA lens. C) Z projection of the acquired cross-sectional image of C. elegans (kept in the middle of a glass slide and coverslip) PVD neurons, nuclei of intestinal cells [14]. *Reprinted with permission from the Optical Society.*

Another combination of light-sheet-based imaging techniques with a microfluidics platform for 3D interrogation is the work of Rasmi *et al* [23]. As shown in Figure 2-14 (A), the system consists of two orthogonal illumination and detection arms and a microfluidics device for flow-based translation of worms through the fixed 4.5µm-thick light sheet, eliminating the need for worm immobilization. The system was optimized to acquire consecutive frames with a 35 µm distance of a worm moving at a 6 µl/min flow rate, and the camera operating at 565 fps (Figure 2-14 (B)).

Martin *et al*. [88] also developed a sophisticated light-sheet-based imaging method, termed line excitation array detection (LEAD) fluorescence microscopy, for 3D high-speed flow cytometry of *C. elegans*. As shown in Figure 2-14 (C), LEAD is a complex optical system consisting of an illumination arm for generating a virtual 3-µm light-sheet, a detection arm with a photomultiplier

array (PMT), and a speed detection arm to measure the speed as worms pass through the light-sheet. The proposed system could acquire 800k frames per second of a worm moving at 1 m/s speed through a microfluidic channel. The system's high-speed functionality was demonstrated by 3D imaging of populations of polyglutamine aggregation model *C. elegans* in ~1ms per animal speed (Figure 2-14 (D)).

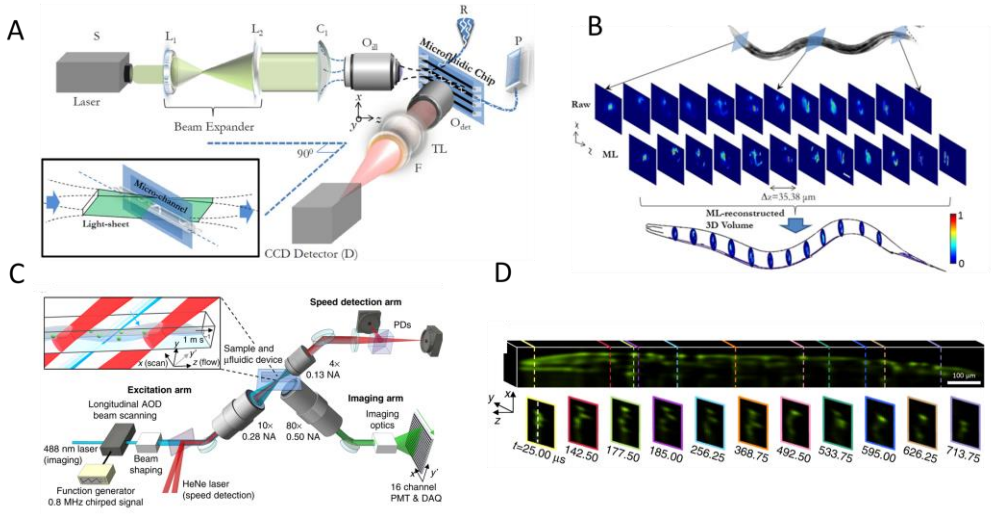

Figure 2-14. Light-sheet microscopy systems compatible with microfluidic devices for C. elegans imaging. A) Schematic of the microfluidic-based light-sheet imaging system. Laser beam expands via the relay lenses (L), focuses by cylindrical (C) and objective lens (O), then exciting the moving C. elegans inside the microchannel. The inset is a close-up image of the light sheet crossing the microfluidic chip. [23] *B) C. elegans imaging. The cross-sectional raw and deconvolved images are shown in two rows.* [23] *C) schematic of the LEAD system for whole animal flow cytometry of C. elegans. At 0.8 MHz, a longitudinal TeO2 AOD powered by chirped frequency scans the laser excitation beam over an angled plane on the sample. The excited plane is imaged using 14 channels of a 16-channel photomultiplier tube (PMT) array, with each scan cycle recording a complete frame. A microfluidic device provides populations of hundreds of C. elegans at one m/s rate (inset). Two light sheets created by a HeNe laser, and two photodiodes (PDs) are used to measure the speed of nematode within the imaging area.* [88] *D) volumetric image of the protein aggregation model of C. elegans* [88]. *(Panels A and B reprinted with permission from AIP publishing. Panels C and D reprinted under the terms of the Creative Commons Attribution Non-Commercial License).*

More recently, compact LSFM platforms have been proposed, enabling light-sheet imaging of *C. elegans* using conventional wide-field microscopes. For example, Hsieh *et al*. [20] proposed a compact LSFM platform using the volume holographic optical element (VHLSFM) as a replacement for the bulky illumination optics of LSFM (Figure 2-15 (A)). The suggested technique generated light sheets of the same quality as conventional LSFM systems. VHLSFM's performance was validated by imaging the oocytes inside the immobilized *C. elegans* and comparing them to the same cross-sectional images acquired with the conventional widefield. The optical sectioning feature of the proposed system enabled resolving finer features inside the nematode compared to WF, as seen in Figure 2-15 (B).

In another compact and cost-effective platform, Zhao *et al*. [19] developed a light-sheet add-on plugin to the conventional inverted microscope. As seen in Figure 2-13 (C), a fibre-coupled laser is focused with a cylindrical lens and coincides with the focal plane of the inverted microscope's objective. This setup was applied for rapid functional volumetric imaging of behaving *C. elegans* larvae, expressing GCaMP in its body wall muscles (Figure 2-15 (D)). Muscle activity changes were further quantified by analyzing the variations of GcaMP6 intensity. This add-on plugin, combined with the sub-voxel-resolving algorithm, shows a 10-fold resolution enhancement compared with the host inverted microscope. However, mechanical translational components are required in the abovementioned platforms to scan the sample to acquire volumetric information. This sample mounting and scanning approach hinder their application for fast and large-scale studies.

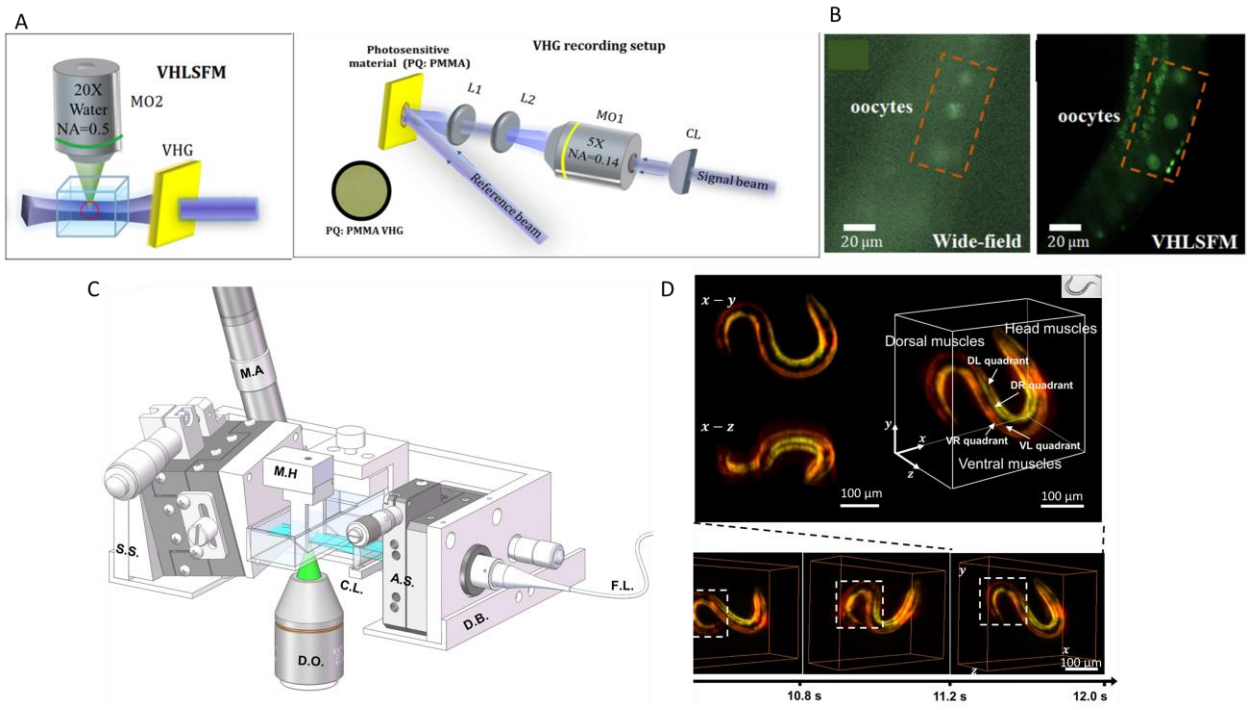

Figure 2-15. Compact LSFM systems. A) Schematic of the VHLSFM. Setup for VHG consists of the objective lens (MO1), relay lens (L), and cylindrical lens (CL). A photo of the fabricated VHG is shown in the inset. [20] *B) Images of oocytes inside C. elegans acquired with VHLSFM (right) and wide-field microscope (left). Panel A and B Reprinted with permission from the Optical Society. C) The schematic of the add-on device which consists of multiple compact mechanical components and optical elements* [19]. *D) Volumetric imaging of muscular activities of behaving C. elegans larva. Panel C and D reprinted with permission from John Wiley and Sons.*

In an essence, the reviewed LSFM platforms for *C. elegans* imaging require either dedicated/costly light-sheet systems or sample immobilization in gel-based media which is not suitable for large-scale continuous imaging studies.

Chapter 3
Device Design and Experimental Methodology

3.1. Conceptual Design: Optofluidic LSFM Platform

The design principle of the proposed optofluidic LSFM platform in this thesis is shown in Figure 3-1. It was designed with the consideration of two criteria. The first criterion was to enhance the throughput of conventional LSFM by combining this platform with PDMS-based microfluidic devices. This combination was pursued in an effort to facilitate rapid LSFM imaging of groups of *C. elegans* via continuous/serial passing of the worms in the PDMS microfluidic device. The second criterion was the cost-effectiveness and compactness of the LSFM platform. The primary consideration in achieving this goal was to design a platform compatible with the commonplace and widely-used conventional wide-field fluorescent microscope, thus increasing its accessibility in regular biology labs. At the same time, the use of microfluidics enabled the integration of illumination optics of LSFM within the same device used for worm translation via an integrated micro-lens. This miniaturization was a practical step toward making the LSFM setup inexpensive and compact.

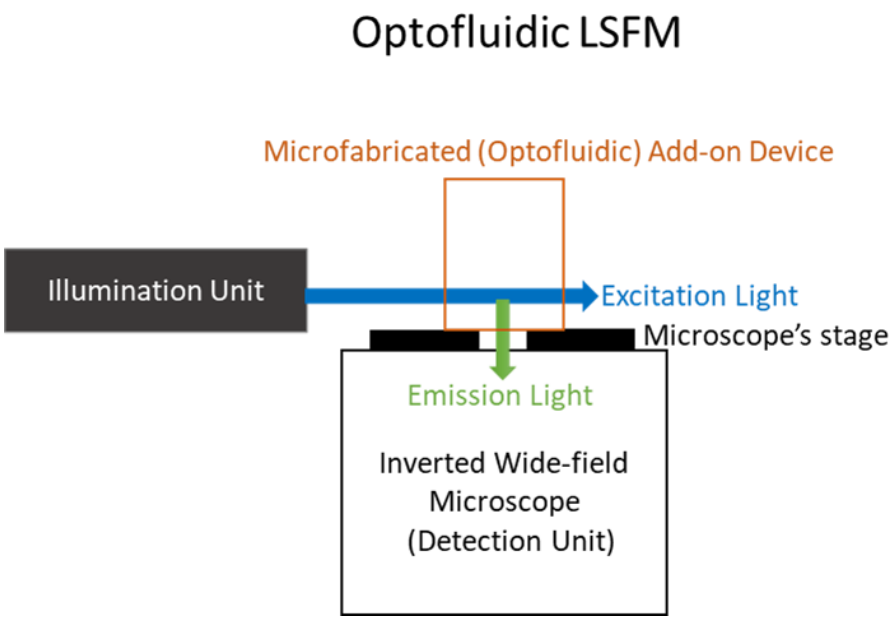

Figure 3-1. *Conceptual design of the optofluidic LSFM platform. LSFM is integrated with the inverted wide-field microscope by the development of a microfabricated add-on optofluidic device. This device could be placed on the stage of an inverted microscope. An external side illumination unit was used as the source of the excitation beam, and the emission beam was collected via the host inverted microscope.*

3.2. Overview of the Developed Optofluidic LSFM Platform

The experimental setup of the developed low-cost optofluidic LSFM platform is shown in Figure 3-2 (A). Optofluidic add-on devices with various designs were placed on the imaging platform of a conventional WF microscope (DM IL LED microscope; Leica, Wetzlar, Germany) for light-sheet imaging. Two optofluidic devices were designed in this thesis, a primary device for immobilization-free and rapid light-sheet imaging of *C. elegans* (thesis objective 1), and a modified device for continuous and quantitative fluorescent imaging of groups of *C. elegans* (thesis objective 2). These devices enabled volumetric imaging of *C. elegans* with the standard microscope and without sample immobilization and/or mechanical scanning. The input beam to

the add-on devices was provided by a free-space and low-cost laser diode source passing through an iris (λ: 488nm, 3mW, OXlasers A-B60F, China; Figure 3-1 (A)).

The schematic working principle of the primary optofluidic device is shown in Figure 3-2 (B). The input laser beam is produced by a free-space laser. After passing through an iris, the laser beam enters the optofluidic device through a hollow (air) channel before hitting the cylindrical PDMS lens. The integrated PDMS lens of the add-on device created the illumination light sheet, replacing the native epi-illumination of the inverted fluorescent microscope. Selective excitation by the sharp planar light sheet offered improvement in the axial resolution in comparison to the epi-illumination mode of the host microscope. The fluorescent light emitted by the sample was collected using the inverted widefield microscope's native air objective lens (N PLAN 20X/0.35NA). Optically sectioned images were recorded with a 5 megapixels CMOS camera with a pitch size of 0.31 µm (GS3-U3-51S5M-C, Point Grey, Canada) and through the native objective lens of the WF microscope.

A

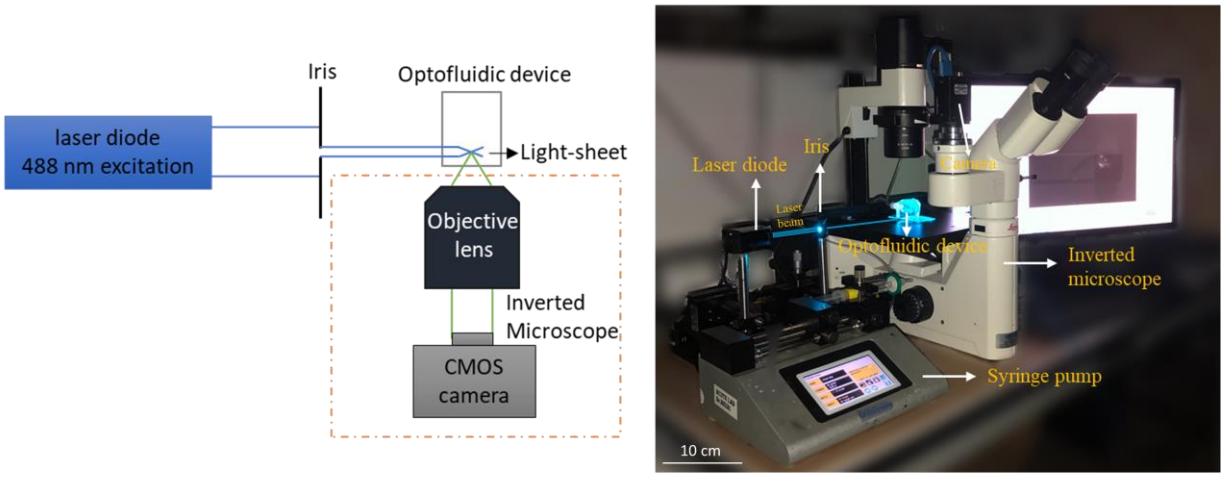

B

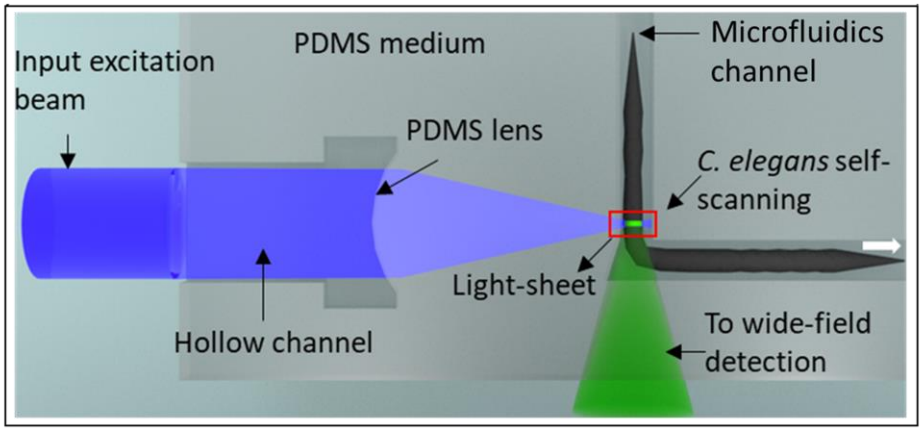

Figure 3-2. Optofluidic LSFM platform: Experimental setup and working principle. A) Schematic illustration and the experimental setup of the optofluidic LSFM platform. The experimetal setup included a free-space and low-cost laser source and an iris that were used to generate the input excitation beam of the optofluidic device. C. elegans were loaded into the device using a syringe pump. The optofluidic add-on device is placed on top of the inverted widefield fluorescent microscope. The generated light-sheet replaced the epi-illumination of the host microscope. The emitted fluorescent was collected by the native objective lens of the microscope and recorded using a CMOS camera. B) Working principle of the primary optofluidic device. Collimated input beam was focused using the integrated PDMS lens and light-sheet was generated inside the microfluidics channel. The cross-section of the worm was contineously imaged as worm traveled through the light-sheet. Optically sectioned images were acquired through the smooth PDMS wall at the bottom of the optofluidic add-on device.

To enable flow-based imaging of samples, a syringe pump (legato 180, KD scientific, USA) was used to pass the *C. elegans* through the stationary light-sheet at a reasonably constant flow rate. For detailed visualization of the neuronal system in the primary device, the flow velocity was chosen as ~90 µm/sec in which a whole worm was scanned in ~10 seconds with the camera operating at 150 fps. For fast imaging of *C. elegans* with primary device, considering that our LSFM system images the cross-section of the worm, the active area of the camera was reduced to only cover the required field of view. This in return enabled using higher frame rates up to 300 fps, corresponding to 100 µm × 100 µm imaging area/region of interest (ROI) (Figure 3-3 (C)). In this configuration, the flow velocity was chosen as ~450 $\mu m.sec^{-1}$. In both imaging speed cases, at least one frame was acquired per a sample movement equal to the light sheet beam waist to ensure Nyquist sampling. For the continuous imaging of groups of *C. elegans* using the modified device the flow rate was adjusted correspondingly to enable imaging worms at certain throughputs (see chapter 4, section 2).

3.3. Optofluidic Add-on Devices: Design and Fabrication

This section provides procedure of the design and fabrication of the optofluidic devices. An add-on device on top of the inverted microscope stage is shown in Figure 3-3 (A). These devices were fabricated using standard soft- and photo-lithography techniques.

3.3.1. Mechanical Design

The top- and side-view microscopic images of the primary optofluidic device are shown in Figure 3-3 (B) and (C), respectively. The device consisted of two parts: the microfluidic channel for *C. elegans* transport, and the integrated PDMS lens for light-sheet generation. For *C. elegans* transportation, the microfluidic channel was design in an L-shape form to minimize the aberrations caused by the presence of the worm in the optical path of the detection objective lens. Microchannel cross-sectional dimensions were approximately 50 µm × 65 µm to enable smooth passing of a single ~50µm-diameter adult worm through the imaging plane with minimal lateral movement. The bottom section of the L-shape channel was designed in an inverse taper shape (~20°) to accommodate the 0.35 numerical aperture of the objective lens (Figure 3-3 (B)). In such an arrangement, the emitted fluorescent light from the sample passed through a small section of the channel (i.e., the PDMS device wall thickness) and air before reaching the objective lens. To minimize the degradation of image quality, the PDMS device was cut carefully to obtain a ~400µm-thick PDMS wall. To remove the surface roughness of the cut PDMS-air interface, an additional step (see section 3.3.3) was taken to make the rough facet as optically flat as possible.
To enable continuous and smooth flow of *C. elegans* inside the microfluidics channel, the L-shape bend of the channel was re-designed in the modified device to facilitate smoother passage of worms through the light-sheet (provided in detail in chapter 4, section 2).

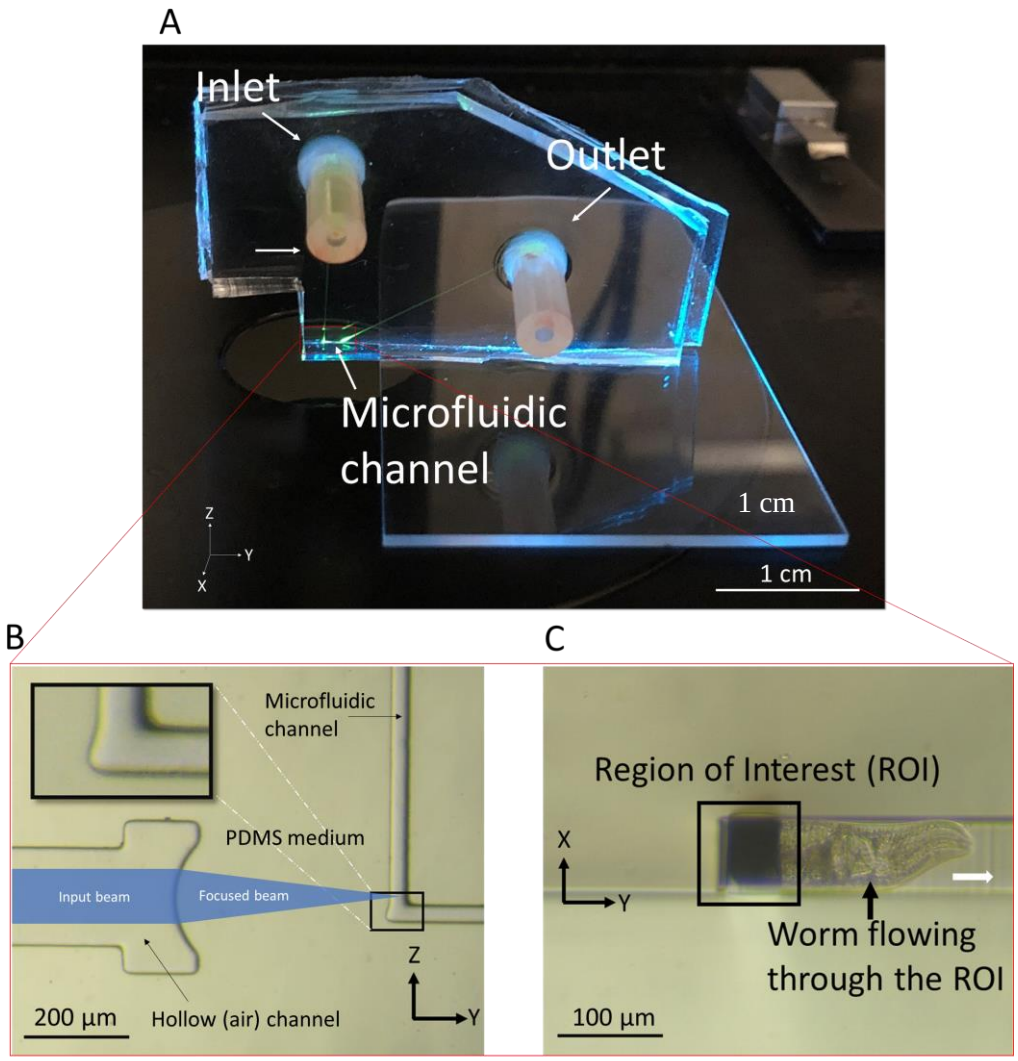

Figure 3-3. The developed primary optofluidic add-on LSFM device. A) the PDMS optofluidic device on top of the inverted fluorescent microscope as a light-sheet add-on (scale bar: 1 cm). Top-view (B) (scale bar 200 µm) and side-view (C) (scale bar 100 µm) bright-field images of the primary optofluidic device taken by the inverted microscope. The laser beam path inside the device is schematically shown in blue (B). The magnified inset of the image B shows the inverse tapered area of the channel designed to accommodate the numerical aperture of the detection lens. A worm flowing through the region of interest is shown in (C).

3.3.2. Optical Design

The illumination part of the optofluidic devices for light-sheet generation was designed and optimized using Zemax OpticStudio® (version 20.1.2). To do so, an air micro-cavity within the PDMS chip was simulated, Figure 3-4. Given the refractive index mismatch of air and PDMS (1 vs ~1.42), the cavity's distal end was shaped in form of a convex cylindrical lens to enable the on-chip generation of the light sheet across the cross section of the microfluidic channel. The intrinsic manufacturing precision of monolithic photo- and soft-lithography enabled proper alignment of the light-sheet with respect to the microfluidics channel during the fabrication stage. Given the ~50-µm diameter of *C. elegans*, at least 50 µm light-sheet length (defined as twice the Rayleigh length) was desired to uniformly illuminate the worm along its cross-section. To achieve this light-sheet length with the 488-nm excitation laser, a light-sheet thickness of ~2.3 µm (i.e., full-width at half-maximum, FWHM, at the focus) was required based on the gaussian beam optics. Zemax simulations determined that a 200-µm radius of curvature of the air-PDMS interface of micro-cavity can satisfy the required light-sheet specifications. Furthermore, the Zemax ray optics module and the native merit function were used to optimize the distance between the curved interface and the microfluidics channel to locate the beam focus at the center of the microfluidic channel, Figure 3-4 (A). Zemax physical optics tool determined an optimized uniform light-sheet illumination across the microchannel with beam thickness of 2.3 µm at the channel center from an input gaussian beam with $1/e^2$ diameter of 90 µm, as shown in Figure 3-4 (B). Simulations also demonstrated that light sheet thickness can be changed between 2-3 µm by changing the input beam diameter in the range of ~60 µm to ~120 µm which can be beneficial for tuning the resolution based on the different stages of *C. elegans* under study.

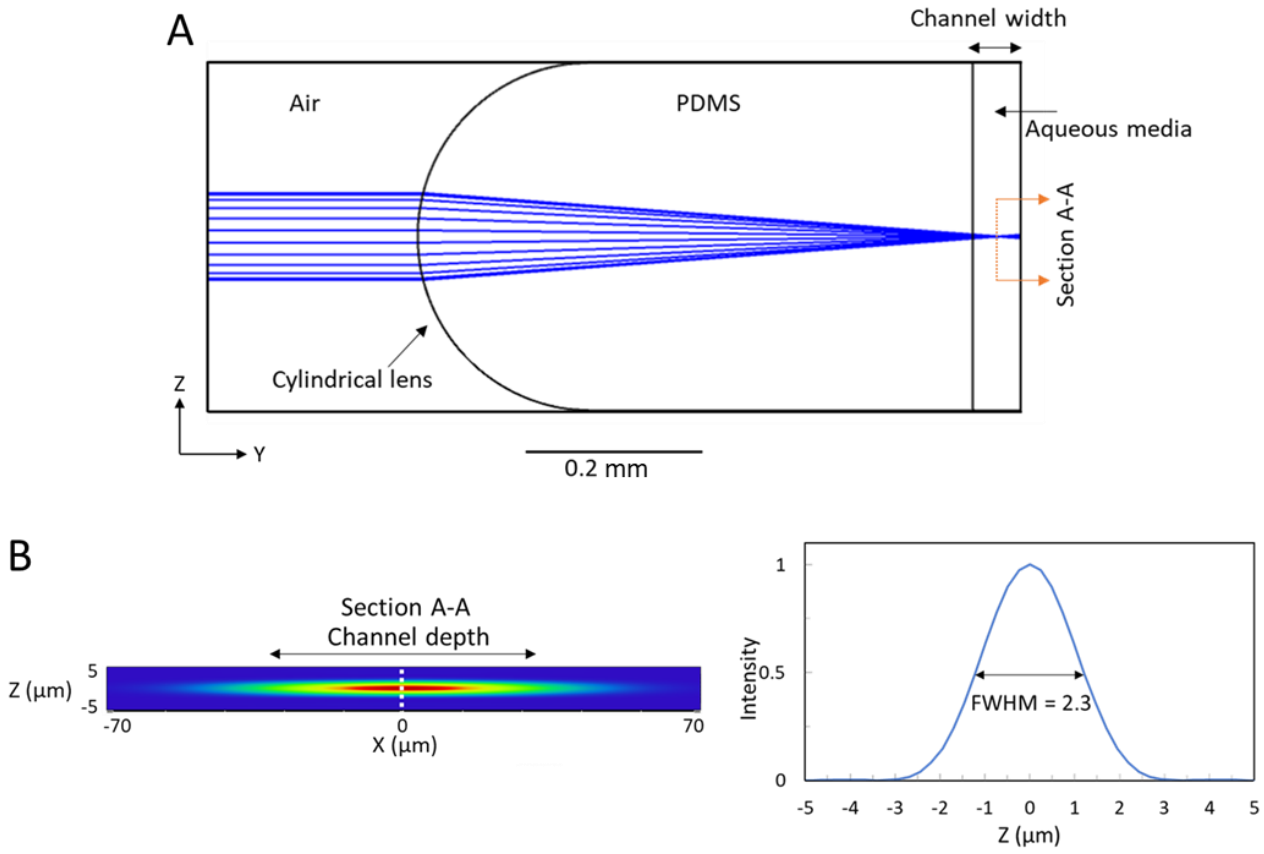

Figure 3-4. Optical simulation using Zemax OpticStudio®. A) lateral view of the ray tracing simulation used for determining the geometrical position, radii of curvature, and aperture size. The coupled beam is focused owing to the refractive index mismatch of air and PDMS, and consequently the light-sheet is generated within the width of the channel. B) Cross-sectional light intensity profile of the light-sheet at the center of the channel at the focus (section A-A in panel A), simulated using physical optics propagation tool. The FWHM measurement for the light-sheet thickness using intensity distribution along z axis at x=0 is also shown in right image.

3.3.3. Microfabrication

The fabrication procedure of the optofluidic devices is depicted schematically in Figure 3-5.

In this project, only manufacturing of photomasks was outsourced. Briefly, microfluidic chip patterns were designed in house via CAD software. CAD designs were then sent to CAD/Art Services (Bandon, USA), where a laser photoplotter (LP9008M-UR, Orbotech, Israel) was utilized to imprint the CAD designs onto the polystyrene masks (Fujifilm, Tokyo, Japan).

Silicon (Si) wafers with a diameter of 4 inch and a thickness of about 0.5 mm were obtained from Wafer World Incorporation (West Palm Beach, USA). MicroChem Corporation (Newton, USA) supplied the negative photoresist SU-8 2075 and the SU-8 developer. PDMS was obtained from Dow Corning Corporation (Midland, USA).

The Si wafer was washed consecutively with acetone (30 seconds), isopropyl alcohol (IPA; 30 seconds), and deionized water (two minutes) before a final heating stage at 110℃ for evaporation of the molecular water layer. Then, Si wafer surface was treated for 30 seconds by oxygen plasma exposure (PDC-001-HP Harrick Plasma, USA) for enhancement of the photoresist adhesion. To fabricate the mold, four milliliters of SU-8 2075 photoresist was poured at the center of the Si wafer and spun using a spinner machine (Brewer Science® Cee® 200X, USA) at 3500 rpm for 30 s to obtain a 65 μm-thick layer. After soft-baking the wafer at 65˚C for 3 minutes and 95˚C for 6 minutes, the wafer was exposed through the abovementioned photomask to 365 nm light for 20 s (UV-KUB 2, KLOE, France) at a power density of 10 mW/cm^2. Then, the wafer was post-baked for 20 minutes at 65˚C and for 4 minutes at 95˚C. To remove the uncured SU8, the mold was rinsed for 2 minutes in SU-8 developer. Finally, the hard-bake process for 25 minutes at 150˚C was performed to achieve the final master silicon mold.

PDMS elastomer and curing agent (Dow Corning, USA) were mixed at 10:1 ratio, degasified, and poured on the Si-SU8 master mold above to make the negative replica (Figure 3-5 (1)). After curing for 2 hours at 80°C, the cured PDMS layer was bonded to another flat PDMS layer using oxygen plasma (PDC-001-HP Harrick Plasma, USA) at 870 mTorr pressure and 30W for 30s (Figure 3-5 (2)). The bonded devices were heated for 15 minutes at 70 C to enhance bonding.

To make the devices compatible with light-sheet imaging on an inverted microscope, they were cut close to the light-sheet plane (Figure 3-5 (3)), leaving a ~400 μm thick PDMS wall between the light-sheet plane and the edge of the device. Cutting the devices caused roughness at the air-PDMS interface (Figure 3-5 (4)). To make the roughed facet optically flat, the devices were contacted from the rough side on a glass slide that was coated with a very thin layer of uncured PDMS (Figure 3-5 (5-6)). After being cured for 30 min at 70°C, devices were separated from the glass to achieve a roughness-free surface. To facilitate the vertical positioning of the add-on devices on the inverted microscope stage, they were bonded to glass slides at a location away from the optical path (see Figure 3-3 (A)).

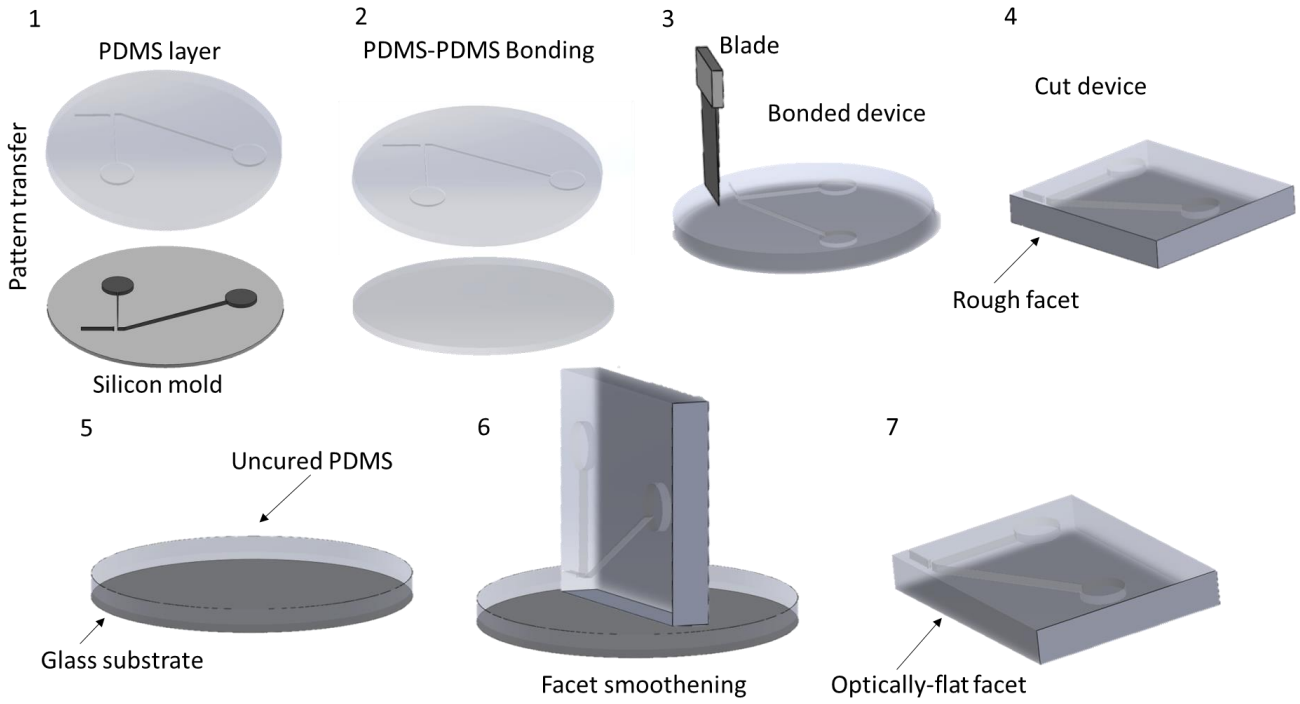

Figure 3-5. Fabrication procedure of the optofluidic devices. (1) Design pattern on the silicon mold was transferred to the PDMS layer by curing the PDMS on the mold and then peeling it off. (2) The PDMS layer with the pattern was bonded to another flat thin layer of PDMS via oxygen plasma surface treatment. This step was to seal the microfluidics channels. (3) The bonded device was cut very close to the light-sheet plane using blade to collect the emission fluorescent through the side facet of the chip. Rough facet in the PDMS-air interface was created as a result of cutting, degrading the final image quality (4). Additional step was taken to make the facet optically flat. PDMS was spin-coated on the substrate to create a thin layer (500 µm) of uncured PDMS on the glass slide (5). Then, the device was placed on top of the substrate to contact the rough facet with the uncured PDMS layer (6). The device was peeled off once cured, leaving a device with an optically flat facet (7).

3.4. Optical Characterization

A beam profiler camera (WinCamD-UHR–½"CMOS Beam Profiler; DataRay; USA) was used to characterize the output beam of the laser. Optical characterization of the optofluidic devices was carried out using the Rhodamine fluorescent dye (Rhodamine 110 chloride, Sigmaaldrich). To do so, Rhodamine solution was inserted into the microfluidics channel. In order to measure the thickness of the light-sheet, the add-on devices were placed on the inverted microscope in top-view orientation (Figure 3-3 (B)) while imaging the Rhodamine solution fluorescently.

The imaging resolution of the LSFM platform were determined from images of 500-nm fluorescent beads (FP-0556-2, fluorescent Nile red particles, Spherotech). The beads were diluted in aqueous solution and flowed through the stationary light-sheet across the whole field of view by a syringe pump at a flow rate of 0.01 µL/min. The experimental lateral and axial resolutions of the system were measured by analyzing the acquired consecutive frames of the passing beads.

3.5. Sample Preparation and Experimental Procedures

3.5.1. *C. elegans* Preparation

C. elegans strains that were used in this thesis were NW1229 (a transgenic strain expressing green fluorescent protein (GFP) pan-neuronally; F25B3.3::GFP + dpy-20(+)) and BZ555 (a transgenic strain expressing GFP in dopaminergic neurons; dat-1p::GFP). These strains were acquired from the *Caenorhabditis* Genetics Center (USA, Saint Paul). Worms were grown on standard nematode growth medium (NGM) agar plates and kept at room temperature (approximately 22 °C) in a biological safety cabinet. To avoid any possibility of contamination, the cabinet was pre-sterilized

with UV light and cleaned with a 70% ethanol in water solution. Sigma-Aldrich (USA, St. Louis) supplied all the chemicals. This section discusses the details of *C. elegans* maintenance procedures.

3.5.1.1. Preparation of Nematode-growth Media and Bacterial Culture

The worm plates were prepared based on the standard protocols outlined in the Wormbook [89]. Briefly, the NGM-plates were seeded at room temperature with a "lawn" of *Escherichia coli* (*E. coli*) strain OP50. The OP50 supply was generated by inoculating L-Broth media with a single colony of *E. coli* OP50 from the streak plate and cultured overnight at 37℃ in a shaker-incubator. The L-Broth medium was made by autoclaving a mixture of 10 grams Bacto-tryptone, 5 grams Bacto-yeast, and 5 grams sodium chloride in 1-liter distilled water. Following centrifugation of the inoculated enriched media to concentrate the bacterial culture, the plates were seeded with 100 µl of the *E. coli OP50* source and dried overnight. All studies were performed on newly prepared plates containing the bacterial culture.

3.5.1.2. Chunking

To sustain the worms' viability, they were transferred to new NGM plates by a technique called 'Chunking,' which was necessary because of the bacterial lawn consumption and the creation of worm aggregates. A sterilized scalpel was utilized to cut and transfer a 0.5 cm^2 piece of agar containing elderly or starving worms from an old NGM plate to a freshly made bacterial-seeded NGM plate. The new plate was then returned to the biosafety cabinet to grow for worm synchronization. When mold or fungal contamination occurred on a plate, the chunking process was repeated twice within five minutes. A small piece of agar from the contaminated plate was cut and placed at the side of the fresh plate, away from the bacterial lawn. Worms were allowed to crawl towards the new bacterial lawn within five minutes. A new agar cut was then made from the

new plate and placed on another bacterial-seeded agar plate to ensure that the patch remained viable and free of contamination.

3.5.1.3. Synchronization and Chemical Exposure

All experiments were performed with age-synchronized, well-fed gravid hermaphrodite adult worms (~ 60 hours). The synchronized worms were obtained using the conventional alkaline hypochlorite treatment method [90]. The synchronization procedure is depicted in Figure 3.6 (A). Briefly, gravid hermaphrodite adult worms were washed off the NGM plate using M9 buffer (3 g KH2PO4, 6 g Na2HPO4, 5 g NaCl, and 1 ml 1 M MgSO4 in 1 L distilled water) in a 15 ml Eppendorf tube and treated with a solution of 3.875 ml double-distilled water, 125 µL 1 M NaOH, and 1 ml commercial bleach for 10 minutes. This treatment dissolves the worm cuticle but does not affect the worm eggs. After the treatment, the eggs were collected by centrifuging the sample at 1500 rpm for two minutes. The eggs were hatched to L1 larvae overnight in a tube with M9 buffer rotating using RotoFlex™ tube rotator (RK-04397-40, Cole-Parmer, Canada). For control experiments, the hatched larvae were seeded on top of freshly prepared NGM plates and collected on the day of the experiment. To obtain chemically exposed worms, the hatched larvae were treated with 50 mM of 6-OHDA toxicant in a dark room for 1 hour [91]. Figure 3-6 (B) shows the approximate culture times at room temperature to obtain a certain worm age for use in our tests.

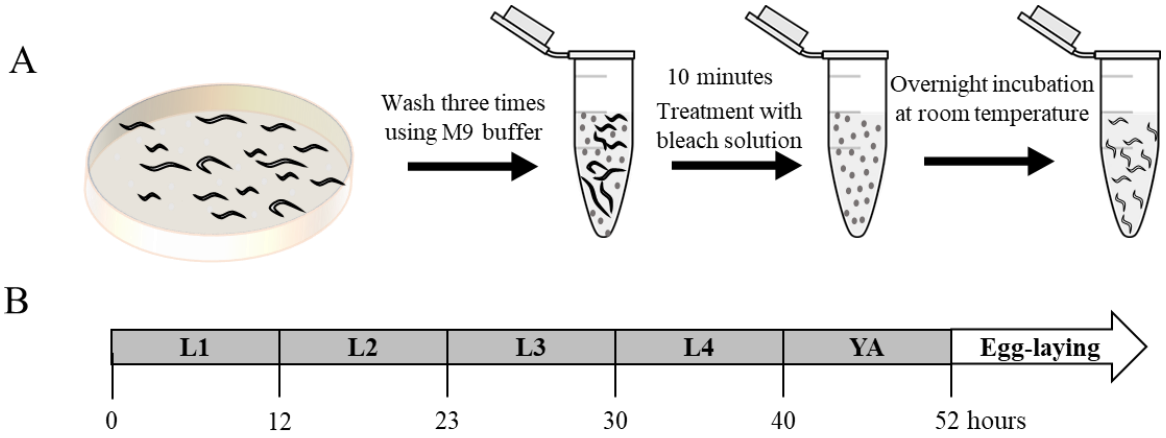

Figure 3-6. Synchronization process using 5 ml of bleach solution (3.875 mL of double-distilled water, 125 µL of NaOH, and 1 mL of commercial bleach). (B) Culture time needed to obtain specific C. elegans larvae stages.

3.5.2. Worm Loading into LSFM Devices

Depending on the nature of the experiment, worms were either picked individually or washed off the plates prior to loading into the devices. Worm picking was carried out with the aid of a platinum wire obtained from the Wormstaff (USA). In this process, firstly, the wire was gently scrubbed on the border of the bacterial lawn that was on a pre-seeded NGM plate to make the tip sticky for worm picking. To load the worm into a LSFM device, the wire with the picked worm was dipped into the device inlet.

To wash the worms off the plates, 2 milliliters of M9 buffer was pipetted over the worm plate to collect the worms and transfer them to a 15 milliliters Eppendorf tube. The tube was then kept upright for 15 minutes for sedimentation of all adult worms while the smaller worms floated in the supernatant. Subsequently, 1.5 milliliters of the supernatant were discarded, leaving around 0.5 milliliters of M9 with adult worms. The worm concentration was determined by counting the worms in a 5 µl droplet of M9 buffer taken manually using a pipette. This procedure was repeated

three times, and the average was reported as the worm concentration. Then, worms were loaded into the device at the desired concentration of the experiments using a syringe pump. The loaded worms were then imaged at various flow rates (details in chapter 4).

3.6. Data Processing

3.6.1. Image Analysis

In this thesis, all images of samples including rhodamine, fluorescent beads, and *C. elegans* were acquired in 8-bit monochrome format. A microscope calibration slide was used to measure the eventual pixel size of the imaging system. To do so, the number of pixels across the 1 mm marking of the slide was measured, and the pitch/pixel size of the image was determined using Fiji software for the objective lenses used in the studies [92]. Once the camera frames were captured in experiments, light-sheet images were imported to Fiji as an image stack. The volume viewer plugin of Fiji was used to reconstruct the 3D volumetric image of the *C. elegans* from the acquired 2D cross-sectional images. Volume viewer plugin produced the volumetric representation considering the Z-Aspect ratio of the stack of images. Z-Aspect ratio was calculated based on measurement of average worm speed via image processing and under the assumption of uniform passage of worm through the light sheet. Once the corresponding average spatial distance between consecutive frames were determined, the value was imported to the software as the Z voxel size over the lateral pitch size.

For the flow characterization experiments, ImageJ software was used to measure the worm passing time through the light-sheet. Firstly, the camera was configured to provide the relative acquisition time of each frame (aka. timestamp) in the header information. Then, acquired image stacks with

embedded timestamp were imported to ImageJ. Correspondingly, the passing time of each worm was measured by subtracting the time that the worm entered and exited the light-sheet plane inside the microchannel.

For the fluorescent intensity analysis, MATLAB software was used to quantify the average fluorescent intensity of each video frame, and subtract it from the background intensity. The background intensity was measured using the first frame of each video in which the worm was not in the region of interest. All data points were transferred to Microsoft Excel (Microsoft Corp., WA, USA) for normalization of the data with respect to the control experiments. The same code was used to obtain the intensity histogram of entire frames of a video.

3.6.2. Statistical Analysis

Minitab Software was used to conduct all statistical analyses in this study. Since one-way ANOVA assumes similar variance among groups, Levene's test was first used to determine the homogeneity of variances. If the outcome of the test was significant ($p<0.05$), Welch's ANOVA was used instead of one-way ANOVA. If the ANOVA indicated a significant difference in mean values, a Tukey HSD post-hoc pairwise comparison was performed to determine the pairs of means that differ significantly. If the variance homogeneity assumption was satisfied, a Games-Howell post hoc test was used rather than Tukey HSD.

Chapter 4
Results and Discussion

4.1. LSFM Imaging of *C. elegans* with the Primary Add-On Optofluidic Device

This section provides the imaging results obtained via the use of the primary optofluidic add-on device with the inverted fluorescent microscope for immobilization-free, rapid, and high-resolution imaging of *C. elegans* (thesis objective 1). To do so, the device was first optically characterized; then, the feasibility of light-sheet imaging of neuronal expressions of *C. elegans* was examined.

4.1.1. Optical Characterization

Once the add-on device was fabricated, optical characterization tests were carried out to measure the light-sheet thickness and the experimental resolution of the LSFM imaging system. To observe the light sheet inside the microfluidic channel, the L-shaped microchannel was filled with a fluorescent rhodamine solution and imaged in a top-view orientation while illuminated by an input beam diameter ($1/e^2$ width) of ~90 µm. The bright-field and fluorescent images of the device with rhodamine solution are depicted in Figure 4-1 (A) and (B), respectively. From the intensity measurements in Figure 4-1 (C), a full width half maximum (FWHM) of 2.4 µm was measured as

the light-sheet thickness (at the focus) at the middle of the channel, also depicted by a dashed-line in Figure 4-1 (B).

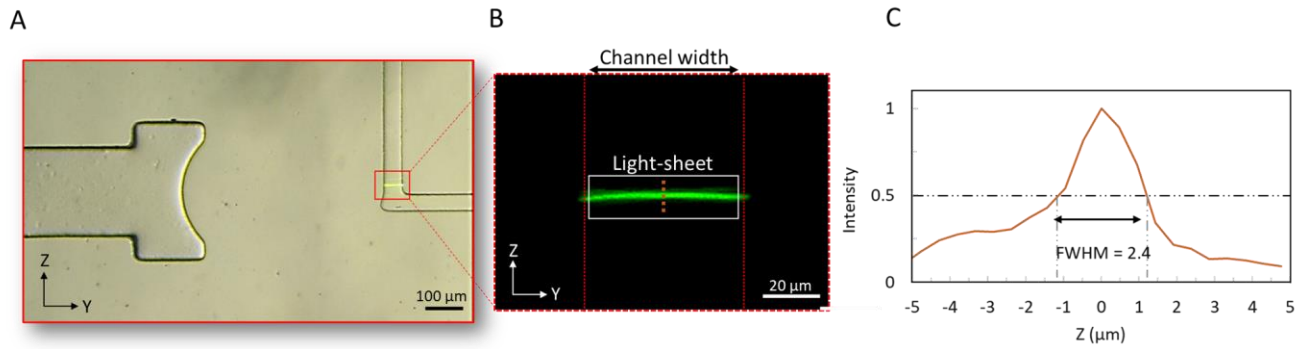

Figure 4-1. Optical characterization of the add-on optofluidic device. A) Overlaid bright-field and light-sheet images of the device filled with rhodamine fluorescent dye (100 µm scale bar). B) Magnified GFP image of the L-shaped microchannel showing the generated light-sheet taken by the green filter (525±50 nm band pass) of the microscope (20 µm scale bar). C) A 2.4 µm FWHM was achieved for the light-sheet thickness at focus, at the middle of the channel along the vertical dashed line shown in B).

The small deviation of the measured value from the simulated one (2.4 µm vs. 2.3 µm; see section 3.3.2 for simulation) can be due to measurement errors. It is worth noting that, when imaging *C. elegans*, the light-sheet thickness can be slightly different from the characterized value due to additional refractions and aberrations caused by worms' tissue.

To measure the experimental resolution of the system, 500-nm fluorescent beads were imaged as point source. Figure 4-2 shows the imaging results from the fluorescent beads. The consecutive frames of the passing bead were acquired with 0.55 µm axial step size, Figure 4-2 (A), using the 20X/0.35NA objective lens. Axial step size was measured via particle trajectory method and found to be reasonably constant. Figure 4.2 (B) shows the cross-sectional image of the resolved bead at the center of the light sheet; the normalized intensity profile of Figure 4-2 (C) across the center of

the image suggests a lateral resolution of 1.1 μm as the FWHM. The measured lateral resolution was ~13% inferior to the theoretical resolution of the detection lens (0.95 μm) which can be due to the aberrations induced by PDMS material in the detection path. Figure 4-2 (D) depicts the image of a passing bead along the axial direction. The intensity profile at the center of the bead, Figure 4-2 (E), demonstrates achievement of a 2.4 μm FWHM in the axial direction, which is in good agreement with the simulated light-sheet thickness of 2.3 μm. The three-dimensional experimental point spread function (PSF) of the LSFM system is visualized in Figure 4-2 (F). In this experiment, fluorescent beads were flowed across the light-sheet in an aqueous solution with the refractive index of ~1.33 which is reasonably close to the refractive index of the *C. elegans* (~1.37) [93]. However, spherical aberrations can be induced in the final images of the *C. elegans* due to this slight mismatch of refractive indices, and also inhomogeneity in the refractive indices of *C. elegans'* internal structures.

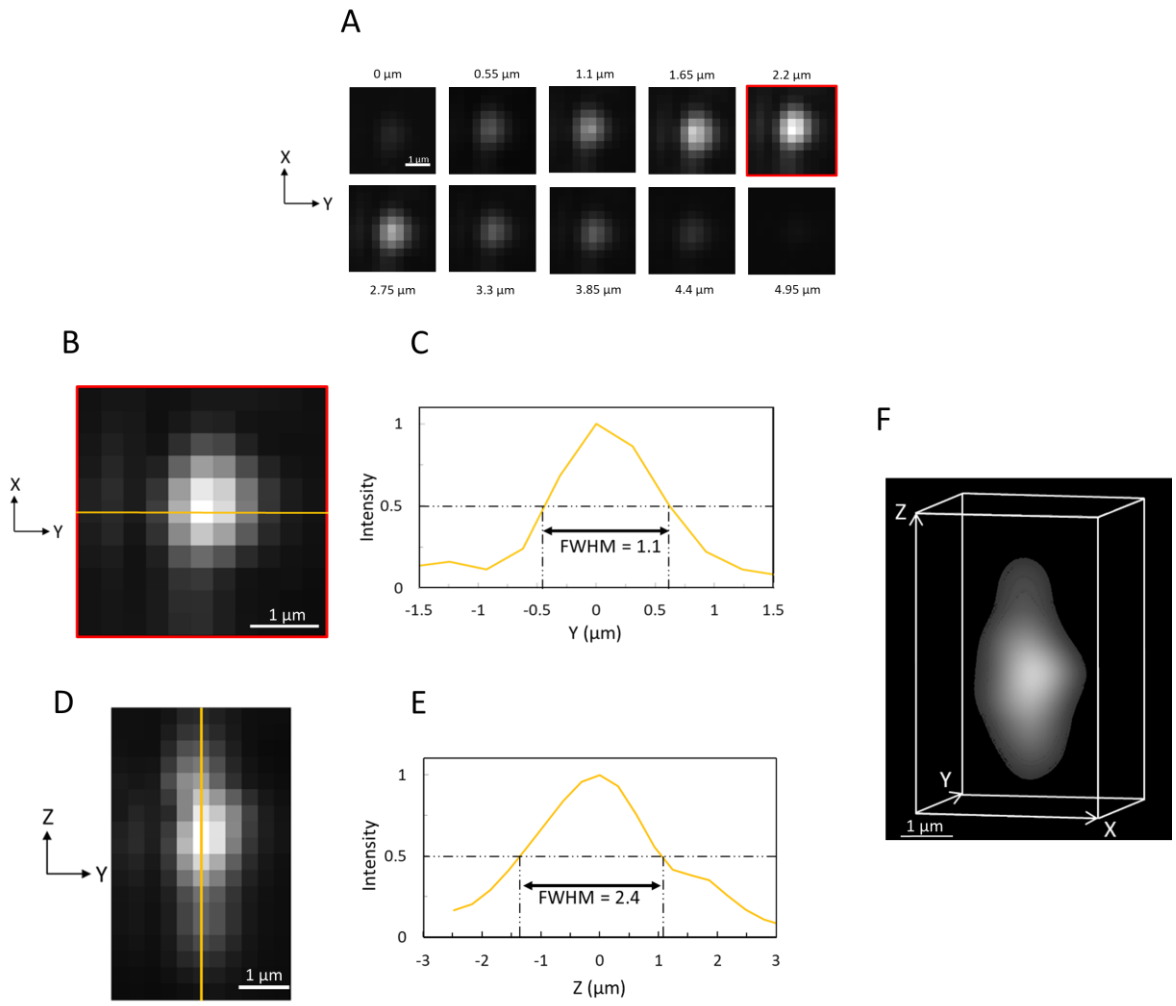

Figure 4-2. Resolution measurement of the optofluidic LSFM platform. A) Acquired images of a 500 nm fluorescent bead passing through the light-sheet. Images are shown at different time points corresponding to 0.55 µm axial spacing. B) Magnified image of the central plane of the bead in (A). C) The intensity profile along the line in (B) showing a lateral FWHM of 1.1 µm. D) Axial reconstruction of the stack of images in (A). E) The axial intensity profile along the line shown in (D). F) 3D experimental PSF acquired with volumetric rendering of the stack of images in (A). Scale bars in panels (A), (B) and (D) correspond to 1 µm.

4.1.2. LSFM imaging of *C. elegans* Neuronal System

To investigate the feasibility of performing light-sheet imaging with the low-cost add-on device, two *C. elegans* strains were imaged. Figure 4.3 depicts the LSFM images obtained from an NW1229 *C. elegans* with pan-neuronal GFP expression. In this experiment, a gravid adult worm was loaded into the device at the flow velocity of 90 $\mu m.sec^{-1}$ and was continuously imaged during the ~10-second period that took for the entire worm to pass through the stationary light sheet. The key characteristic of the NW1229 *C. elegans* is the clustering of neurons in the head and tail, connected across through a ventral cord, as shown in the Figure 4-3 (A) [94], [95]. Figure 4-3 (B) shows representative cross-sectional LSFM images of NW1229 neurons at different locations along the length of the worm. Characteristic fluorescent expressions of NW1229 can be clearly resolved. For example, sensory dendrites, head neuronal ganglia, ventral and dorsal nerve cords, and tail neurons are visualized with high contrast and resolution using the developed low-cost platform. Figure 4-3 (B(i)) shows several fluorescent expressions extending from the brain to the tip of the nose. These expressions are consistent with those of the dendrites of the sensory neurons. The contrast obtained from the dendrites of the sensory neurons with the low-cost add-on is comparable with those previously reported using conventional LSFM systems [14], [15], [23]. Figures 4-3 (B(ii-iii)) show the characteristic clustering of neurons inside the brain. In the mid-body, Figure 4-3 (B(iv-v)), the ventral and the dorsal nerve cords (orange and blue arrows, respectively), the ventral cord motor neurons (purple arrow), and the body commissures (white arrow) are clearly resolved. As expected, these neurons are mostly distributed close to the circumference of the worm cross section [94]. Visualization of the ventral cord neurons along the

worm body with high contrast and at high resolution is specifically useful for studies targeting neurodegenerative disorders such as Alzheimer's disease and Parkinson's disease [96], [97].

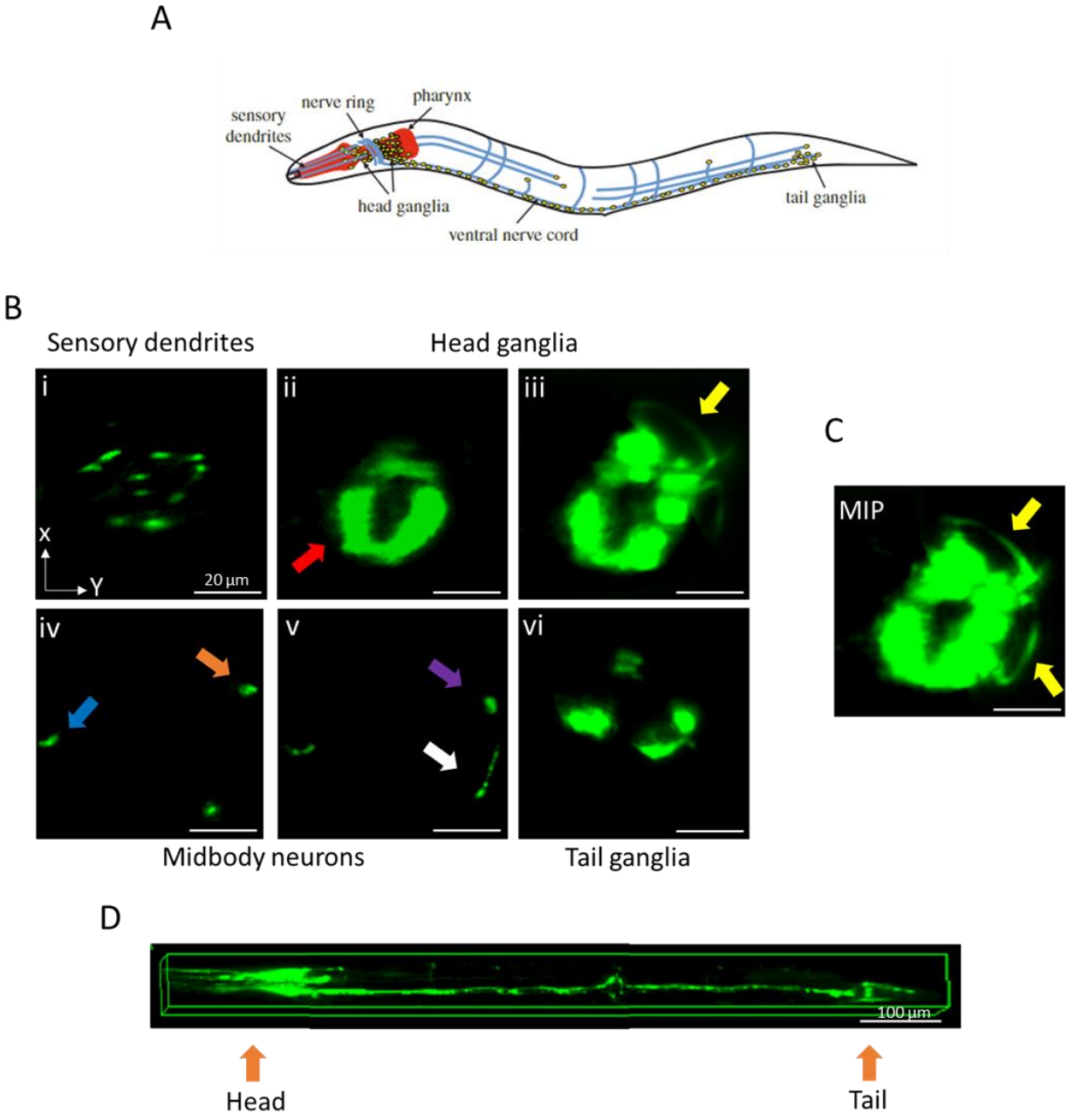

Figure 4-3. Light-sheet imaging of adult NW1229 C. elegans with the optofluidic device. A) Overview of the nervous system of the C. elegans [95], *reprinted with permission from Ref.* [95]. *B) Representative cross-sectional images of the pan-neuronally GFP expressing worm acquired with the optofluidic device under a conventional fluorescent microscope: (i) Cross-sectional image of the sensory dendrites; (ii-iii) Neurons in the brain of the C. elegans. The nerve ring is shown with a red arrow in (ii), and commissures are shown with yellow arrows in (iii); (iv-v) Cross-sectional images of the midbody section in which, orange and blue arrows indicate the ventral and dorsal nerve cords, respectively. Purple arrow shows the ventral nerve cord motor neurons and white arrow correspond to the body commissure; (vi) Cross-sectional image of the tail ganglia. D) The maximum intensity projection (MIP) of the acquired frames in the head region showing the nerve ring and head commissures. Scale bars in (A) and (C) correspond to 20 µm. D) Volumetric reconstruction of the worm. This 3D image was produced by stacking ~1500 two-dimensional light-sheet frames (100 µm scale bar).*

Lastly, neurons in the tail ganglia are visualized in Figure 4-3 (B(vi)), highlighting the most distal part of the worms' neuronal system. Figure 4-3 (C) is the maximum intensity projection of the frames acquired from the brain, showing the commissures (yellow arrows) [98]. Volumetric visualization of the worm's entire neuronal system could be achieved by stacking the ~1500 two-dimensional light-sheet cross-sectional images as shown in Figure 4-3 (D).

Figure 3-4 compares the *C. elegans* images obtained with the optofluidic device while excited with the light-sheet illumination, and the epi-fluorescence illumination of the host inverted microscope. The acquired cross-sectional images of the sensory dendrites (also showed in Figure 4-3 (B(i)) in both illumination modes are shown in Figure 4-4 (A). Also, acquired image of the nerve ring in the head is compared in Figure 4-4 (B). Significant enhancement of image contrast can clearly be recognized in the images obtained with the low-cost add-on, as the indicated neuronal features are clearly resolved when illuminated with the light-sheet. This improvement is attributed to the

elimination of out-of-focus fluorescent light of head ganglia region due to the selective planar excitation with the light-sheet.

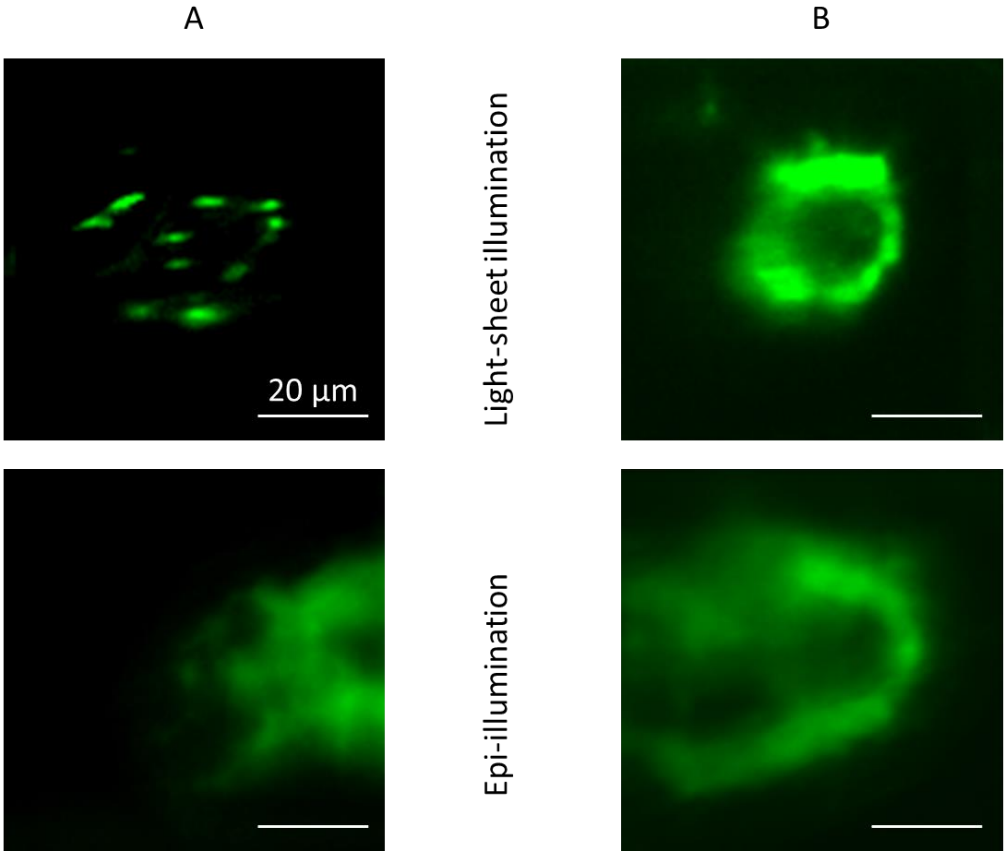

Figure 4-4. Comparing the image contrast of the C. elegans within the optofluidic device when operating in the epifluorescence mode (bottom) and the proposed light-sheet mode (top). Contrast enhancement is notable as the dendrites (A) and nerve ring (B) are only identified in the image acquired with the light-sheet illumination using low-cost add-on device. Scale bars represent 20 µm.

The results presented in Figures 4-3 and 4-4 confirm the ability of the developed low-cost optofluidic LSFM platform in visualizing the neuronal system of the worm with high contrast and resolution. Possibility of rendering the volumetric fluorescent expression of the entire worm for studying the neuronal processes in their natural 3D milieu has also been demonstrated.

4.1.3. Rapid LSFM Imaging of *C. elegans*

To explore the possibility of improving the imaging speed, an NW1229 worm was imaged while flowing at a higher velocity of 450 µm.sec^{-1}. Acquired LSFM images at such high speed (Figure 4-5) demonstrate the possibility of rapidly imaging the entire nervous system of the worm without compromising the resolution. At such high flow velocity, the entire worm was imaged in ~2 seconds with ~600 acquired cross-sectional images which still ensures Nyquist sampling. For example, Figure 4-5 (i) shows fluorescent expressions associated with dendrites of sensory neurons which is very comparable to those captured at the lower velocity in Figure 4-3 (B(i)). Similarly, the ventral nerve cord (orange arrow), dorsal nerve cord (blue arrow) and midbody commissure (white arrow) in worm's midbody region are resolved with contrast and resolution comparable to those obtained at the low velocity, Figure 4-5 (iii-iv) vs. Figure 4-3 (B(iv-v)). These results confirm the ability of the optofluidic add-on device in rapid (~2s) imaging of *C. elegans* with high contrast and without the need for worm immobilization. This demonstration can open the door for downstream utilization of the developed low-cost optofluidic LSFM add-on for continuous and high-throughput imaging of *C. elegans* (see section 4.2).

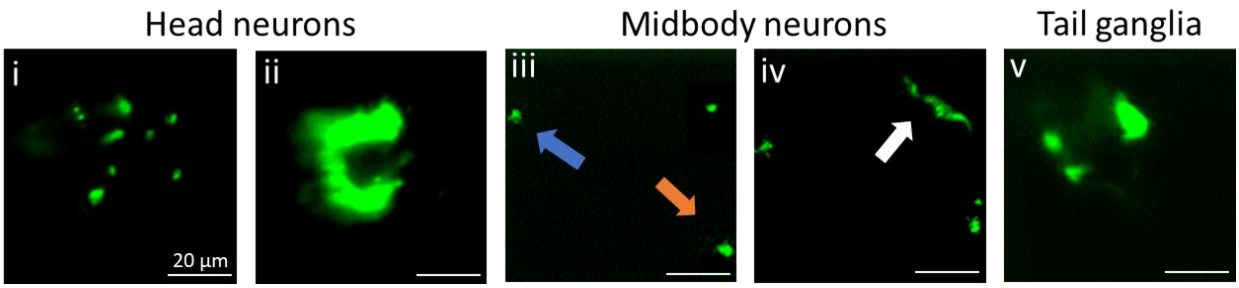

Figure 4-5. Fast cross-sectional image acquisition of C. elegans NW1229 strain at 450 µm.sec^{-1} velocity using the add-on optofluidic device. Fluorescent expressions in (i) correspond to sensory dendrites. Axon bundles in head ganglia is observed in (ii). (iii-iv) show the neuronal features in the midbody region such as ventral nerve cord (orange arrow), dorsal nerve cord (blue arrow), and the commissure (white arrow). Tail neurons are shown in (v). Scale bars correspond to 20 µm.

To test performance of developed primary design in LSFM imaging of other *C. elegans* strains, we also carried out imaging on the BZ555 *C. elegans* strain. This strain expresses GFP in its DNs (Figure 3-6 (A)) [31] and is widely exploited as a model for studying PD. Figure 4-6 (B) depicts representative cross-sectional light-sheet images of the anterior DNs of a BZ555 strain flowing at a velocity of 450 µm.sec^{-1} in the channel; here, the DNs and their axonal/dendritic processes are clearly resolved. Dendrites of the four CEP neurons (blue arrows) are shown in Figure 4-6 (B(i)). CEP neurons cell bodies (red arrows) along with the axons (orange arrow) are clearly visualized in Figures 4-6 (B(ii-iii)). ADE neurons (yellow arrows) are shown with high contrast in Figure 4-6 (B(iv-v)). Figure 4-6 (B(vi)) is a maximum intensity projection image showing the two CEP neuron pairs and their axonal processes in a single image. Presented LSFM images of BZ555 *C. elegans* strain demonstrate the possibility of resolving a DN or a pair of DNs in a single frame which normally cannot be achieved with the host wide field microscope.

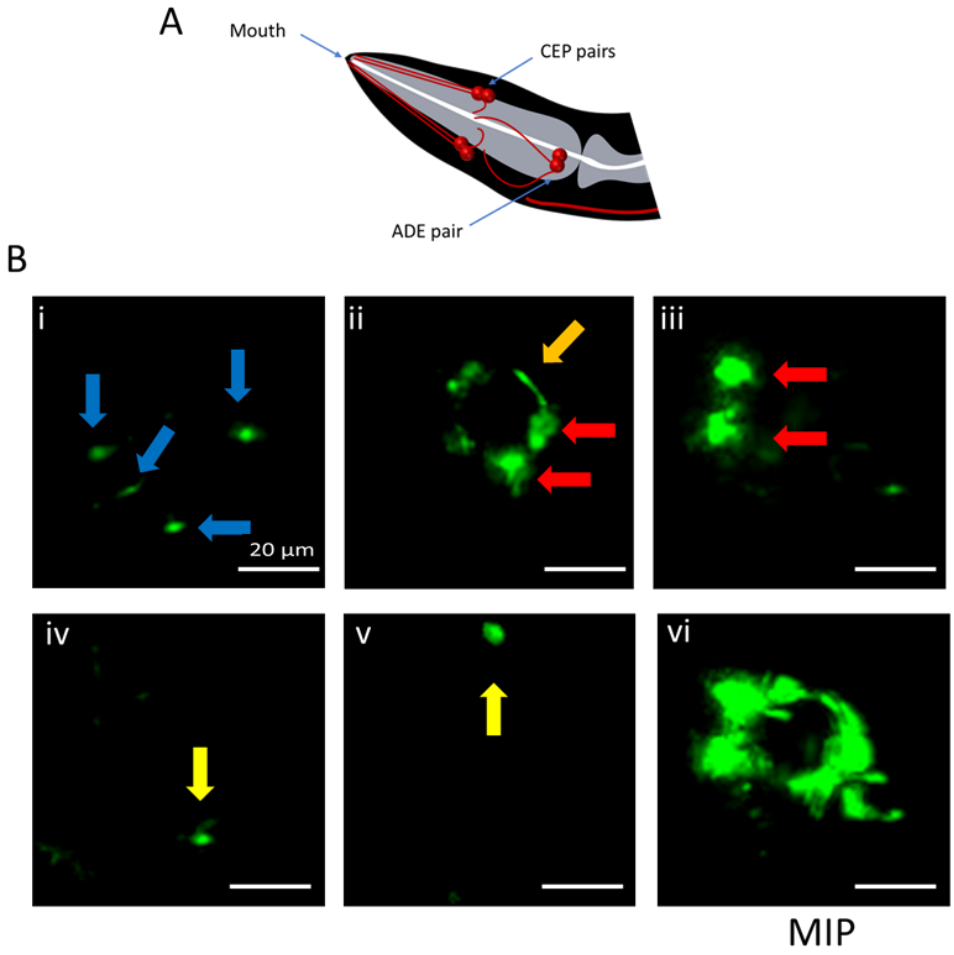

Figure 4-6. LSFM imaging of adult BZ555 C. elegans with the optofluidic device. A) Schematic presentation of the head DNs. The fluorescent light-sheet images acquired with low-cost add-on device are shown in (B): (i) Cross-section image of the dendrites of the four CEP neurons; (ii-iii) CEP neuron pairs (red arrows) and their axonal processes shaping the nerve ring (orange arrow); (iv-v) ADE pair (yellow arrows); (vi) Maximum intensity projection image showing the two CEP pair and their axonal processes. Scale bars correspond to 20 µm.

As described in the above section, the developed optofluidic LSFM platform can be potentially utilized for continuous imaging of groups of *C. elegans*. Typically, large-scale studies in the *C. elegans* research are conducted via parallel or serial immobilization of *C. elegans* in the microfluidics devices using various techniques reviewed in chapter 2. However, in these approaches, images are typically acquired laterally from the top-view and not from the cross-section. As such, the imaging performance of these methods is limited due to the intrinsic compromise between imaging speed and resolution as high NA objectives do not offer a large enough field of view to image the entire ~1mm long worm at once. The proposed optofluidic LSFM, on the other hand, combines the planar illumination of the light-sheet microscopy with the continuous flow of the microfluidics platform to enable rapid and high-resolution LSFM imaging of worm cross sections without the need for immobilization. Flow-based translation of *C. elegans* and continuous acquisition of cross-sectional images intrinsically makes the platform suitable for continuous and potentially high-throughput imaging, which is discussed in the following section. The possibility of quantitative fluorescence imaging with our add-on device for light-sheet screening of the effect of chemical neurotoxic exposure is also investigated and presented in the following section.

4.2. Continuous Imaging of *C. elegans* Groups

This section is dedicated to design modifications of the optofluidic device for improving the performance of the solution in continuous imaging of *C. elegans*. The section first discusses the modification made, followed by discussion of results of optical characterization of the modified device. The modified device is then utilized in a study for selecting the operating flow rate for continuous imaging. Eventually, the optimized device is used for testing the feasibility of continuous light-sheet imaging of *C. elegans*. The section concludes by presenting and discussing quantitative data on fluorescence expression of groups of *C. elegans* exposed to neurotoxin that were continuously imaged with modified device (thesis objective 2).

4.2.1. Device Modification

The possibility of imaging groups of *C. elegans* continuously was first investigated with the primary optofluidic device introduced in section 3 of chapter 3. Although the primary device enabled high-resolution and immobilization-free light-sheet imaging of *C. elegans*, preliminary experiments indicated that the 90° microchannel bend design with an inverse tapered shape (Figure 3-3 (B)) could lead to worm flow blockage at the sharp bend when multiple worms were loaded in the device (Figure 4-7 (A), top image). As a result, an adjustment was made to the 90° bend to facilitate better passage of worms through the channel and the light sheet. For this purpose, the inverse tapered shape of the bend in the primary device was changed to a bend with 50 μm radius of curvature, as seen in Figure 4-7 (A), bottom image. Another modification to the device design was narrowing the input channel from 0.6 mm to 0.2 mm to facilitate worm loading into the inlet

channel. This modification was essential as in the original design, the worms could resist against the low-velocity flow in the initially-wide inlet channel.

To investigate the worm passage efficiency in the primary and modified devices, an experiment was conducted to measure the worms passing time duration across the light-sheet plane (Figure 4-7 (B)). In this study, synchronized adult worms (N=20) were loaded into both primary and modified devices at a flow rate of 40 µL/min and their passing behaviours through the channel were studied. The experiments were repeated three times for each device design.

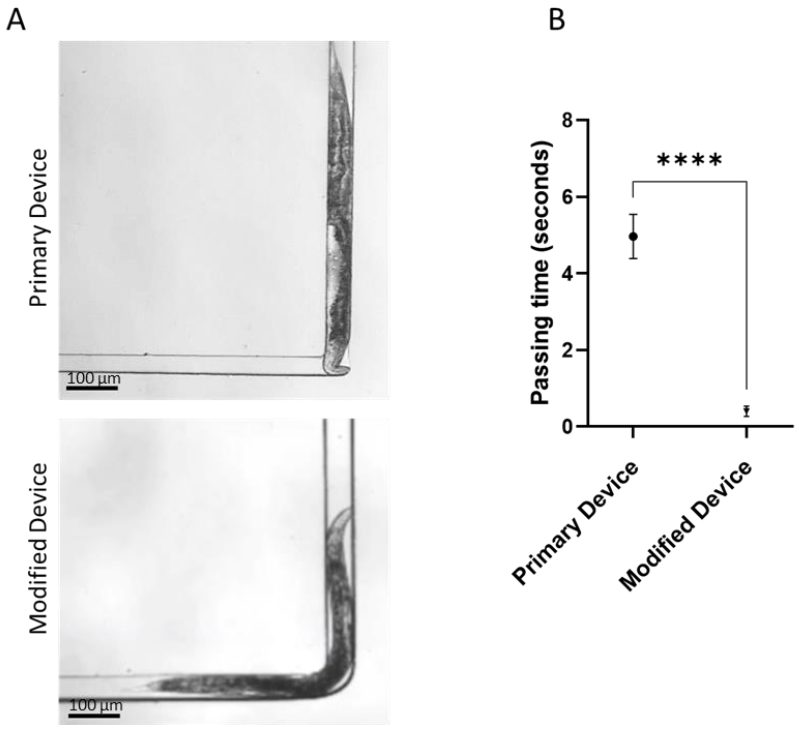

Figure 4-7. Worm passing in the primary and the modified LSFM optofluidic devices. A) Microscopic images showing the bend of the two devices. The top image in (A) shows a stuck worm in the sharp bend of the primary device. The bottom image in (A) shows the worm passage through the light sheet plane in the modified device. Scale bars in A correspond to 100 µm. B) The average passing time of the worms against the light sheet in the primary and the modified devices, showing a significant improvement in passing time with the modified device.

The study revealed that in the primary design, worms frequently were stuck at the 90° bend of the channel which resulted in long average passing time of worms through the channel (Figure 4-7(A)-top). In the modified design, on the other hand, worms passed smoothly through the channel (Figure 4-7(A)-bottom). Through image processing, the passing time of worms through the channel were measured. The obtained results showed a significant decrease in the average passing time of the worms through the light sheet in the modified device compared to the primary device (Figure 4-7 (B)). Adjusting the bend resulted in an average passing time of 0.18 ± 0.03 seconds per worm, which was significantly ($p<0.0001$) shorter than the 4.61 ± 0.56 seconds per worm achieved in the primary device. As such, the next set of experiments was carried out with the modified device.

4.2.2. Optical Characterization

Once the improvement in worm passing time in the modified design was confirmed, optical characterization tests were performed to compare the light sheet specifications of the modified device with those of the primary design. Since the excitation optical design of the modified device was the same as the primary device, the light-sheet thickness was expected to be similar in both designs (Figure 4-8 (A)). As seen in the inset of Figure 4-8 (A), the revised curved channel was design in a way that, similar to original design, light-sheet hits the vertical wall of the microchannel. However, replacing the initially designed inverse tapered bend with the 50-µm curvature in the modified device could introduce additional aberrations and image degradations in the final image.

In order to measure the light-sheet thickness, the device was filled with rhodamine solution, and the generated light-sheet was observed inside the microchannel (Figure 4-8 (B)). Intensity measurement along the Z-axis showed 2.55 µm FWHM as the light-sheet thickness at the middle of the microfluidic channel, as shown in Figure 4-8 (C). Minor differences in the light-sheet thickness from the simulated value (2.55 µm vs. 2.3 µm) could be induced by fabrication tolerances.

A 2.55 µm width for the axial point spread function was achieved via measurement of the light-sheet thickness (Figure 4-8 (C)). To measure the lateral resolution of the imaging system, 0.5 µm beads were imaged as a point source. Intensity measurement along the x-direction suggested a 1.2 µm width for the lateral point spread function, as shown in Figure 4-8 (D). The optical characterization results confirmed that imaging performance of the modified device is reasonably close to that of the primary design, albeit with much better performance in continuous imaging.

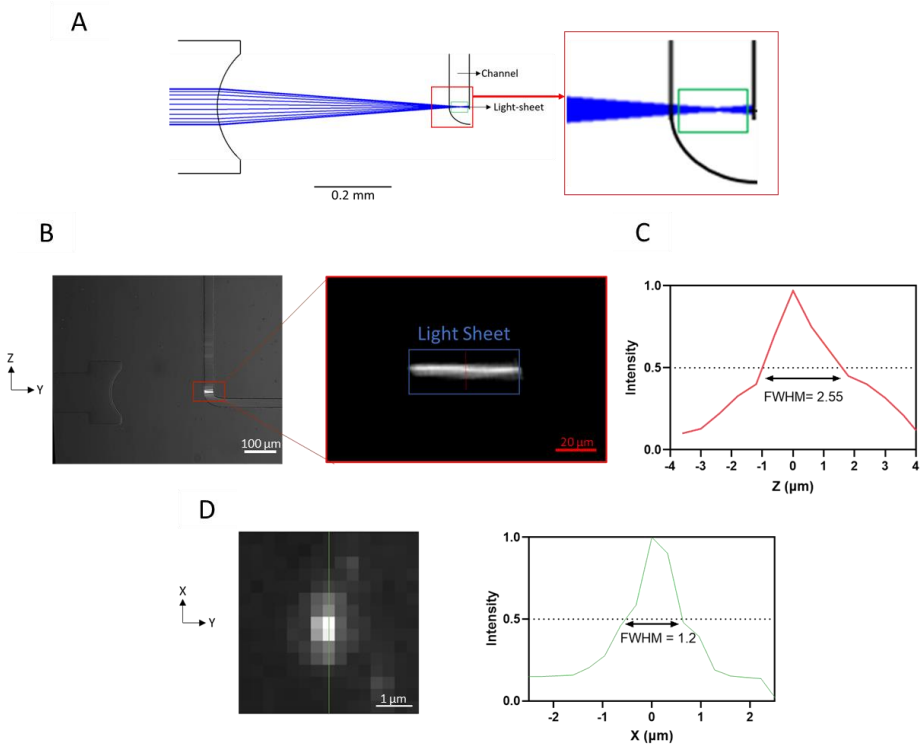

Figure 4-8. Optical design and characterizations results of modified design. A) Optical design of the modified device. Light-sheet hitting the wall of modified microchannel is shown in inset of (A). B) Overlaid bright-field and light-sheet images of the modified device filled with rhodamine fluorescent dye (100 µm scale bar). Inset is magnified fluorescence image of the L-shaped microchannel showing the generated light-sheet taken by the green filter (525±50 nm. band pass) of the microscope (20 µm scale bar). C) Intensity profile of light sheet at focus, showing a 2.55 µm FWHM. D) Image of the central plane of the bead is shown on the left (1 µm scale bar). The intensity profile along the green line suggests an FWHM of 1.2 µm as lateral resolution.

4.2.3. Continuous Imaging of *C. elegans* with the Modified Optofluidic Device

This section discusses the experiments conducted to find the suitable worm concentration, followed by the characterization of the modified device to determine a suitable operating flow rate for continuous imaging. After the determination of these parameters, a study was conducted to establish the feasibility of continuous imaging of groups of worms.

4.2.3.1. Experimental Conditions

Experiments were carried out to determine the appropriate concentration of worms to be used in the continuous imaging study. The aim was not to clog the device in the continuous imaging experiments by overpopulating the device with worms. Three different concentrations of worms (6, 3, and 1 worm/µl) were tested. A preliminary experiment at a flow rate of 40 µl/min was performed using the highest concentration (6 worms/µl), and the channel was clogged by the accumulation of worms in the bend section. Therefore, the solution with the highest concentration was diluted to achieve 3 and 1 worms/µl concentrations. No clogging occurred in these two concentrations. Since the ultimate goal of this study was to image the worms continuously at the

highest possible throughput, the concentration of 3 worms/µl was chosen to continue the experiments.

To produce a blur-free image without motion artifacts, an adequate number of frames throughout the worm length was needed to be acquired. Considering the size of the region of interest, our camera could achieve up to ~300 fps. According to preliminary experiments, although the 40 µl/min was perceived as an appropriate flow rate, an adequate number of frames could not be achieved with our camera due to the high speed of worms in this flow condition. As a result, an experiment was performed to determine a suitable worm speed (or passing time through the light-sheet) at lower flow rates in which our camera could acquire a reasonable number of cross-sectional images.

Figure 4-9 (A) shows the worms passing times through the light sheet at different flow rates of 30, 20, and 15 µl/min using the determined concentration of 3 worms/ul. As expected, the average passing time across the light sheet increased by decreasing the flow rate as the worms moved with lower velocity. The flow rate of 30 µl/min resulted in a worm average passing time of 0.19 ± 0.03 seconds, which correspondingly leads to the acquisition of ~60 frames throughout the ~1mm length of the worm. As shown in Figure 4-9 (B), a preliminary experiment with this flow rate resulted in the acquisition of blurry images, indicating that the sampling rate was not sufficient due to the worm's high velocity. Therefore, the flow rate was further reduced to 20 µL/min, with which an average passing time of 0.65 ± 0.11 seconds was achieved. In this configuration, ~195 frames were acquired per worm. In addition, the quality of light-sheet images at this condition improved, as shown in Figure 4-9 (C).

On the other hand, at a lower flow rate of 15 µL/min, the average passing time increased substantially to 4.45 ± 0.39 seconds since some worms were resisting against the flow at the bend.

As such, based on the above observations and measurements, the flow rate of 20 µL/min was selected as the operating flow rate for continuous imaging. It should be noted that the decision to reduce the flow rate was due to the limitations of the camera used in our setup and should not be seen as a fundamental limitation of the developed technology.

The presented characterization tests above were carried out in horizontal orientation of the device (Figure 4-7 (A)), which enabled observation of the worm's movement within the microchannel using the inverted microscope's native optics. These measurements are expected to be applicable to the final vertical orientation of the device for light-sheet imaging (Figure 3-3 (A)), as gravitational forces are insignificant in microfluidic settings due to the scaling laws.

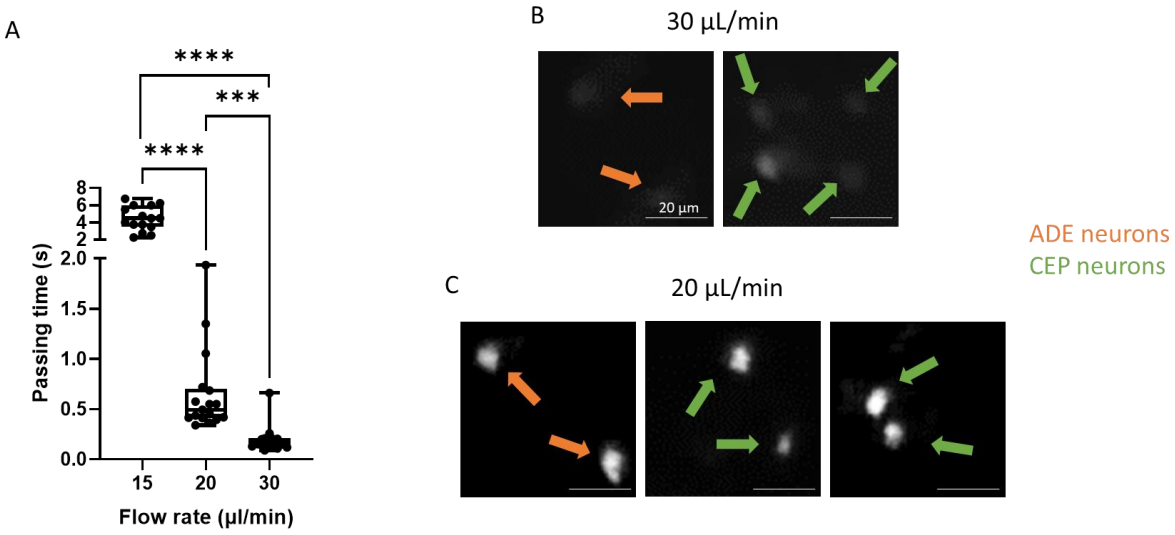

Figure 4-9. Preliminary experiments to set conditions for continuous LSFM imaging of C. elegans. A) Passing time of worms across the light sheet spot at different flow rates in the horizontal orientation of the modified device (for at least N=40 worms for each flow rate). A significant reduction in the average passing times of worms was observed by increasing the flow rate. B) Cross-sectional LSFM images of ADE and CEP neurons of BZ555 worms at the flow rate of 30 µl/min, indicating the blurriness of the image. C) Representative cross-sectional images showing the DNs in the head of the C. elegans acquired while worms were passing at the flow rate of 20 µl/min. Scale bars correspond to 20 µm. Orange and green arrows show ADE and CEP neurons, respectively.

4.2.3.2. Continuous LSFM Imaging of BZ555 C. elegans

Once the modified device was characterized optically and fluidically, the device was placed vertically on the inverted microscope stage to perform continuous light-sheet imaging of BZ555 *C. elegans* worms. In this experiment, 20 adult worms were loaded into the modified device at the flow rate of 20 µl/min and continuously imaged while passing through the light-sheet. The experiment was repeated three times to examine the reproducibility of results. An average of 16 worms out of 20 were observed passing through the light sheet. The rest of the worms could have been trapped in the device reservoir or the inlet tubes. Due to the inconsistencies in the passing velocity of the worms, an average of 14 worms in each experiment were successfully imaged (i.e., individual neurons were resolved). These velocity variations also contributed to the errors of the average passing time at 20 µL/min (provided in the previous section). The imaging results obtained from the three experiments suggested a throughput of approximately 12 ± 2 worms per minute using the modified add-on optofluidic device. Figure 4-9 (C) provides the representative cross-sectional images of the DNs of the *C. elegans* BZ555 strain. The obtained cross-sectional light-sheet images of *C. elegans* neurons confirmed the modified optofluidic device's ability to image *C. elegans* at single-neuron resolution, with a comparable image quality to that of the primary device (Figure 4-6), and at the throughput of 12 worms/minute. The obtained results qualitatively suggest that the modified optofluidic LSFM device has the promise of enabling high-throughput and high-content imaging of this organism via the simple and low-cost addition of an optofluidic device to a regular inverted fluorescent microscope.

4.2.4. Proof of Concept Application of Continuous LSFM Imaging to Neurodegeneration Studies

Here, we aimed to demonstrate the application of our technology to quantitative testing of neurodegeneration in *C. elegans*. To achieve quantitative fluorescent measurement of neurodegeneration with the proposed low-cost optofluidic LSFM platform, a preliminary chemical exposure study was conducted. A group of BZ555 *C. elegans* was exposed to 50mM 6-OHDA neurotoxin which has been shown in the literature to lead to degeneration of DNs in this strain [97]. LSFM images were acquired with the modified optofluidic device and compared with the unexposed control worms not exposed to 6-OHDA to assess the feasibility of quantifying toxicant-induced neurodegeneration with the modified device. Figure 4-10 depicts the experimental results obtained from imaging the two worm groups 72 hours after exposure of the test group to 50 mM 6-OHDA.

In this neurodegeneration quantification experiment, 20 adult worms per group flowed at 20 µl/min in the device, from which 12 well-imaged worms per group were selected for further image analysis. Firstly, a histogram of the head region of an exposed and a control worm was produced to compare the distributions of fluorescence expressions in the two worms, as shown in Figure 4-10 (A). Figure 4-10 (B) shows the zoomed view of the histogram with pixel intensity value above 100, which is typically the indicator of bright neuronal features. Our LSFM images and data analysis of the two worm groups show that the fluorescent expression is significantly decreased in the exposed worm (red) compared to the control worm (gray). These significant losses in the

signals are consistent with the results of previous studies demonstrating significant attenuation of fluorescence expression due to neuronal loss after 6-OHDA treatment [99].

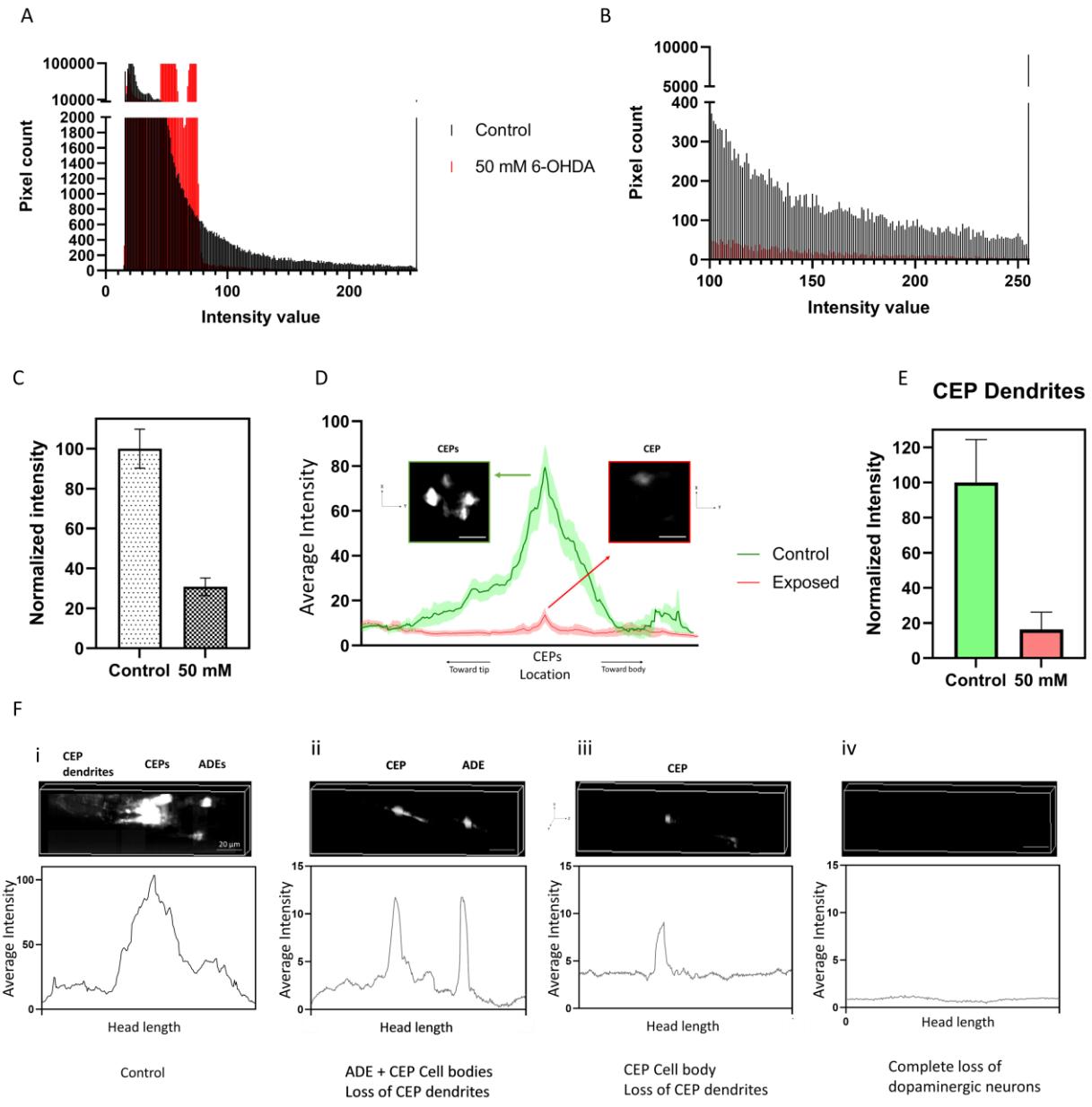

Figure 4-10. Quantitative LSFM imaging of BZ555 C. elegans strain treated with 50mM 6-OHDA neurotoxin. A) Histogram of a control (gray, not exposed) and an exposed (red, 50 mM 6-OHDA) worm showing the distribution of pixel intensity values in the head region of the two worms. (B) A magnified histogram of (A), demonstrating the distribution and number of pixels with an intensity value above 100 in two worms (one per each group). C) Normalized intensity plot of the control and exposed worms neuronal intensity in the head (N=12), highlighting the significant overall intensity reduction in the 50mM 6-OHDA exposed group. D) Average frame intensity change of the two worm groups along their head region (from nose to roughly the location of ADE neurons), plotted based on the location of CEP cell bodies (maximum peak intensity). Cross-sectional LSFM image samples of each group at the peak intensity region is also shown, demonstrating significant degeneration of CEPs in the exposed worm (scale bar 20 µm). E) Normalized intensity plot of the control and exposed groups indicating the significant overall intensity loss of the CEP dendrites in the exposed group. F) Average intensity plot of the control sample along with the 3D image showing DNs in the head (i), an exposed worm with CEP and ADE neurons and partial loss of dendrites (ii), an exposed worm with a single CEP neuron and complete loss of CEP dendrites and ADE pairs (iii), and an exposed worm with complete loss of head dopaminergic neurons (iv). Scale bars represent 20 µm.

To compare the signals from the two groups statistically, we quantified the average fluorescent intensity of the LSFM frames acquired from worms in the two exposed and control groups. As shown in Figure 4-10 (C), a significant reduction (~70%) in the overall intensity of the 6-OHDA exposed worms was observed compared to the control group. This demonstrated our system's ability in continuous imaging and quantification of neurodegeneration in worms exposed to neurotoxins.

Having quantified the overall neuronal intensity of the two groups, we then attempted to identify the specific locations of neurodegeneration (i.e., one of the main values of LSFM over epi-fluorescent imaging). Figure 4-10 (D) represents the average fluorescent intensity of individual frames across the worms' head length in the two groups. The maximum intensity peaks in the two curves correspond to the frames containing the CEP neuron pairs. Example frames containing CEP

pairs are also shown for representative worms from each group in Figure 4-10 (D). As shown in Figure 4-10 (D), a significant reduction in the average intensity of head neurons was observable in the 6-OHDA exposed worms (red line) as compared to the control worms (green line). An overall intensity reduction of ~84% in the CEP dendrites (extended from the tip of the worm to the nerve ring) was also measured as depicted in Figure 4-10 (E).

Careful interrogation of LSFM images of the exposed worms demonstrated the presence of several neurotoxin-induced phenotypes. Individual intensity plots and corresponding volumetric images of different phenotypes are presented in Figure 4-10 (F-ii to F-iv). Figure 4-10 (F-i) provides the intensity profile of a control worm with the pronounced expression of CEP and ADE neurons (as also seen in the corresponding 3D image). Figure 4-10 (F-ii) represents a 6-OHDA exposed worm with a CEP and an ADE neuron with partial loss of their processes (Dendrites/Axons), which is in agreement with the two peaks of the corresponding intensity plot across the head. An exposed worm with only a single CEP neuron and complete loss of the CEP dendrites is shown in Figure 4-10 (F-iii). Lastly, a worm with a complete loss of DNs is shown in Figure 4-10 (F-iv).

Results shown in Figure 4-10 confirmed the ability of the optofluidic LSFM platform in quantifying the fluorescence expression of *C. elegans* and detecting different phenotypes occurring as a result of chemical exposure with single neuron resolution, without immobilization, and in a continuous manner. The results of this preliminary study demonstrate the potential of the developed technology for chemical screening applications which frequently require quantitative analysis of large populations of *C. elegans* at high throughput and imaging resolution. We will provide some suggestions in the next chapter for the ways that this technology can be improved to better meet the above technological needs.

4.3. Closing Remarks

The experimental results of Figures 4-3 to 4-6 confirm the ability of the developed low-cost optofluidic platform to rapidly acquire high-contrast LSFM images of *C. elegans*. Given the fact that LSFM systems are expensive and scarce, the developed platform has great potential to make significant contributions to the field of biology by offering a low-cost solution for converting the commonplace conventional widefield microscopes to an LSFM system. Another significance of the developed low-cost solution is its ability to continuously image the cross-sections of *C. elegans* as they pass through the stationary light sheet. This feature is specifically important in biological studies involving whole-body interrogation of large groups of *C. elegans*, which is achieved and demonstrated in Figure 4-9. The optical sectioning ability of the developed add-on enables volumetric visualization of individual neuronal features. This capability opens the door for studying the effects of environmental toxicants on specific neurons with a conventional microscope, which is achieved and demonstrated in Figure 4-10. This attribute is of value because the conventional fluorescence microscope typically images worms from top over the worm length and, hence, is unable to focus on specific neurons in a single image. This is because the depth of focus of moderate and high NA objectives are normally smaller than the diameter of a worm.

Chapter 5
Thesis Summary and Future Work

This section provides the summary of the thesis, followed by recommendations for future research.

5.1. Thesis Summary

We have designed and developed low-cost add-on PDMS-based optofluidic chips for rapid, immobilization-free, and continuous LSFM imaging of *C. elegans* with a conventional fluorescent microscope. The add-on devices integrate the illumination path of the LSFM within the PDMS chip, enabling continuous imaging of the cross-section of *C. elegans* as they pass through a microfluidic channel. An on-chip light-sheet was generated with a 2.4-µm thickness, enhancing the axial resolution of the host inverted wide-field microscope. The experimental resolution of the system was measured using the microbeads, suggesting FWHM width of the point spread function as 1.1 µm and 2.4 µm in the lateral and axial directions, respectively. Experimental results from imaging NW1229 and BZ555 strains of *C. elegans*, expressing fluorescent pan-neuronally or in dopamine neurons respectively, confirmed the ability of the system in producing optically sectioned and high-contrast images of the entire neuronal network in few seconds. The possibility of generating volumetric images of *C. elegans* neuronal system from cross-sectional images was also examined.

Furthermore, modifications to the primary device enabled continuous imaging of groups of *C. elegans* with the low-cost optofluidic LSFM. The modified device was optically characterized,

and a light-sheet thickness of 2.55 µm was achieved. Fluidic characterization of the device determined 20 µL/min as the operating flow rate of the experiment, taking into consideration of the camera capturing speed. Experimental results on the BZ555 strain offered continuous imaging of groups of worms at a throughput of 12 worms/minute. Furthermore, quantitative imaging of control and 6-OHDA exposed (50mM) BZ555 *C. elegans* demonstrated the ability of the platform in detecting, quantifying, and differentiating between different toxin-induced phenotypes.

This work has great potential to make significant contributions to the field of biology by offering a low-cost solution for converting the commonplace conventional wide-field microscopes to an LSFM platform for high content and potentially high-throughput fluorescent imaging of *C. elegans*.

5.2. Limitations and Recommendations for Future Research

In this thesis, we used the optofluidic LSFM device to image groups of *C. elegans* continuously at a certain throughput. However, there existed non-uniformities in the velocity profile of each worm as it passed through the light-sheet, as well as between velocity profiles of different worms. The experimental results in this thesis showed that increasing the system's operating flow rate leads to more uniform velocities, which would necessitate higher camera capturing speeds.

In this thesis, we assessed the feasibility of performing continuous imaging of groups of *C. elegans* with the proposed platform. We also examined the possibility of quantitative fluorescent imaging of groups of worms with a primary chemical exposure assay. However, chemical screening assays typically require imaging a large number of samples and screening multiple chemicals. Increasing the camera capturing speed and enhancing the sample loading procedure can be pursued in the

future to enable the proposed optofluidic LSFM system to image in a high-throughput manner. For example, if a camera acquires at a high frame rate (1000 frames per second), higher flow rates than those utilized in this thesis can be used for worm translation, leading to faster worm speeds and increased throughput. This improvement would be critical in minimizing worm speed variations and image artifacts, as higher flow rates result in less deviations of worm speed, as presented in this thesis. However, we estimate that slight non-uniformities in worm speed will occur even at higher flow rates, necessitating the use of sensors for instantaneous speed measurements. These measurements can be used post image acquisition to compensate datasets for nonuniform motion artifacts and produce precise volumetric images.

Applying the modifications mentioned above can eventually enable the proposed system to obtain a significantly large number of datasets from worm populations in a short time. As such, employing/developing machine learning algorithms can be pursued to compensate for motion artifacts and/or for phenotype classification based on historic datasets.

In this thesis, we optimized the proposed optofluidic LSFM system for imaging ~50-µm diameter adult *C. elegans*. However, the proposed light-sheet-based imaging system can potentially be employed for imaging other stages of *C. elegans* or other biological samples such as cells and Drosophila embryos, as well as in flow cytometry. For instance, slight changes to the aperture size of the cylindrical lens and the microfluidic channel's width are expected to enable imaging early stages of *C. elegans*, which is not straightforward in other imaging approaches requiring immobilization as the small worms are more likely to move.

In this thesis, we demonstrated the feasibility of light-sheet imaging of *C. elegans* at a single-neuron resolution, which is sufficient for lots of applications, including screening. In light of this and the aberrations induced by utilizing high-NA lenses, we chose a 0.35 numerical aperture

detection objective. Given that the cross-section of the worm is being imaged in the developed platform, one can utilize higher-NA lenses for applications requiring better resolution. This would require some optimization to the design of the PDMS device to minimize the aberrations.

In this study, a cylindrical lens was used to create the light sheet and illuminate the sample from one side. However, one can apply modifications to the design of the microfluidic device to enable dual-side illumination to achieve a more homogeneous point spread function. Also, designing acylindrical lenses can be pursued to achieve aberration-free light-sheets to enhance the axial resolution of the imaging system.

Following the suggestions above, the proposed low-cost optofluidic LSFM can potentially be employed by many biology labs for high-content and high-throughput light-sheet imaging of *C. elegans* with a conventional fluorescence microscope.

References

[1] J. Huisken and D. Y. R. Stainier, "Selective plane illumination microscopy techniques in developmental biology," *Development*, vol. 136, no. 12, pp. 1963–1975, 2009.

[2] H. Deschout *et al.*, "On-chip light sheet illumination enables diagnostic size and concentration measurements of membrane vesicles in biofluids," *Nanoscale*, vol. 6, no. 3, pp. 1741–1747, 2014.

[3] P. Paiè, F. Bragheri, A. Bassi, and R. Osellame, "Selective plane illumination microscopy on a chip," *Lab on a Chip*, vol. 16, no. 9, pp. 1556–1560, 2016.

[4] J. C. M. Gebhardt *et al.*, "Single-molecule imaging of transcription factor binding to DNA in live mammalian cells," *Nature methods*, vol. 10, no. 5, pp. 421–426, 2013.

[5] J. Apfeld and S. Alper, "What can we learn about human disease from the nematode C. elegans?," *Methods in molecular biology (Clifton, NJ)*, vol. 1706, p. 53, 2018.

[6] D. Teschendorf and C. D. Link, "What have worm models told us about the mechanisms of neuronal dysfunction in human neurodegenerative diseases?," *Molecular Neurodegeneration*, vol. 4, no. 1, p. 38, 2009, doi: 10.1186/1750-1326-4-38.

[7] R. M. Power and J. Huisken, "A guide to light-sheet fluorescence microscopy for multiscale imaging," *Nature methods*, vol. 14, no. 4, pp. 360–373, 2017.

[8] L. Breimann, F. Preusser, and S. Preibisch, "Light-microscopy methods in C. elegans research," *Current Opinion in Systems Biology*, vol. 13, pp. 82–92, 2019.

[9] J. Huisken and D. Y. R. Stainier, "Even fluorescence excitation by multidirectional selective plane illumination microscopy (mSPIM)," *Optics letters*, vol. 32, no. 17, pp. 2608–2610, 2007.

[10] P. J. Keller, A. D. Schmidt, J. Wittbrodt, and E. H. K. Stelzer, "Reconstruction of zebrafish early embryonic development by scanned light sheet microscopy," *science*, vol. 322, no. 5904, pp. 1065–1069, 2008.

[11] J. Huisken, J. Swoger, F. Del Bene, J. Wittbrodt, and E. H. K. Stelzer, "Optical sectioning deep inside live embryos by selective plane illumination microscopy," *Science*, vol. 305, no. 5686, pp. 1007–1009, 2004.

[12] B.-C. Chen *et al.*, "Lattice light-sheet microscopy: imaging molecules to embryos at high spatiotemporal resolution," *Science*, vol. 346, no. 6208, 2014.

[13] O. E. Olarte, J. Andilla, E. J. Gualda, and P. Loza-Alvarez, "Light-sheet microscopy: a tutorial," *Advances in Optics and Photonics*, vol. 10, no. 1, pp. 111–179, 2018.

[14] R. McGorty, H. Liu, D. Kamiyama, Z. Dong, S. Guo, and B. Huang, "Open-top selective plane illumination microscope for conventionally mounted specimens," *Optics Express*, vol. 23, no. 12,

p. 16142, 2015, doi: 10.1364/oe.23.016142.

[15] J. Van Krugten, K. TARIS, and E. J. G. Peterman, “Imaging adult C. elegans live using light-sheet microscopy,” *Journal of microscopy*, vol. 281, no. 3, pp. 214–223, 2021.

[16] M. Rieckher *et al.*, “A customized light sheet microscope to measure spatio-temporal protein dynamics in small model organisms,” *PLoS one*, vol. 10, no. 5, p. e0127869, 2015.

[17] Y. Wu *et al.*, “Inverted selective plane illumination microscopy (iSPIM) enables coupled cell identity lineaging and neurodevelopmental imaging in Caenorhabditis elegans,” *Proceedings of the National Academy of Sciences*, vol. 108, no. 43, pp. 17708–17713, 2011.

[18] H. Jiang *et al.*, “Droplet-based light-sheet fluorescence microscopy for high-throughput sample preparation, 3-D imaging and quantitative analysis on a chip,” *Lab on a Chip*, vol. 17, no. 13, pp. 2193–2197, 2017.

[19] F. Zhao *et al.*, “Efficient and cost-effective 3D cellular imaging by sub-voxel-resolving light-sheet add-on microscopy,” *Journal of biophotonics*, vol. 13, no. 6, p. e201960243, 2020.

[20] T.-Y. Hsieh, S. Vyas, J.-C. Wu, and Y. Luo, “Volume holographic optical element for light sheet fluorescence microscopy,” *Optics Letters*, vol. 45, no. 23, pp. 6478–6481, 2020.

[21] Z. Guan *et al.*, “Compact plane illumination plugin device to enable light sheet fluorescence imaging of multi-cellular organisms on an inverted wide-field microscope,” *Biomedical optics express*, vol. 7, no. 1, pp. 194–208, 2016.

[22] F. Cutrale and E. Gratton, “Inclined selective plane illumination microscopy adaptor for conventional microscopes,” *Microscopy research and technique*, vol. 75, no. 11, pp. 1461–1466, 2012.

[23] C. K. Rasmi *et al.*, “Integrated light-sheet imaging and flow-based enquiry (iLIFE) system for 3D in-vivo imaging of multicellular organism,” *Applied Physics Letters*, vol. 111, no. 24, p. 243702, 2017.

[24] L. Hood, “Systems biology: integrating technology, biology, and computation,” *Mechanisms of ageing and development*, vol. 124, no. 1, pp. 9–16, 2003.

[25] A. Zabihihesari, A. J. Hilliker, and P. Rezai, “Fly-on-a-chip: microfluidics for Drosophila melanogaster studies,” *Integrative Biology*, vol. 11, no. 12, pp. 425–443, 2019.

[26] M. D. Adams *et al.*, “The genome sequence of Drosophila melanogaster,” *Science*, vol. 287, no. 5461, pp. 2185–2195, 2000.

[27] A. Khalili and P. Rezai, “Microfluidic devices for embryonic and larval zebrafish studies,” *Briefings in functional genomics*, vol. 18, no. 6, pp. 419–432, 2019, doi: 10.1093/bfgp/elz006.

[28] T. Kaletta and M. O. Hengartner, “Finding function in novel targets: C. elegans as a model

organism," *Nature reviews Drug discovery*, vol. 5, no. 5, pp. 387–399, 2006.

[29] S. Brenner, "The genetics of Caenorhabditis elegans," *Genetics*, vol. 77, no. 1, pp. 71–94, 1974.

[30] L. Ma, Y. Zhao, Y. Chen, B. Cheng, A. Peng, and K. Huang, "Caenorhabditis elegans as a model system for target identification and drug screening against neurodegenerative diseases," *European Journal of Pharmacology*, vol. 819, pp. 169–180, 2018.

[31] K. Youssef, A. Tandon, and P. Rezai, "Studying Parkinson's disease using Caenorhabditis elegans models in microfluidic devices," *Integrative biology : quantitative biosciences from nano to macro*, vol. 11, no. 5, 2019, doi: 10.1093/intbio/zyz017.

[32] M. Markaki and N. Tavernarakis, "Modeling human diseases in Caenorhabditis elegans," *Biotechnology Journal*, vol. 5, no. 12, pp. 1261–1276, 2010, doi: 10.1002/biot.201000183.

[33] R. H. Fu *et al.*, "Acetylcorynoline attenuates dopaminergic neuron degeneration and α-synuclein aggregation in animal models of Parkinson's disease," *Neuropharmacology*, vol. 82, pp. 108–120, 2014, doi: 10.1016/j.neuropharm.2013.08.007.

[34] Y. Cho, C. L. Zhao, and H. Lu, "Trends in high-throughput and functional neuroimaging in Caenorhabditis elegans," *Wiley Interdisciplinary Reviews: Systems Biology and Medicine*, vol. 9, no. 3, p. e1376, 2017.

[35] D. Midkiff and A. San-Miguel, "Microfluidic technologies for high throughput screening through sorting and on-chip culture of C. elegans," *Molecules*, vol. 24, no. 23, p. 4292, 2019.

[36] M. Petrascheck, X. Ye, and L. B. Buck, "A high-throughput screen for chemicals that increase the lifespan of Caenorhabditis elegans," *Annals of the New York Academy of Sciences*, vol. 1170, no. 1, pp. 698–701, 2009.

[37] O. E. Olarte, J. Andilla, D. Artigas, and P. Loza-Alvarez, "Decoupled illumination detection in light sheet microscopy for fast volumetric imaging," *Optica*, vol. 2, no. 8, pp. 702–705, 2015.

[38] L. P. O'Reilly, C. J. Luke, D. H. Perlmutter, G. A. Silverman, and S. C. Pak, "C. elegans in high-throughput drug discovery," *Advanced Drug Delivery Reviews*, vol. 69–70, pp. 247–253, 2014, doi: 10.1016/j.addr.2013.12.001.

[39] B. P. Gupta and P. Rezai, "Microfluidic approaches for manipulating, imaging, and screening C. elegans," *Micromachines*, vol. 7, no. 7, p. 123, 2016, doi: 10.3390/mi7070123.

[40] H. E. Kinser and Z. Pincus, "High-throughput screening in the C. elegans nervous system," *Molecular and Cellular Neuroscience*, vol. 80, pp. 192–197, 2017, doi: 10.1016/j.mcn.2016.06.001.

[41] G. Aubry and H. Lu, "A perspective on optical developments in microfluidic platforms for Caenorhabditis elegans research," *Biomicrofluidics*, vol. 8, no. 1, p. 11301, 2014, doi: 10.1063/1.4865167.

[42] N. A. Bakhtina and J. G. Korvink, “Microfluidic laboratories for C. elegans enhance fundamental studies in biology,” *RSC Advances*, vol. 4, no. 9, pp. 4691–4709, 2014, doi: 10.1039/c3ra43758b.

[43] S. Mondal, S. Ahlawat, K. Rau, V. Venkataraman, and S. P. Koushika, “Imaging in vivo Neuronal Transport in Genetic Model Organisms Using Microfluidic Devices,” *Traffic*, vol. 12, no. 4, pp. 372–385, 2011, doi: 10.1111/j.1600-0854.2010.01157.x.

[44] N. Chronis, M. Zimmer, and C. I. Bargmann, “Microfluidics for in vivo imaging of neuronal and behavioral activity in Caenorhabditis elegans.,” *Nature methods*, vol. 4, no. 9, pp. 727–731, Sep. 2007, doi: 10.1038/nmeth1075.

[45] Y. Wang, J. Wang, W. Du, X. J. Feng, and B.-F. Liu, “Identification of the neuronal effects of ethanol on C. elegans by in vivo fluorescence imaging on a microfluidic chip,” *Analytical and bioanalytical chemistry*, vol. 399, no. 10, pp. 3475–3481, 2011.

[46] K. E. McCormick, B. E. Gaertner, M. Sottile, P. C. Phillips, and S. R. Lockery, “Microfluidic devices for analysis of spatial orientation behaviors in semi-restrained Caenorhabditis elegans,” *PLoS ONE*, vol. 6, no. 10, p. e25710, 2011, doi: 10.1371/journal.pone.0025710.

[47] S. E. Hulme, S. S. Shevkoplyas, J. Apfeld, W. Fontana, and G. M. Whitesides, “A microfabricated array of clamps for immobilizing and imaging C. elegans,” *Lab on a Chip*, vol. 7, no. 11, pp. 1515–1523, 2007, doi: 10.1039/b707861g.

[48] H. Bringmann, “Agarose hydrogel microcompartments for imaging sleep-and wake-like behavior and nervous system development in Caenorhabditis elegans larvae,” *Journal of neuroscience methods*, vol. 201, no. 1, pp. 78–88, 2011.

[49] J. Krajniak, Y. Hao, H. Y. Mak, and H. Lu, “C.L.I.P.-continuous live imaging platform for direct observation of C. elegans physiological processes,” *Lab on a Chip*, vol. 13, no. 15, pp. 2963–2971, 2013, doi: 10.1039/c3lc50300c.

[50] J. Krajniak and H. Lu, “Long-term high-resolution imaging and culture of C. elegans in chip-gel hybrid microfluidic device for developmental studies,” *Lab on a Chip*, vol. 10, no. 14, pp. 1862–1868, 2010, doi: 10.1039/c001986k.

[51] M. M. Crane *et al.*, “Autonomous screening of C. elegans identifies genes implicated in synaptogenesis,” *Nature methods*, vol. 9, no. 10, pp. 977–980, 2012.

[52] K. Chung, M. M. Crane, and H. Lu, “Automated on-chip rapid microscopy, phenotyping and sorting of C. elegans,” *Nature Methods*, vol. 5, no. 7, pp. 637–643, 2008, doi: 10.1038/nmeth.1227.

[53] H. S. Chuang, H. Y. Chen, C. S. Chen, and W. T. Chiu, “Immobilization of the nematode caenorhabditis elegans with addressable light-induced heat knockdown (ALINK),” *Lab on a Chip*, vol. 13, no. 15, pp. 2980–2989, 2013, doi: 10.1039/c3lc50454a.

[54] T. V. Chokshi, A. Ben-Yakar, and N. Chronis, “CO2 and compressive immobilization of C. elegans on-chip,” *Lab on a Chip*, vol. 9, no. 1, pp. 151–157, 2009, doi: 10.1039/b807345g.

[55] P. Rezai, S. Salam, P. R. Selvaganapathy, and B. P. Gupta, “Effect of pulse direct current signals on electrotactic movement of nematodes Caenorhabditis elegans and Caenorhabditis briggsae,” *Biomicrofluidics*, vol. 5, no. 4, p. 44116, 2011.

[56] P. Rezai, S. Salam, P. R. Selvaganapathy, and B. P. Gupta, “Electrical sorting of Caenorhabditis elegans,” *Lab on a Chip*, vol. 12, no. 10, pp. 1831–1840, 2012.

[57] P. Rezai, A. Siddiqui, P. R. Selvaganapathy, and B. P. Gupta, “Behavior of Caenorhabditis elegans in alternating electric field and its application to their localization and control,” *Applied Physics Letters*, vol. 96, no. 15, p. 153702, 2010, doi: 10.1063/1.3383223.

[58] P. Rezai, A. Siddiqui, P. R. Selvaganapathy, and B. P. Gupta, “Electrotaxis of Caenorhabditis elegans in a microfluidic environment,” *Lab on a Chip*, vol. 10, no. 2, pp. 220–226, 2010, doi: 10.1039/b917486a.

[59] X. Ding *et al.*, “On-chip manipulation of single microparticles, cells, and organisms using surface acoustic waves,” *Proceedings of the National Academy of Sciences*, vol. 109, no. 28, pp. 11105–11109, 2012.

[60] M. Cornaglia, T. Lehnert, and M. A. M. Gijs, “Microfluidic systems for high-throughput and high-content screening using the nematode: Caenorhabditis elegans,” *Lab on a Chip*, vol. 17, no. 22, pp. 3736–3759, 2017, doi: 10.1039/c7lc00509a.

[61] X. Heng *et al.*, “Optofluidic microscopy—a method for implementing a high resolution optical microscope on a chip,” *Lab on a Chip*, vol. 6, no. 10, pp. 1274–1276, 2006.

[62] X. Cui *et al.*, “Lensless high-resolution on-chip optofluidic microscopes for Caenorhabditis elegans and cell imaging,” *Proceedings of the National Academy of Sciences*, vol. 105, no. 31, pp. 10670–10675, 2008.

[63] D. Lange, C. W. Storment, C. A. Conley, and G. T. A. Kovacs, “A microfluidic shadow imaging system for the study of the nematode Caenorhabditis elegans in space,” *Sensors and Actuators B: Chemical*, vol. 107, no. 2, pp. 904–914, 2005.

[64] S. O. Isikman, I. Sencan, O. Mudanyali, W. Bishara, C. Oztoprak, and A. Ozcan, “Color and monochrome lensless on-chip imaging of Caenorhabditis elegans over a wide field-of-view,” *Lab on a Chip*, vol. 10, no. 9, pp. 1109–1112, 2010.

[65] W. Bishara, H. Zhu, and A. Ozcan, “Holographic opto-fluidic microscopy,” *Optics express*, vol. 18, no. 26, pp. 27499–27510, 2010.

[66] A. F. Coskun, I. Sencan, T.-W. Su, and A. Ozcan, “Lensfree fluorescent on-chip imaging of

transgenic Caenorhabditis elegans over an ultra-wide field-of-view," *PloS one*, vol. 6, no. 1, p. e15955, 2011.

[67] P. Liu, R. J. Martin, and L. Dong, "Micro-electro-fluidic grids for nematodes: a lens-less, image-sensor-less approach for on-chip tracking of nematode locomotion," *Lab on a chip*, vol. 13, no. 4, pp. 650–661, 2013.

[68] J. Wu, G. Zheng, and L. M. Lee, "Optical imaging techniques in microfluidics and their applications," *Lab on a Chip*, vol. 12, no. 19, pp. 3566–3575, 2012.

[69] H. Schneckenburger and V. Richter, "Laser Scanning versus Wide-Field—Choosing the Appropriate Microscope in Life Sciences," *Applied Sciences*, vol. 11, no. 2, p. 733, 2021.

[70] A. R. Hardham, "Confocal microscopy in plant–pathogen interactions," in *Plant Fungal Pathogens*, Springer, 2012, pp. 295–309.

[71] T. J. Van Ham, K. L. Thijssen, R. Breitling, R. M. W. Hofstra, R. H. A. Plasterk, and E. A. A. Nollen, "C. elegans model identifies genetic modifiers of α-synuclein inclusion formation during aging," *PLoS Genetics*, vol. 4, no. 3, p. e1000027, 2008, doi: 10.1371/journal.pgen.1000027.

[72] J. M. Girkin and M. T. Carvalho, "The light-sheet microscopy revolution," *Journal of Optics*, vol. 20, no. 5, p. 53002, 2018.

[73] M. Weber, M. Mickoleit, and J. Huisken, "Light sheet microscopy," *Methods in cell biology*, vol. 123, pp. 193–215, 2014.

[74] K. Greger, J. Swoger, and E. H. K. Stelzer, "Basic building units and properties of a fluorescence single plane illumination microscope," *Review of Scientific Instruments*, vol. 78, no. 2, p. 23705, 2007.

[75] Z. Elisa, B. Toon, S. C. De Smedt, R. Katrien, N. Kristiaan, and B. Kevin, "Technical implementations of light sheet microscopy," *Microscopy research and technique*, vol. 81, no. 9, pp. 941–958, 2018.

[76] U. Krzic, S. Gunther, T. E. Saunders, S. J. Streichan, and L. Hufnagel, "Multiview light-sheet microscope for rapid in toto imaging," *Nature methods*, vol. 9, no. 7, pp. 730–733, 2012.

[77] Y. Wu *et al.*, "Spatially isotropic four-dimensional imaging with dual-view plane illumination microscopy," *Nature biotechnology*, vol. 31, no. 11, pp. 1032–1038, 2013.

[78] M. Weber and J. Huisken, "Omnidirectional microscopy," *nature methods*, vol. 9, no. 7, pp. 656–657, 2012.

[79] H.-U. Dodt *et al.*, "Ultramicroscopy: three-dimensional visualization of neuronal networks in the whole mouse brain," *Nature methods*, vol. 4, no. 4, pp. 331–336, 2007.

[80] E. Zagato *et al.*, "Microfabricated devices for single objective single plane illumination microscopy

(SoSPIM)," *Optics express*, vol. 25, no. 3, pp. 1732–1745, 2017.

[81] P. J. Keller and M. B. Ahrens, "Visualizing whole-brain activity and development at the single-cell level using light-sheet microscopy," *Neuron*, vol. 85, no. 3, pp. 462–483, 2015.

[82] T. F. Holekamp, D. Turaga, and T. E. Holy, "Fast three-dimensional fluorescence imaging of activity in neural populations by objective-coupled planar illumination microscopy," *Neuron*, vol. 57, no. 5, pp. 661–672, 2008.

[83] F. O. Fahrbach, F. F. Voigt, B. Schmid, F. Helmchen, and J. Huisken, "Rapid 3D light-sheet microscopy with a tunable lens," *Optics express*, vol. 21, no. 18, pp. 21010–21026, 2013.

[84] R. Regmi, K. Mohan, and P. P. Mondal, "Light sheet based imaging flow cytometry on a microfluidic platform," *Microscopy research and technique*, vol. 76, no. 11, pp. 1101–1107, 2013.

[85] M. Silhankova and H. C. Korswagen, "Migration of neuronal cells along the anterior–posterior body axis of C. elegans: Wnts are in control," *Current opinion in genetics & development*, vol. 17, no. 4, pp. 320–325, 2007.

[86] L. Gao, "Extend the field of view of selective plan illumination microscopy by tiling the excitation light sheet," *Optics express*, vol. 23, no. 5, pp. 6102–6111, 2015.

[87] I. Albert-Smet, A. Marcos-Vidal, J. J. Vaquero, M. Desco, A. Muñoz-Barrutia, and J. Ripoll, "Applications of light-sheet microscopy in microdevices," *Frontiers in neuroanatomy*, vol. 13, p. 1, 2019.

[88] C. Martin, T. Li, E. Hegarty, P. Zhao, S. Mondal, and A. Ben-Yakar, "Line excitation array detection fluorescence microscopy at 0.8 million frames per second," *Nature Communications*, vol. 9, no. 1, p. 4499, 2018, doi: 10.1038/s41467-018-06775-0.

[89] T. Stiernagle and I. WormBook, "The C. elegans Research Community," *WormBook*, pp. 1551–8507, 2006.

[90] M. Porta-de-la-Riva, L. Fontrodona, A. Villanueva, and J. Cerón, "Basic Caenorhabditis elegans methods: Synchronization and observation," *Journal of Visualized Experiments*, no. 64, p. e4019, 2012, doi: 10.3791/4019.

[91] S. Salam *et al.*, " A microfluidic phenotype analysis system reveals function of sensory and dopaminergic neuron signaling in C. elegans electrotactic swimming behavior ," in *Worm*, 2013, vol. 2, no. 2, p. e24558, doi: 10.4161/worm.24558.

[92] J. Schindelin *et al.*, "Fiji: An open-source platform for biological-image analysis," *Nature Methods*, vol. 9, no. 7, pp. 676–682, Jul. 2012, doi: 10.1038/nmeth.2019.

[93] R. Xiong and K. Sugioka, "Improved 3D cellular morphometry of Caenorhabditis elegans embryos using a refractive index matching medium," *Plos one*, vol. 15, no. 9, p. e0238955, 2020.

[94] Zf. Altun, “DH 2011. Nervous system, general description,” *WormAtlas doi*, vol. 103908.

[95] C. Fang-Yen, M. J. Alkema, and A. D. T. Samuel, “Illuminating neural circuits and behaviour in Caenorhabditis elegans with optogenetics,” *Philosophical Transactions of the Royal Society B: Biological Sciences*, vol. 370, no. 1677, p. 20140212, 2015.

[96] K. A. McVey, I. B. Snapp, M. B. Johnson, R. Negga, A. S. Pressley, and V. A. Fitsanakis, “Exposure of C. elegans eggs to a glyphosate-containing herbicide leads to abnormal neuronal morphology,” *Neurotoxicology and teratology*, vol. 55, pp. 23–31, 2016.

[97] F. Calahorro and M. Ruiz-Rubio, “Caenorhabditis elegans as an experimental tool for the study of complex neurological diseases: Parkinson’s disease, Alzheimer’s disease and autism spectrum disorder,” *Invertebrate neuroscience*, vol. 11, no. 2, pp. 73–83, 2011.

[98] H. Hutter, “Five-colour in vivo imaging of neurons in Caenorhabditis elegans,” *Journal of microscopy*, vol. 215, no. 2, pp. 213–218, 2004.

[99] R. Nass, D. H. Hall, D. M. Miller, and R. D. Blakely, “Neurotoxin-induced degeneration of dopamine neurons in Caenorhabditis elegans,” *Proceedings of the National Academy of Sciences of the United States of America*, vol. 99, no. 5, pp. 3264–3269, 2002, doi: 10.1073/pnas.042497999.